Synthesis and evaluation of porous titanium scaffolds prepared with the space holder method for bone tissue engineering

Arifvianto, Budi

DOI
10.4233/uuid:7f631f4e-3ffa-42fc-9ed1-c98af583ea28

Publication date
2017

Document Version
Final published version

Citation (APA)
Arifvianto, B. (2017). *Synthesis and evaluation of porous titanium scaffolds prepared with the space holder method for bone tissue engineering*. [Dissertation (TU Delft), Delft University of Technology]. https://doi.org/10.4233/uuid:7f631f4e-3ffa-42fc-9ed1-c98af583ea28

Important note
To cite this publication, please use the final published version (if applicable).
Please check the document version above.

SYNTHESIS AND EVALUATION OF POROUS TITANIUM SCAFFOLDS PREPARED WITH THE SPACE HOLDER METHOD FOR BONE TISSUE ENGINEERING

Proefschrift

ter verkrijging van de graad van doctor
aan de Technische Universiteit Delft,
op gezag van de Rector Magnificus prof.ir. K.C.A.M. Luyben;
voorzitter van het College voor Promoties,
in het openbaar te verdedigen op woensdag 25 oktober 2017 om 10:00 uur

door

Budi ARIFVIANTO

Master of Biotechnology
Universitas Gadjah Mada, Yogyakarta, Indonesië
geboren te Yogyakarta, Indonesië

This dissertation has been approved by the

Promotor	: Prof.dr. F.C.T. van der Helm
Copromotor	: Dr. J. Zhou

Composition of the doctoral committee:

Rector Magnificus	Chairman
Prof.dr. F.C.T. van der Helm	Technische Universiteit Delft, promotor
Dr. J. Zhou	Technische Universiteit Delft, copromotor

Independent members:

Dr. A.A. Zadpoor	Technische Universiteit Delft
Prof. dr. ir. N.N.J. Verdonschot	Radboud Universitair Medisch Centrum
Prof. dr. R.G.H.H. Nelissen	Leids Universitair Medisch Centrum
Prof. dr. ir. L. Froyen	Katholieke Universiteit Leuven
Prof. dr. I.M. Richardson	Technische Universiteit Delft
Prof. dr. ir. H.H. Weinans	Technische Universiteit Delft, reserve member

Keywords: synthesis, evaluation, titanium scaffold, space holder method, bone tissue engineering

Printed by : Proefschriftmaken

Cover design by : Yazdi Ibrahim Jenie

ISBN 978-94-6186-851-0
An electronic version of this dissertation is available at
http://repository.tudelft.nl/.

Synthesis and evaluation of porous titanium scaffolds prepared with the space holder method for bone tissue engineering

Budi Arifvianto

Contents

Chapter 1

Introduction

Parts of this chapter are adapted from:
Fabrication of metallic biomedical scaffolds with the space holder method: A review
B. Arifvianto and J. Zhou, Materials, Vol. 7, 2014, pp. 3588-3622.

1.1. Bone defect reconstruction and tissue engineering approach

Up till now, loss of function and impaired life quality of a patient as a result of large bone defects remain a serious problem in the society [1]. As noted by Calori et al. [2], large bone defects can be caused by trauma, tumour or infection that leads to large bone resection and complex non-unions. Basically, the bone tissue has a capability of healing by itself when fractured. However, impaired healing may occur, leading to delayed union or non-union when a bone segment is excised above a critical size [2, 3], for instance, 3 cm for the forearm, 5 cm for the femur and tibia, and 6 cm for the humerus [2].

In recent years, bone tissue engineering has received increasing attention within the biomedical research community as an alternative approach to bone defect reconstruction. With this approach, damaged bone tissue can be repaired and remodelled with new bone cells in a scaffold implanted at the defect site [4]. This new approach is considered highly promising in overcoming the major deficiencies of autogenous bone grafts, which have been used as gold standard implants for many years to support the formation of new bone cells [5]. Autogenous bone grafts contain living cells that can differentiate into osteoblasts for bone tissue regeneration (osteogenic). They also encourage local or additional cells to differentiate into osteoblasts (osteoinductive) and serve as templates that support newly formed bone cells (osteoconductive) [5]. Their clinical applications can, however, be seriously limited by disease transmission and infection from donor to recipient, donor site morbidity, bone defect size, viability of the host bed and the availability of autogenous bone grafts [5, 6]. These limitations have stimulated the development of synthetic materials for scaffolds that may eventually replace autogenous grafts [7, 8, 9].

Scaffolds for bone tissue engineering are designed with porous structures to facilitate cellular activities, such as the migration and proliferation of osteoblasts and mesenchymal cells, as well as the transport of nutrients and oxygen required for vascularization during bone tissue development [7, 8, 10]. With bone tissue grown and developed appropriately in porous structures, osseointegration and stability of implants are improved, as indicated by increased fixation strength, as a result of mechanical interlocking between porous implants and surrounding host bone tissue [8, 11].

1.2. Titanium scaffolds for bone tissue engineering

Bone tissue engineering scaffolds have been made from various materials [9]. Ceramic biomaterials such as hydroxyapatite and β-tricalcium phosphate [12] are well known for their biocompatibility and bioactivity, but they are too brittle for applications that require sufficient mechanical strength and fracture toughness [8, 9, 13]. Polymeric biomaterials are biocompatible and biodegradable, but most of them possess poor mechanical properties [9]. Metallic scaffolds have been acknowledged as the most suitable materials for porous implants for bone tissue engineering.

Titanium and its alloys, for example, have demonstrated a combination of excellent mechanical properties and biocompatibility [14, 15, 16], allowing their use as load-bearing implants and bone tissue scaffolds [17, 18, 19, 20]. The major limitation of these metallic biomaterials is related to their high elastic moduli that lead to stress shielding and bone resorption over time. For instance, the elastic moduli of solid titanium and Ti-6Al-4V alloy are 100-105 GPa and 112 GPa, respectively [21]; being almost three to eight times higher than the Young's modulus of cortical bone tissue reported in the literature, i.e., 14.1 – 27.6 GPa [22]. With porous structure, however, the mismatch in elastic modulus between metallic implant and host bone tissue can be reduced [9, 21].

1.3. Design requirements of titanium scaffolds for bone tissue engineering

Currently, several review articles have been published with a purpose to specify optimum porosity and pore sizes required for bone tissue ingrowth in a scaffold based on both in vitro and in vivo studies. However, it is important to note that the in vitro bone regeneration in a scaffold showed an opposite trend when it was compared with the results from in vivo studies [8, 23].

Highly porous scaffolds, e.g., those with porosity of 90%, is generally required to ensure cell delivery and tissue ingrowth [24], owing to a very large number of interconnected pores for the diffusion of oxygen, nutrients and waste required for bone cell activities within the scaffold. As such, the mechanical properties of the scaffold might however be compromised. As a consequence, the in vivo bone tissue regeneration was altered, since the mechanical loading on a scaffold would determine bone apposition [23]. In the case of scaffolds prepared from metallic biomaterials, such as titanium or its alloys, a highly porous structure in those materials may, to

some extent, not be a problem, owing to the excellent mechanical properties of their solid matrix material [23].

The influences of pore sizes on the performance of a scaffold for bone tissue engineering have so far been reviewed as well. Initially, Hulbert et al. [25] considered that 100 μm was the minimum requirement of pore size for scaffolds for bone tissue engineering. Later, on the basis of the studies conducted up to 2005, Karageorgiou and Kaplan [8] recommended a pore size of 300 μm for scaffolds. Chang et al. [13] showed that an 8-week post-implanted hydroxyapatite scaffold with a pore size of 300 μm possessed the highest compressive strength compared with scaffolds with pore sizes of 50, 100 and 500 μm, indicating a better osteoconduction capacity of the scaffold with a 300 μm pore size than the others. Through a study with the distal femoral cortex of rabbits, Gotz et al. [26] observed delayed onset of bone remodelling in the surface-laser-textured Ti-6Al-4V alloy having 100 μm pores compared with the same implants with 200 and 300 μm pores. Kuboki et al. [27] demonstrated that 300-400 μm could be considered as an optimum pore size range for bone-forming efficacy in porous blocks prepared from hydroxyapatite material. Murphy et al. [10] revealed that 325 μm was an optimum pore size, as indicated from the largest number of osteoblasts that could be generated in a collagen-glycosaminoglycan scaffold after 7-day seeding in a culture medium. From their study, it was also stressed that the importance of pore size parameter was related to its capacity in facilitating cell proliferation and migration [10], in addition to oxygen and nutrients supplies for ostoegenesis within a scaffold [8, 23]. Bobyn et al. [11] demonstrated the highest fixation strength of a porous-surfaced cobalt-based alloy with a pore size range of 200-400 μm after implanted for 12 weeks in a cortical canine bone. On the basis of these reports, it can be concluded that pore sizes in the range of 200 – 500 μm should be considered in the design of scaffolds for bone tissue engineering.

1.4. Fabrication of biomedical titanium scaffolds: the space holder method

Currently, various methods for the fabrication of metallic scaffolds have been presented in the literature, for example, powder sintering, expansion of pressurized gas bubbles, powder deposition, rapid prototyping and space holder method [9, 21, 22, 28]. Powder sintering, as a traditional powder metallurgy method, has been widely used for its simplicity in generating porous structures needed for scaffolds. With this method, metal powder particles are compacted and sintered. Pores are formed from the interstices of powder particle arrangements [28, 29, 30, 31]. As such, pore sizes and pore shape of sintered powder compacts depend on the sizes and shape of starting powder particles [28, 29, 31] and maximum porosity achievable is limited to 35% [31]. Powder sintering may be coupled with the space holder method so as to reach higher porosity levels and better control over porous structure in scaffolds [32, 33].

Scaffold fabrication with the space holder method relies on temporary particles added to a metallic matrix powder, i.e., space holding particles that act as a pore former. Figure 1.1 schematically illustrates the main steps involved in metallic scaffold fabrication with the space holder method. Space-holding particles are first mixed and compacted together with metallic matrix powder particles and then removed, either before or during sintering, leaving new pores

behind in the matrix. The space holder method highly resembles the fugitive filler method [34], and therefore their names may be used interchangeably. A number of space holder materials have been utilized, such as carbamide ($CO(NH_2)_2$) [35, 36, 37, 38, 39], ammonium hydrogen carbonate (NH_4HCO_3) [40, 41], sodium chloride (NaCl) [42, 43], starch [44], saccharose [45], polymethyl-methacrylate (PMMA) [46], magnesium (Mg) [47, 48], steel [49] and paraformaldehyde [50].

Earlier designed metallic scaffolds produced with the space holder method exhibited characteristics and performance that could meet the criteria of scaffolds for bone tissue engineering, i.e., high porosity (45%–80%), interconnected pores, appropriate pore sizes (200–500 μm) and adequate mechanical properties in terms of elastic modulus and compressive strength [32]. A series of in vitro cell compatibility tests showing bone cell attachment, proliferation and differentiation in the Ti-Nb-Zr alloy scaffold confirmed the biocompatibility of the scaffold produced with the space holder method [51]. This finding was attributed to the ability of the space holder method to produce high-porosity scaffolds (up to 70%) with interconnected pores, considering the great importance of porosity for bone cell activities [35, 52].

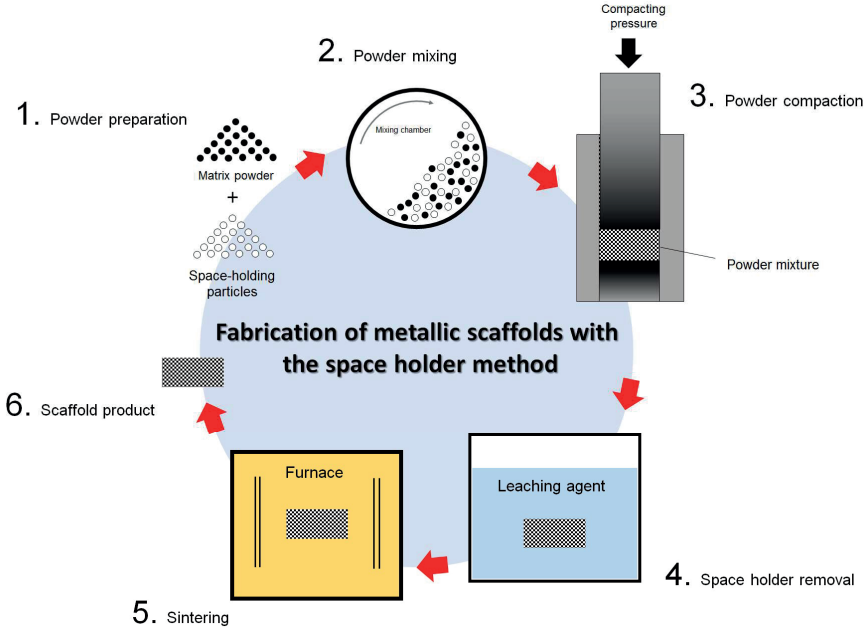

Fig. 1.1. Fabrication route for metallic scaffolds with the space holder method. In principle, the prepared space-holding particles and metallic matrix powder (Step 1) are first mixed (Step 2) and compacted together to form scaffold green body (Step 3). Then, the space-holding particles are removed, leaving new pores behind in the matrix (Step 4). In the end, the porous matrix material is sintered (Step 5) to form the final form of the scaffold (Step 6).

1.5. Problem definition

Up till now, many studies have been conducted on scaffold fabrication with the space holder method. Despite a large number of studies on the subject, the mechanisms involved in the scaffold fabrication with this method have not yet been fully understood. Processing parameters had been studied mostly by trial-and-error rather than in a systematic manner and on the basis of the concepts of powder metallurgy that are actually the underlying principle of the space holder method. These have led to difficulties in ensuring the reproducibility of scaffold properties. Moreover, many of the studies on the performance of metallic scaffolds as well as on the fabrication procedures overlap each other, resulting in difficulties in tracking the research progress and in establishing standardized procedures for metallic scaffold fabrication with this method. In the end, all these facts may result in the uncertainties of the scaffold performance to heal the bone defect of the patient.

1.6. Aim of this thesis

This thesis is aimed to provide a fundamental knowledge of the mechanisms involved in the fabrication of biomedical titanium scaffolds with the space holder method. The work reported in this thesis is directed towards giving an insight into the way to control the porous structure of biomedical titanium scaffolds through adjusting the process parameters of the space holder method. To serve this purpose, a series of experimental studies were performed systematically to investigate the influences of process parameters applied in the fabrication of titanium scaffolds on their porous architecture and relevant properties. On the basis of the knowledge of the mechanisms involved in the fabrication process, titanium scaffolds with porous structures that could meet the requirements for bone tissue engineering were proposed at the end of this thesis.

1.7. Outline of this thesis

The outline of the research in this thesis is schematically illustrated in Fig. 1.2. Chapter 2 gives a critical review of a large number of papers published since 2000 on the technical capabilities of the space holder method, its limitations and challenges for the fabrication of biomedical titanium scaffolds. This chapter provides a solid foundation for the research reported for this thesis. As discussed in this chapter, powder compaction and space holder removal are selected to be studied in an attempt to control the porous structure of titanium scaffolds in this research. In Chapters 3-6, all these parameters and their relationships with the mechanisms involved in the scaffold fabrication and the pore characteristics of the scaffolds are presented.

As noted in Chapter 2, the importance of powder compaction in the fabrication of titanium scaffold with the space holder method is recognized, as it governs not only the structural integrity but also the porous structure of the scaffold. An appropriate compacting pressure is called for, since too high compacting pressures may lead to shape distortions of macro-pores in the scaffold. In Chapter 3, a method is described, based on the mechanics of uniaxial compaction

of powder mixtures for the determination of the critical compacting pressure that can be applied to the preparation of titanium scaffolds without causing excessive deformation or breakage of carbamide space holder. The compaction behaviours of the powders under the pressures applied are also discussed in this chapter.

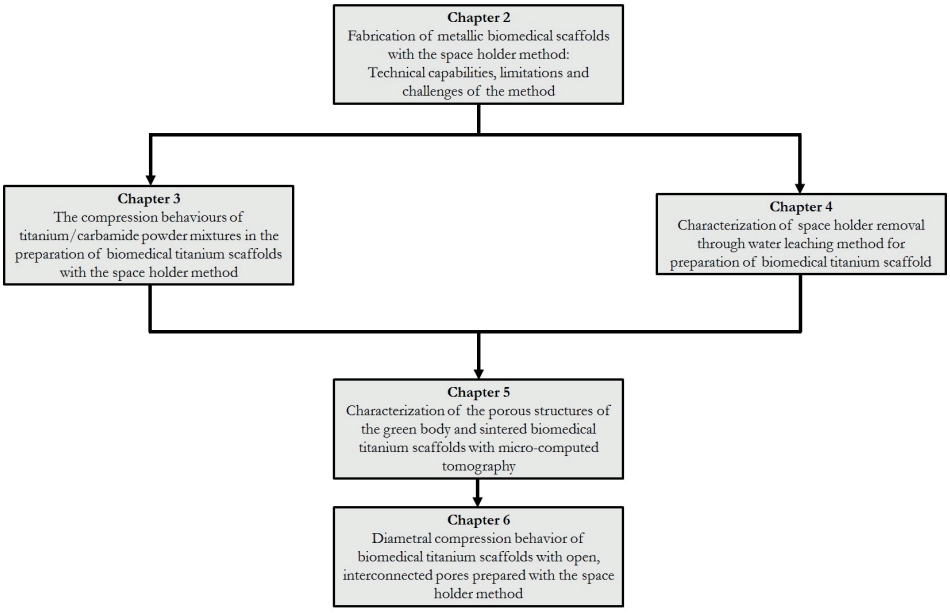

Fig. 1.2. Outline of the research in this thesis

Porous structure of titanium scaffold is achieved after the removal of space-holding particles from the compacted titanium/carbamide powder mixture. In this research, the water leaching technique was utilized for removing carbamide space-holding particles from the scaffold preform. As discussed in Chapter 2, this technique entails some complexities, particularly with regard to the duration required for the leaching process. A too long immersion period for leaching potentially deteriorates structural integrity and, in some cases, ruins the scaffold preform during and after the leaching. On the other hand, a too short immersion period of time may result in the contamination of the scaffold preform due to incomplete removal of space-holding particles. In Chapter 4, a new technique for the characterization of space holder removal with water leaching is described. By using this technique, the mechanisms involved and appropriate duration for the leaching process to remove the carbamide space holder from titanium scaffold preforms were then determined.

Sintering determines the final porous structure and performances of the scaffolds produced. As discussed in Chapter 2, there are two types of pores produced after the sintering of the titanium scaffold preform prepared with the space holder method, i.e., macro- and micro-pores.

They originate from the space occupied by space-holding particles and inter-particle necks of sintered titanium powder particles, respectively. Although this fabrication technique has been widely reported in the literature, the information on the transformation of space-holding particles in the green body into macro-pores in the scaffold interior and the corresponding 3-dimensional (3D) changes of the scaffold porous structure is still lacking. As a consequence, the question remains unanswered as to whether the final porous structure of the scaffold could be controlled from the space holder volume fraction in its green structure. As presented in Chapter 5, the changes in the porous structure of titanium scaffold prior to and after sintering were characterized by using micro-computed tomography (micro-CT). In addition, by using the characterization technique developed in Chapter 4, the efficiencies of water leaching in the removal of space-holding particles from titanium scaffold preforms were determined.

To evaluate the performances of titanium scaffolds after being prepared with the optimized space holder method, the physical and mechanical properties of the scaffolds needed to be determined. As seen in Chapter 6, the porous structure, the presence of open, interconnected pores within the scaffolds, and the mechanical properties of the scaffolds fabricated through the fabrication steps reported in Chapters 3-5 were characterized. Micro-computed tomography (micro-CT) analysis and permeability tests were carried out to investigate the porous structures and pore interconnections. In addition, the elastic moduli and yield strengths of the scaffolds were determined by performing diametral compression tests.

References

[1] I. Drosse, E. Volkmer, R. Capanna, P. De Biase, W. Mutschler and M. Schieker, "Tissue engineering for bone defect healing: An update on a multi-component approach," *Injury,* vol. 39, pp. S9-S20, 2008.

[2] G. M. Calori, E. Mazza, M. Colombo and C. Ripamonti, "The use of bone-graft substitutes in large bone defects: Any specific needs?," *Injury,* vol. 42, pp. S56-63, 2011.

[3] E. Lucarelli, D. Donati, A. Cenachi and P. M. Fornasari, "Bone reconstruction of large defects using bone marrow derived autologous stem cells," *Transfusion and Apheresis Science,* vol. 30, pp. 169-174, 2004.

[4] A. Vats, N. S. Tolley, J. M. Polak and J. E. Gough, "Scaffolds and biomaterials for tissue engineering: A review of clinical applications," *Clinical Otolaryngology,* vol. 28, pp. 165-172, 2003.

[5] P. Lichte, H. C. Pape, T. Pufe, P. Kobbe and H. Fischer, "Scaffolds for bone healing: Concepts, materials and evidence," *Injury,* vol. 42, pp. 569-573, 2011.

[6] K. J. L. Burg, S. Porter, T. Pufe, P. Kobbe and H. Fischer, "Biomaterials developments for bone tissue engineering," *Biomaterials,* vol. 21, pp. 2347-2359, 2001.

[7] S. Bose, M. Roy and A. Bandyopadhyay, "Recent advances in bone tissue engineering scaffolds," *Trends in Biotechnology,* vol. 30, pp. 546-554, 2012.

[8] V. Karageorgiou and D. Kaplan, "Porosity of 3D biomaterial scaffolds and osteogenesis," *Biomaterials,* vol. 26, pp. 5474-5491, 2005.

[9] G. Ryan, A. Pandit and D. P. Apatsidis, "Fabrication methods of porous metals for use in orthopaedic applications," *Biomaterials,* vol. 27, pp. 2651-2670, 2006.

[10] C. M. Murphy, M. G. Haugh and F. J. O'Brien, "The effect of mean pore size on cell attachment, proliferation and migration in collagen-glycosaminoglycan scaffolds for bone tissue engineering," *Biomaterials,* vol. 31, pp. 461-466, 2010.

[11] J. D. Bobyn, R. M. Pilliar, H. U. Cameron and G. C. Weatherly, "The optimum pore size for the fixation of porous-surfaced metal implants by the ingrowth of bone," *Clinical Orthopaedic and Related Research,* vol. 150, pp. 263-270, 1980.

[12] L. Galois and D. Mainard, "Bone ingrowth into two porous ceramics with different pore sizes: An experimental study," *Acta Orthopaedica Belgica,* vol. 70, pp. 598-603, 2004.

[13] B. S. Chang, C. K. Lee, K. S. Hong, H. J. Youn, H. S. Ryu, S. S. Chung and K. W. Park, "Osteoconduction at porous hydroxyapatite with various pore configurations," *Biomaterials,* vol. 21, pp. 1291-1298, 2000.

[14] M. Niinomi, "Mechanical properties of biomedical titanium alloys," *Materials Science and Engineering A,* vol. 243, pp. 231-236, 1998.

[15] M. Niinomi, "Recent research and development in titanium alloys for biomedical applications and healthcare goods," *Science and Technology of Advanced Materials,* vol. 4, pp. 445-454, 2003.

[16] H. J. Rack and J. I. Qazi, "Titanium alloys for biomedical applications," *Materials Science and Engineering C,* vol. 26, pp. 1269-1277, 2006.

[17] J. Chen, E. Paetzell, J. Zhou, L. Lyons and W. Soboyejo, "Osteoblast-like cell ingrowth, adhesion and proliferation on porous Ti-6Al-4V with particulate and fiber scaffolds," *Materials Science and Engineering C,* vol. 30, pp. 647-656, 2010.

[18] L. M. de Vasconcellos, F. N. Oliveira, O. de Leite, L. G. de Vasconcellos, R. F. do Prado, C. J. Ramos, M. L. Graca, C. A. Cairo and Y. R. Carvalho, "Novel production method of porous surface Ti samples for biomedical application," *Journal of Materials Science: Materials in Medicine,* vol. 23, pp. 357-364, 2012.

[19] S. Fujibayashi, M. Neo, H. -M. Kim, T. Kokubo and T. Nakamura, "Osteoinduction of porous bioactive titanium metal," *Biomaterials,* vol. 25, pp. 443-450, 2004.

[20] A. Fukuda, M. Takemoto, T. Saito, S. Fujibayashi, M. Neo, D. K. Pattanayak, T. Matsushita, K. Sasaki, N. Nishida, T. Kokubo and T. Nakamura, "Osteoinduction of porous Ti implants with a channel structure fabricated by selective laser melting," *Acta Biomaterialia,* vol. 7, pp. 2327-2336, 2011.

[21] R. Singh, P. D. Lee, R. J. Dashwood and T. C. Lindley, "Titanium foams for biomedical applications: A review," *Materials Technology,* vol. 25, pp. 127-136, 2010.

[22] K. Alvarez and H. Nakajima, "Metallic scaffolds for bone regeneration," *Materials,* vol. 2, pp. 790-832, 2009.

[23] A. A. Zadpoor, "Bone tissue regeneration: The role of scaffold geometry," *Biomaterials Science,* vol. 3, pp. 231-245, 2015.

[24] T. S. Karande, J. L. Ong and C. M. Agrawal, "Diffusion in musculoskeletal tissue engineering scaffolds: Design issues related to porosity, permeability, architecture, and nutrient mixing," *Annals of Biomedical Engineering,* vol. 32, p. 1728–1743, 2004.

[25] S. F. Hulbert, F. A. Young, R. S. Mathews, J. J. Klawitter, C. D. Talbert and F. H. Stelling, "Potential of ceramic materials as permanently implantable skeletal prostheses," *Journal of Biomedical Materials Research,* vol. 4, pp. 433-456, 1970.

[26] H. E. Gotz, M. Muller, A. Emmel, U. Holzwarth, R. G. Erben and R. Stangl, "Effect of surface finish on the osseointegration of laser-treated titanium alloy implants," *Biomaterials,* vol. 25, pp. 4057-4064, 2004.

[27] Y. Kuboki, Q. Jin and H. Takita, "Geometry of carriers controlling phenotypic expression in BMP-induced osteogenesis and chondrogenesis," *Journal of Bone and Joint Surgery,* vol. 83A, pp. S105-S115, 2001.

[28] D. Dunand, "Processing of titanium foams," *Advanced Engineering Materials,* vol. 6, pp. 369-376, 2004.

[29] M. Guden, E. Celik, A. Hizal, M. Altindis and S. Cetiner, "Effects of compaction pressure and particle shape on the porosity and compression mechanical properties of sintered Ti6Al4V powder compacts for hard tissue implantation," *Journal of Biomedical Materials Research B: Applied Biomaterials,* vol. 85, pp. 547-555, 2008.

[30] I. -H. Oh, N. Nomura, N. Masahashi and S. Hanada, "Mechanical properties of porous titanium compacts prepared by powder sintering," *Scripta Materialia,* vol. 49, pp. 1197-1202, 2003.

[31] I. -H. Oh, N. Nomura, N. Masahashi and S. Hanada, "Microstructures and mechanical properties of porous titanium compacts prepared by powder sintering," *Materials Transactions,* vol. 43, pp. 443-446, 2002.

[32] C. E. Wen, M. Mabuchi, Y. Yamada, K. Shimojima, Y. Chino and T. Asahina, "Processing of biocompatible porous Ti and Mg," *Scripta Materialia,* vol. 45, pp. 1147-1153, 2001.

[33] C. E. Wen, Y. Yamada, K. Shimojima, Y. Chino, T. Asahina and M. Mabuchi, "Processing and mechanical properties of autogenous titanium implant materials," *Journal of Materials Science: Materials in Medicine,* vol. 13, pp. 397-401, 2002.

[34] T. F. Hong, Z. X. Guo and R. Yang, "Fabrication of porous titanium scaffold materials by a fugitive filler method," *Journal of Materials Science: Materials in Medicine,* vol. 19, pp. 3489-3495, 2008.

[35] S. N. Dezfuli, S. K. Sadrnezhaad, M. A. Shokrgozar and S. Bonakdar, "Fabrication of biocompatible titanium scaffolds using space holder technique," *Journal of Materials Science: Materials in Medicine,* vol. 23, pp. 2483-2488, 2012.

[36] G. Kotan and A. S. Bor, "Production and characterization of high porosity Ti-6Al-4V foam by space holder technique powder metallurgy," *Turkish Journal of Engineering and Environmental Science,* vol. 31, pp. 149-156, 2007.

[37] C. F. Li, Z. G. Zhu and T. Liu, "Microhardness of pore walls in porous titanium prepared with novel powder metallurgy," *Powder Metallurgy,* vol. 48, pp. 237-240, 2005.

[38] W. Niu, C. Bai, G. Qiu and Q. Wang, "Processing and properties of porous titanium using space holder technique," *Materials Science and Engineering A,* vol. 506, pp. 148-151, 2009.

[39] O. Smorygo, A. Marukovich, V. Mikutski, A. A. Gokhale, G. J. Reddy and J. V. Kumar, "High-porosity titanium foams by powder coated space holder compaction method," *Materials Letters,* vol. 83, pp. 17-19, 2012.

[40] A. Laptev, M. Bram, H. P. Buchkremer and D. Stöver, "Study of production route for titanium parts combining very high porosity and complex shape," *Powder Metallurgy,* vol. 47, pp. 85-92, 2004.

[41] D. S. Li, Y. P. Zhang, X. Ma and X. P. Zhang, "Space-holder engineered porous NiTi shape memory alloys with improved pore characteristics and mechanical properties," *Journal of Alloys and Compounds,* vol. 474, pp. L1-L5, 2009.

[42] Y. Torres, J. J. Pavón and J. A. Rodríguez, "Processing and characterization of porous titanium for implants by using NaCl as space holder," *Journal of Materials Processing Technology,* vol. 212, pp. 1061-1069, 2012.

[43] X. Zhao, H. Sun, L. Lan, J. Huang, H. Zhang and Y. Wang, "Pore structures of high-porosity NiTi alloys made from elemental powders with NaCl temporary space-holders," *Materials Letters,* vol. 63, pp. 2402-2404, 2009.

[44] A. Mansourighasri, N. Muhamad and A. B. Sulong, "Processing titanium foams using tapioca starch as a space holder," *Journal of Materials Processing Technology,* vol. 212, pp. 83-89, 2012.

[45] J. Jakubowicz, G. Adamek and M. Dewidar, "Titanium foam made with saccharose as a space holder," *Journal of Porous Materials,* vol. 20, pp. 1137-1141, 2013.

[46] A. Manonukul, N. Muenya, F. Léaux and S. Amaranan, "Effects of replacing metal powder with powder space holder on metal foam produced by metal injection moulding," *Journal of Materials Processing Technology,* vol. 210, pp. 529-535, 2010.

[47] Z. Esen and S. Bor, "Processing of titanium foams using magnesium spacer particles," *Scripta Materialia,* vol. 56, pp. 341-344, 2007.

[48] Z. Esen and S. Bor, "Characterization of Ti–6Al–4V alloy foams synthesized by space holder technique," *Materials Science and Engineering A,* vol. 528, pp. 3200-3209, 2011.

[49] P. J. Kwok, S. M. Oppenheimer and D. C. Dunand, "Porous titanium by electro-chemical dissolution of steel space-holders," *Advanced Engineering Materials,* vol. 10, pp. 820-825, 2008.

[50] B. Dabrowski, W. Swieszkowski, D. Godlinski and K. J. Kurzydlowski, "Highly porous titanium scaffolds for orthopaedic applications," *Journal of Biomedical Materials Research B: Applied Biomaterials,* vol. 95, pp. 53-61, 2010.

[51] X. Wang, Y. Li, J. Xiong, P. D. Hodgson and C. Wen, "Porous TiNbZr alloy scaffolds for biomedical applications," *Acta biomaterialia,* vol. 5, pp. 3616-3624, 2009.

[52] S. R. Bhattarai, K. A. Khalil, M. Dewidar, P. H. Hwang, H. K. Yi and H. Y. Kim, "Novel production method and in-vitro cell compatibility of porous Ti-6Al-4V alloy disk for hard tissue engineering," *Journal of Biomedical Materials Research A,* vol. 86, pp. 289-299, 2008.

Chapter 2

Fabrication of metallic biomedical scaffolds with the space holder method

Technical capabilities, limitations and challenges of the method

This chapter is adapted from:
Fabrication of metallic biomedical scaffolds with the space holder method: A review
B. Arifvianto and J. Zhou, Materials, Vol. 7, 2014, pp. 3588-3622.

2.1. Introduction

As described in Chapter 1, the space holder method has been recognized as one of viable techniques for the fabrication of biomedical titanium scaffolds. Up till now, many studies have been conducted to investigate the feasibility of this method as well as to determine the performance of the resulting scaffolds. Furthermore, several review articles on scaffold materials and fabrication technology have been published and these articles all mention the space holder method as one of the effective methods for the fabrication of metallic scaffolds [1, 2, 3]. In addition, general principle of the space holder method has been clearly described in these review articles.

Despite a clear description of the general principle of the method, the procedures used for scaffold fabrication with the space holder method have not yet been collated. All the review articles authored by Ryan et al. [1], Singh et al. [2] and Banshiddi et al. [4] do not provide detailed information on the fabrication procedures or the hurdles that remain towards the large-scale fabrication of scaffolds with controllable, reproducible mechanical properties and architectural characteristics. Moreover, many of the papers on the performance of metallic scaffolds as well as on the fabrication procedures overlap each other, resulting in difficulties in tracking the research progress and in establishing standardized procedures for metallic scaffold fabrication with this method.

In this chapter, the fabrication technology of metallic biomedical scaffolds with the space holder method is reviewed. On the basis of a critical review of a large number of papers published since 2000, the technical capabilities of this method, its limitations and challenges are elucidated.

This chapter begins with a discussion on the importance of powder selection and preparation on the properties of metallic biomedical scaffolds prepared with the space holder method (Section 2.2). Technological aspects encountered in each fabrication step of metallic scaffolds with the space holder method are critically reviewed in Sections 2.3 – 2.6. Finally, concluding remarks are given in Section 2.7.

2.2. Powder selection and preparation

The fabrication of metallic scaffolds with the space holder method begins with the mixing of metal matrix powder and space-holding particles (see Figure 1.1 in Chapter 1). It is important to note that appropriate matrix powder particles must be selected and prepared, before scaffold fabrication can be started. This is mainly because the properties of the resultant scaffolds are to some extent dictated by the characteristics of both metal matrix powder and space-holding particles [5, 6, 7, 8, 9].

2.2.1. Elemental and alloyed matrix powders

Basically, the porous structure of a scaffold stems from the arrangements of metal matrix powder particles that build up the scaffold framework. Pure titanium and magnesium are among powdered metallic materials that have been processed as the matrices of scaffolds [10, 11]. Since the mechanical and biological properties of those pure metallic scaffolds are often not satisfactory, scaffolds prepared from alloy powders, such as Ti-6Al-4V [5, 12, 13], NiTi [14, 15, 16], Ti-6Ta-4Sn [17], Ti-5Mn [18], Ti-7.5Mo [19, 20], Ti-10Mo [21], AZ91 [22] and Mg-Zn [23] are preferred.

In general, there are two techniques that may be used for the preparation of alloy powders, i.e., the pre-alloying (PA) technique and blended elemental (BE) technique [24]. In the PA technique, the addition of one or more elements to the base metal is performed before the alloy is atomized into a powder form. By contrast, the BE technique is deployed by blending elemental powder particles in, e.g., a planetary ball milling machine running at a prescribed ball-to-powder ratio for a certain duration. During the blending process, elemental powder particles are plastically deformed and cold welded [19, 20] and alloying takes place during sintering after cold compaction of blended elemental powders, in addition to alloying that may have already taken place during intensive mixing.

Alloying elements must be carefully selected, based on the considerations on possible toxic and allergic side-effects [25]. Several alloying elements have been found to be toxic and inappropriate for biomedical applications, such as aluminium (Al), nickel (Ni), iron (Fe), vanadium (V) and cobalt (Co) [26], while other elements such as zirconium (Zr), niobium (Nb) and tantalum (Ta), molybdenum (Mo) and tin (Sn) have been taken as safe alloying elements [25, 26]. Table 2.1 shows a number of examples of scaffolds that have been developed from powdered alloys with the space holder method.

Table 2.1. Bone tissue engineering scaffolds developed from powdered alloys with the space holder method

Alloyed powder	Method of alloying*	References
Ti-6Al-4V	PA	[12, 27]
NiTi	PA, BE	[6, 14, 15]
Ti-5Mn	BE	[18]
Ti-7.5Mo	BE	[19, 20]
Ti-6Ta-4Sn	BE	[17]
Ti-16Sn-4Nb	BE	[28]
316L stainless steel	PA	[29]
AZ91	PA	[22]
Mg-Zn	BE	[23]

*PA = pre-alloying technique and BE = blended elemental technique

2.2.2. Morphology of matrix powder particles

The properties of a metallic scaffold are influenced by the morphological characteristics of metal matrix powder particles. Guden et al. [5] reported higher porosity and larger pore sizes, as a result of the sintering of a compacted angular powder, in comparison with a compacted spherical powder. The compressive strength and elastic modulus of the sintered angular matrix powder were lower than those of the sintered spherical powder [5]. With increasing porosity, the mechanical properties of the scaffolds deteriorated. The better mechanical properties of the scaffolds from the sintered spherical powder were attributed to lower porosity, as a result of a higher deformation capacity of spherical particles than that of angular ones under the same compacting pressure [5]. It is important to distinguish the mechanical properties in the sintered state from those in the green state (after compaction). Interestingly, the use of angular matrix powder particles led to a higher green strength of scaffolds [7], while the green body of scaffolds prepared from compacted spherical powder particles tended to collapse, especially during the removal of space-holding particles, due to less mechanical interlocking between initially spherical powder particles in compacts.

2.2.3. Sizes of matrix powder particles

The quality of a sintered scaffold and densification during sintering depend on the sizes of matrix powder particles. Bram et al. [9] showed fully densified scaffold framework as a result of the sintering of powder particles having sizes finer than 16 μm. However, the sintering of powder particles of larger sizes resulted in scaffold framework with voids and sintering necks [9]. In addition, Chen et al. [8] showed downsizing titanium particles through ball milling from 19.79 to 5.89 μm significantly increased the surface energy and apatite-inducing ability of the resulting titanium scaffolds.

2.2.4. Types of space-holding particles

As the porous architecture and mechanical properties of scaffolds are greatly affected by space-holding particles used in scaffold fabrication, the properties and geometrical characteristics of space-holding particles must be considered. The selection of space-holding particles must be based on the following criteria:

a. biocompatibility and non-cytotoxicity
b. chemical stability
c. removal capability
d. mechanical properties.

In order to minimize the adverse effects on the resultant scaffolds due to contamination by the residues of space-holding particles, Bor et al. and Kim et al. [30, 31, 32, 33, 34, 35] used a pure magnesium powder as the space holder. In addition, food-grade powders, such as sodium chloride [14, 15, 36, 37, 38], saccharose [39], dextrin corn starch [40] and tapioca starch [41] have been devised as safe space holders. Reactions between matrix powder and space-holding particles or binder must be avoided and hence chemically stable space-holding particles are preferred. Any reaction between decomposed space-holding particles and scaffold framework may deteriorate the mechanical properties of the resulting scaffolds [35]. Moreover, reactions between space-holding particles and binder that is used in the fabrication process must also be avoided, because they may distort the shape and sizes of space-holding particles and the resulting macro-pore geometry of scaffolds. In addition, space-holding particles must be able to be removed quickly from scaffold preforms in order to prevent contaminations by space holder residues.

Finally, the strength of space holder material is critical, because it is related to the possibility of deformation and then breakage that may occur during the compaction process (see Section 2.4). Considering these criteria, metallic powders such as magnesium and steel whose mechanical properties are better than organic space holders, such as carbamide and sodium chloride, have been used [42, 43]. Table 2.2 shows a few examples of space holders and the considerations in selecting these materials for metallic biomedical scaffolds.

2.2.5. Sizes of space-holding particles

The sizes of space-holding particles must be selected, based on the desired macro-pore sizes in scaffolds. Spacer powder particles having sizes in a range of 100 - 500 μm are commonly chosen to produce scaffolds with macro-pore sizes of 300 - 400 μm. In addition, appropriate sizes of space-holding particles can result in the formation of interconnected macro-pores in scaffolds. By means of tomographic analysis, Tuncer et al. [7] successfully studied the influence of space-holding particle size on the 3-dimensional porous architecture of titanium scaffolds. It is reported that macro-pore interconnect size in scaffolds increases, when space-holding particles of a larger size are used. This could be attributed to greater packing coordination of larger space-holding particles, as compared with smaller particles after compaction. Greater porosity is then produced in scaffolds. As a consequence of having a larger macro-pore interconnect size, the specific surface area of scaffolds decreases, when space-holding particles of a larger size are used.

Moreover, macro-pore sphericity increases when space-holding particles of a larger size are used. Pore wall thickness increases with increasing space-holding particle size for the same relative density, compared to the one with space-holding particles having a smaller size, resulting in better mechanical properties of scaffolds.

Table 2.2. Space holding particles and considerations in selection for metallic biomedical scaffolds

Space holder material	Reasons of selection	References
Ammonium hydrogen carbonate	Low decomposition temperature	[6, 44, 45]
Carbamide	Highly soluble in water	[46, 47]
Saccharose	Soluble in water, biocompatible	[39]
Sodium chloride	Soluble in water, biocompatible	[14, 36]
Magnesium	Biocompatible, good mechanical properties	[12, 32, 42]
Steel	Good mechanical properties	[43]

2.2.6. Morphology of space-holding particles

Regarding the shape of space-holding particles, Bekoz and Oktay [47] showed decreased compressive strength and elastic modulus of stainless steel foams with the use of an irregularly shaped carbamide space holder. Stainless steel foams with spherical pores exhibited better mechanical properties, as they had smoother pore surfaces that could minimize stress concentrations due to a decreased number of sharp edges in scaffolds. Zhang et al. [48] confirmed that spherical porogens (space holder) resulted in polymeric scaffolds with higher compressive strength and elastic modulus, corresponding to a smaller number of defects in scaffolds, compared to those processed with cubical porogens. At high porosity levels, spherical space holder yielded a more ordered array of macro-pores and interconnections in the interior of scaffolds. With cubical space holder, however, effective geometrical packing in scaffold preforms could not be achieved, resulting in an irregular porous structure.

2.2.7. Size distribution of space-holding particles

The size distribution of space-holding particles must be controlled. In most cases, a narrow distribution of space-holding particle sizes is preferred. In order to investigate the effect of the particle size distribution of space holder, Li et al. [6] compared porous architecture and mechanical properties of NiTi scaffolds prepared with sieved and non-sieved space-holding particles. Through sieving, the size distribution of space-holding particles could be narrowed down to a certain range. From this study, it was found that NiTi scaffolds processed with the non-sieved space holder exhibited lower strength and possessed nearly no superplastic

properties, resulting from randomly distributed macro-pores in scaffolds. This finding confirms the importance of the size uniformity of space-holding particles to the performance of metallic scaffolds.

2.3. Mixing

With the space holder method, mixing of matrix powder and space-holder is conducted as the first step in scaffold fabrication. Porosity and pore interconnectivity of resultant scaffolds can be determined by adjusting the volume fraction of space-holding particles. The porosity of a scaffold is expressed mathematically in Eq. 2.1a,

$$p = \frac{V_{pore}}{V_{sc}} \tag{2.1a}$$

where p is the ratio of pore volume V_{pore} to the total volume of the scaffold V_{sc}. In the space holder method, the scaffold porosity p can be designed by determining the ratio of space holder volume (V_{sh}) to the volume of scaffold preform (V_{scp}), as expressed in Eqs. (2.1b) and (2.1c),

$$p = \frac{V_{sh}}{V_{scp}} \tag{2.1b}$$

$$p = \frac{\left(m_{sh}/\rho_{sh}\right)}{\left(m_{sh}/\rho_{sh} + m_m/\rho_m\right)} \tag{2.1c}$$

Using Eq. 2.1c, scaffold porosity can be defined from the mass m and density ρ of metal matrix powder and space-holding particles. The subscripts *sh* and *m* in Eq. 2.1b correspond to space holder and matrix powder, respectively. Porosity levels of scaffold products are however often found to deviate from designed values, mainly due to micro-pores in scaffold framework and low mixing efficiency. Detailed information on micro-pores is presented in Section 2.6. Low mixing efficiency can be attributed to powder agglomeration and adhesion of mixed powder particles to the inner surface of mixing container wall. As a consequence, the resulting mixture is less uniform, consisting of granular materials with inappropriate homogeneity.

2.3.1. Effect of mixing on porosity and pore distribution

With the space holder method, both open and closed pores can be formed in scaffolds, depending on the volume fraction of space-holding particles added to the mixture [49]. Open pores are built up from coalesced space-holding particles as a consequence of the compaction process, while closed pores are formed from isolated space-holding particles in the mixture. The number of such isolated pores increases as space holder content decreases [50]. Bhattarai et al. [27] observed open pores with interconnected channels in titanium scaffolds at a porosity level of 70%. Poor pore interconnection was achieved in other scaffolds at lower porosity levels [27].

Sharma et al. [51] revealed that the transition from closed or isolated pores to interconnected pores occurred when the total porosity of scaffolds reached 55%.

The importance of the mixing process on the pore distribution of scaffolds has recently been emphasized [6, 51, 52]. As macro-pores are formed from the space occupied by space-holding particles, a homogeneous distribution of these particles in the mixture will lead to a homogeneous macro-pore distribution in scaffolds. Furthermore, as discussed earlier, the mechanical properties of scaffolds are influenced by pore homogeneity. Li et al. [6] showed lower compressive strength of NiTi scaffolds processed with a non-sieved space holder, as compared with that prepared using a sieved space holder. In this case, the non-sieved space holder led to non-uniform and irregularly shaped macro-pores in scaffolds. As a consequence, these scaffolds suffered from severe stress concentrations and collapsed at low stress levels. In addition, it was difficult to obtain a linear correlation between the strength and porosity of scaffolds processed with the non-sieved space holder [6]. Using the finite element method (FEM), Niu et al. [53] confirmed this finding; the relationship between elastic modulus and pore distribution in scaffolds with a random pore distribution could not be predicted, in contrast to scaffolds with a pore distribution in a regular array.

2.3.2. Effect of mixing on segregation

Inhomogeneous distribution of macro-pores in scaffolds, as well as inhomogeneous distribution of space-holding particles in scaffold preforms, is often attributed to powder segregation that occurs during the mixing process. Segregation, or the separation of mixed powder components, occurs due to the differences in size and density between powder components. Two modes of powder segregation have been recognized, i.e., buoyancy and percolation [54, 55]. In the buoyancy mode, powder segregation occurs as a result of the difference in powder density; heavier particles sink to a lower level of the mixture, while lighter ones rise up. Powder segregation with the percolation mode occurs because of the differences in particle size and size distribution; smaller particles tend to fall through the interstices of larger particles and settle at the bed of a mixing container. During the mixing of metallic matrix powder with space holder, segregation in the buoyancy mode and in the percolation mode may simultaneously occur as both smaller but heavier metallic matrix particles and larger but lighter space holding particles are involved in the mixing system. A segregated powder mixture yields clusters of pores in certain regions of scaffolds, after the removal of space holder [52]. It has been reported that matrix particles should be approximately several times smaller than space-holding particles in order to improve the sinterability of metal matrix powder [9]. It has however also been reported that a uniform distribution of pores in titanium scaffolds can be achieved by mixing titanium matrix particles with an average size of 45 μm and a carbamide space holder with an average size of about 51 μm, instead of >223 μm [56].

Segregation occurring during the mixing of metal matrix powder and space holding particles can be minimized by using binders. With a binder added to the mixture, granular materials are formed, composed of space-holding particles coated with smaller metal matrix particles [9, 29, 47, 57]. Such granular materials can then be compacted to form a green body. Binders are mostly

prepared in the liquid form and have to be selected appropriately to avoid contamination due to harmful elements possibly retained in the final scaffold products. The criteria for appropriate binders have been established, based on their biocompatibility and non-toxic properties. In addition, binders must be able to produce an adequate binding strength between metal matrix powder and space-holding particles and not be reactive to both of the powders. Water, for example, may be an inappropriate binder for some water-soluble space holders, such as carbamide, ammonium hydrogen carbonate and sodium chloride, as it reacts with these powders and consequently distorts the sizes and shape of space-holding particles. Up till now, a number of binders have been used for the fabrication of metallic scaffolds, such as polyvinyl-alcohol (PVA) [12, 19, 32, 33, 37, 47, 42, 57], polyethylene-glycol (PEG) [58], polymethyl metacrylate (PMMA) [29], paraffin [22, 49, 59] and ethanol [22, 27, 28, 39, 60]. A multi-component binder consisting of high-density poly-ethylene (HDPE), paraffin wax, poly-ethylene glycol and stearic acid has also been used in the fabrication of scaffolds through powder injection moulding [61, 62]. In addition, binders have been used to increase the green density of scaffold preforms. Detailed information on the green density of scaffold preform can be found in Section 2.4. Jha et al. [37] showed a higher green density of titanium scaffold preforms (1.38 g cm^{-3}) compared to the value from theoretical calculation (1.12 g cm^{-3}), due to the addition of PVA binder. The amount and concentration of binder are of critical importance and should be chosen appropriately so as to optimize the mixing process and obtain a homogeneous mixture of metal matrix powder and space-holding particles.

Table 2.3 lists the examples of the mixing process for metal matrix powder and space-holding particles in the preparation of metallic biomedical scaffolds. Besides binders, mixer type and mixing duration are important factors that may affect the results of the mixing process.

Obviously, mixing of metal matrix powder and space holding particles is a step of critical importance in scaffold fabrication. Any failure in the mixing process, leading to an inhomogeneous distribution of space holder particles and consequently an inhomogeneous distribution of macro-pores in scaffolds, cannot be repaired at the subsequent steps of scaffold fabrication.

2.4. Compaction

2.4.1. Effect of compaction on powder particles

Compaction is performed after mixing to achieve a certain green strength that can keep the mixture of metal matrix powder and space holding particles being intact during the subsequent steps of scaffold fabrication, i.e., space holder removal and sintering. During compaction, granular materials obtained from mixing are densified, forming the green body of scaffolds or scaffold preforms. Stages involved in the powder compaction process have been well described in the literature. Before compaction, loose powder particles or granular materials have no bonding strength, except small area of inter-particle contact. A large number of voids are present in the interstices of loose powder particles or granular materials. When compaction begins, powder particles or granular materials rearrange themselves, fill the voids and increase packing coordination. As compacting pressure increases, the number of contact points and the contact

area of granular materials increase, leading to densification and the formation of a composite green body made of metal matrix powder and space holding particles.

Table 2.3. Mixing process used in the fabrication of metallic biomedical scaffolds with the space holder method

Metal matrix powder	Space holder	Mixer type	Binder	Duration of mixing	References
Titanium	Ammonium hydrogen carbonate	Manual	not defined	3-4 min	[44]
Titanium	Ammonium hydrogen carbonate	V-blender	not defined	8 h	[6]
Titanium	Carbamide	V-blender	PEG	1 h	[58]
Titanium	Carbamide	not defined	Water	1 min	[63]
Titanium, NiTi alloy	Magnesium	not defined	PVA	30 min	[12, 32, 33, 42]
Titanium	Sodium chloride	Turbula mixer	not defined	≥40 min	[36]
Ti-6Al-4V alloy	Carbamide	rolling mixer	Ethanol	1 h	[27, 60]
316L stainless steel	Carbamide	Sigma blade mixer	PMMA	30 min	[29]
Stainless steel	Carbamide	Turbula mixer	Paraffin wax	1 h	[47]
Magnesium	Carbamide	Manual	Paraffin powder and ethanol	not defined	[22]

2.4.2. Effect of compaction on green density and green strength

Powder compaction improves the sinterability of metallic powders. Effective metallurgical bonding between metallic powder particles can be achieved, only when there is no oxide film on powder particle surface [22, 64]. During compaction, surface oxide film may be disrupted, allowing direct contact of compacted powder particles. The disruption of oxide film by compaction occurs due to large shear strains, stress concentrations, scratching and jabbing that occur when metallic powder and space holding particles are pressed against one another under a given compacting pressure [22].

Scaffold preforms prepared with powder compaction are often evaluated in terms of green density ρ_g, as mathematically expressed in Eq. 2.2,

$$\rho_g = m_g / V_g \tag{2.2}$$

where m_g and V_g are the mass and volume of the scaffold preform. The green density of the scaffold preform increases with rising compacting pressure applied to the compact [27, 29, 60]. However, the presence of less-densified space-holding particles than metal matrix powder

particles results in a less significant increase in the green density of scaffold preform. Bakan [69] showed that an increase in compacting pressure from 100 to 500 MPa could considerably enhance the green density of 316L stainless steel powder. Densification of stainless steel powder mixed with 70 vol.% carbamide was however less significant than that of the powder without carbamide under the same compacting pressure. The green density of carbamide powder compacts was found to be independent of compacting pressure applied [29]. Similarly, the green densities of titanium and Ti-6Al-4V scaffolds were found to increase with increasing compacting pressure [27, 60, 65]. Moreover, it was observed that the density of scaffold preforms decreased with increasing volume fraction of carbamide space-holding particles [60]. However, the relationship between the green density of scaffold preforms and the sizes of space-holding particles was unclear [60].

The problems encountered in the compaction of granular materials in the preparation of metallic scaffolds have been recognized in the literature, such as (i) low structural integrity of scaffold preform, (ii) deformation and then breakage of space-holding particles and (iii) inhomogeneous pressure distribution in the compact.

Low green strength is not desired, as it may result in the collapse of scaffold preforms at the subsequent processing steps. Torres et al. [36] reported collapsed titanium matrix particles during the water leaching process for the removal of space-holding particles. Titanium scaffold preforms processed under compacting pressures lower than 200 MPa could not remain intact after the removal of NaCl space-holding particles through water leaching [36]. The ductility of powder material also influences the structural integrity of scaffold preforms. Ductile powder materials usually correspond to more stable green compacts than brittle ones, either before or after the removal of space-holding particles. Binder is therefore often used to improve the green compact stability of brittle powder materials [9].

Deformation and then breakage of space-holding particles in scaffold preforms occur when their critical stresses to fracture are exceeded by the compacting pressures transferred locally to these particles [35, 44]. Fracture of ammonium hydrogen carbonate particles in a mixture with titanium matrix particles under a compacting pressure of 350 MPa has been reported [44]. Under a given compacting pressure, space-holding particles serve as the bridges that separate metal matrix particles. With increasing compacting pressure, metal matrix particles tend to press space-holding particles more strongly. Once their elastic limit and critical strength are exceeded, space-holding particles are deformed and broken. Deformation of magnesium and carbamide space-holding particles during compaction has been reported [22, 35, 63]. Deformation distorted the resulting macro-pore sizes and morphology and consequently induced anisotropic properties of scaffolds [35]. Furthermore, there was a tendency that broken space-holding particles were trapped in scaffold preforms and could not be completely removed through water leaching [36]. Since compaction on the one hand enhances the strength of compacts but on the other hand it may distort space holder geometry, attempts have been made to determine an optimum compacting pressure that balances these opposite results. An optimum compacting pressure can be determined, based on experimental results and theoretical calculation.

2.4.3. Determination of optimum compacting pressure

Several experimental techniques have been used to determine an optimum compacting pressure for scaffold fabrication with the space holder method, such as (i) visual inspection, (ii) microhardness test, (iii) compression test and (iv) shrinkage evaluation. In visual inspection, direct observation of space-holding particles is made after compaction. Bakan [29] showed that compaction under pressures higher than 100 MPa could break carbamide space-holding particles that were embedded in 316L stainless steel matrix powder. Smorygo et al. [63] showed elliptical pores in titanium scaffolds as a result of distorted carbamide space-holding particles after compaction at a pressure of 500 MPa. Gligor et al. [40] established 400 MPa as an optimum compacting pressure to achieve sufficient interparticle bonding strength without deforming space-holding particles. Kotan and Bor [66] reported that the structural integrity of Ti-6Al-4V scaffold preforms could not be maintained after compaction at pressures below 300 MPa and hence a compacting pressure of 450 MPa was used in their research. With the microhardness method, optimum compacting pressures can be determined, based on the uniformity of cell wall microhardness in scaffolds. For example, compaction at a pressure of 250 MPa resulted in titanium scaffold cell walls with uniform microhardness [65]. In addition, the determination of an optimum compacting pressure, based on compressive yield strength and shrinkage, was carried out by Niu et al. [67]. With this method, the maximum compressive yield strength and minimum shrinkage of sintered titanium scaffolds were achieved when a compacting pressure of 200 MPa was applied in preparing scaffolds. Examples of the experimental ways of determining optimum compacting pressures are summarized in Table 2.4.

The determination of an optimum compacting pressure from theoretical calculation has only been reported in a limited number of papers. Jha et al. [37] and Mondal et al. [68] introduced the rule of mixtures as expressed in Eq. 2.3 to estimate an optimum pressure σ for uniaxial die compaction of titanium powder and NaCl space-holding particles:

$$\sigma = (1-x)\bar{\sigma}_m + x \cdot \bar{\sigma}_{sh} \tag{2.3}$$

where $\bar{\sigma}_m$ and $\bar{\sigma}_{sh}$ are the strengths of metal matrix and space-holding powder materials, respectively and x is the volume fraction of the space holder in the mixture. In applying this equation, the applied pressure was assumed to be shared proportionally according to the volume fractions of metal matrix powder and space-holding particles. For instance, in order to produce a titanium scaffold with 80% porosity, a mixture of titanium matrix powder and NaCl space-holding particles has to be prepared with a volume fraction of space holder being 0.8. Since the strengths of titanium powder material and NaCl are 450 MPa and 60 MPa, respectively, the optimum compacting pressure determined using Eq. 2.3 is 138 MPa [37]. In practice, compacting pressure applied to granular materials must be higher than this value in order to overcome inter-particle frictional forces and the friction between powder particles and die wall.

Table 2.4. Experimental determination of optimum compacting pressures for the fabrication of metallic scaffolds with the space holder method

Metal matrix powder	Space holder material	Compacting pressure (MPa)	Method of evaluation	References
Stainless steel	Carbamide	100	Visual inspection	[29]
Titanium	Carbamide	<500	Visual inspection	[63]
Titanium	Corn starch dextrin	400	Visual inspection	[40]
Ti-6Al-4V alloy	Carbamide	450	Visual inspection	[66]
Titanium	Carbamide	250	Microhardness distribution	[65]
Titanium	Carbamide	200	Shrinkage and compressive yield strength of the scaffold	[67]

2.4.4. Effect of compaction on porosity

An inhomogeneous pressure distribution over powder compacts may lead to (i) the variation of green density in the scaffold preform, (ii) an inhomogeneous distribution of space-holding particles as well as an inhomogeneous distribution of resultant macro-pores in the scaffold, and (iii) deteriorated mechanical properties of the scaffold [14, 52, 65, 69]. Detailed information on the variations in green density and green strength of scaffold preforms as a result of not optimum compaction is discussed later in this chapter.

Compaction influences the porosity of scaffolds. Zhao et al. [14] reported reductions in the total porosity of porous NiTi alloy scaffolds with increasing compacting pressure and increases in porosity with increasing volume fraction of NaCl space holder. Since the total porosity of the scaffold is calculated from the sum of macro-porosity and micro-porosity, this finding may indicate that micro-porosity decreases with increasing compacting pressure due to increasing packing coordination (interparticle contact area) in the scaffold [12, 65]. Similarly, Esen and Bor [12] revealed lower porosity levels in Ti-6Al-4V scaffolds from compacted and then sintered powder, in comparison with sintered loose matrix powder. This phenomenon was confirmed in other studies on the removal of space-holding particles. Torres et al. [36] reported that the lowest compacting pressure over a range of 200 – 800 MPa resulted in the highest porosity level in titanium scaffold preforms. As a consequence, the time needed for NaCl removal through water leaching became shorter [36]. Bekoz and Oktay [47] showed that water leaching of carbamide particles ran more slowly through the green body of stainless steel foams that were compacted

at a pressure greater than 200 MPa, confirming a reduced number of micro-pores in scaffold preforms. Furthermore, Li et al. [65] showed a decreased sintering index of titanium scaffolds with increasing compacting pressure. Since an increase in the sintering index means an increase in the shrinkage level of scaffolds during sintering, this finding implies a reduction in micro-porosity by compaction.

The effect of compaction on the macro-porosity of scaffolds has been reported. As discussed earlier, deformation and fracture of space-holding particles that may occur during compaction will distort the sizes and shape of macro-pores in the resulting scaffolds [35]. On the other hand, macro-porosity of scaffolds is unaffected by compaction, since the content of space holder remains unchanged [36]. However, pore interconnections increase with increasing compacting pressure because of the deformation and coalescence of space-holding particles that form interconnected pores in the end [70].

2.4.5. Common compaction techniques

Several techniques of compaction have been used in the fabrication of metallic scaffolds, i.e., (i) uniaxial die compaction [12, 44, 42], (ii) isostatic compaction [7, 15] and (iii) injection moulding [61, 71, 72]. Furthermore, the compaction of metal matrix powder and space-holding particles has been conducted either at room temperature (cold compaction) [37, 44, 65] or elevated temperatures (hot pressing) [15, 35].

As shown in Figure 2.1, uniaxial die compaction is performed with the aid of a pair of punches that move uniaxially through a die filled with powders or granular materials. Once powders are loaded in the die, the upper punch compresses the powders or granular materials. The lower punch supports the compressed powders or granular materials and delivers reaction against the upper punch. Compacted powders or granular materials are then ejected from the die, once compaction is accomplished. Limitations of uniaxial die compaction as a result of (i) inter-particle friction and (ii) the friction between powder particles and die wall have been recognized. These limitations are responsible for the variations in pressure and green density in powder compacts. It is reported that in single-action die compaction, the highest compacting pressure is experienced by the powder particles that are located in the circumference of the cylindrical compact nearby the acting punch. As a consequence, the highest green density of the compact is achieved in this location. On the other hand, the lowest compacting pressure that yields the lowest green density is found in the circumference of the lower part of the compact [69]. With increasing aspect ratio or height-to-diameter ratio of compacts, the variation in green density in powder compacts becomes more pronounced. Since green strength corresponds proportionally to green density, the powder particles located in the region with the lowest green density are prone to collapse.

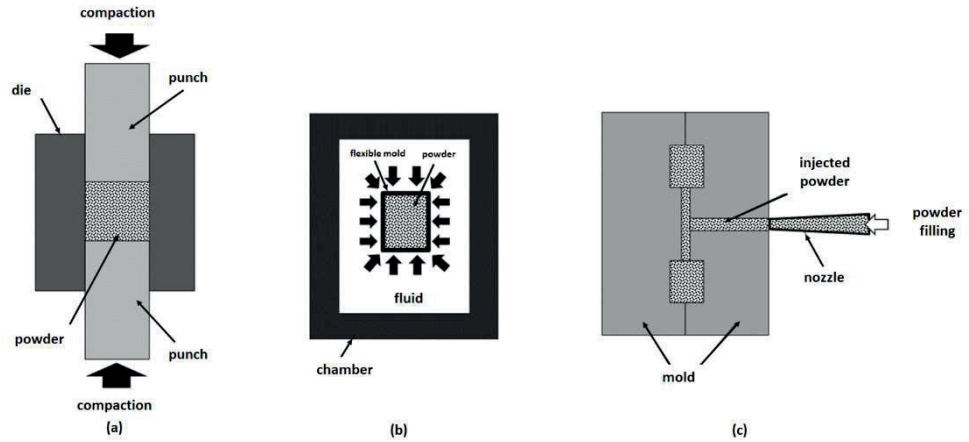

Fig. 2.1. Common techniques of compaction in the fabrication of metallic scaffolds with the space holder method: (a) uniaxial die pressing, (b) isostatic pressing and (c) injection moulding

The variations in compacting pressure and green density in uniaxially compacted powder influence the porous architecture of metallic scaffolds. Zhao et al. [14] showed that the variation in compacting pressure led to the increases in the inhomogeneity of pore distribution in NiTi scaffolds. Li et al. [65] showed the variation in cell wall or framework microhardness in titanium scaffolds, depending on the compacting pressure applied. In their study, the cell wall microhardness of titanium scaffolds processed under a compacting pressure of 150 MPa increased linearly from the center to the edge of scaffolds. This could be attributed to the friction between titanium powder particles and die wall surface, which resulted in a hardening effect on these particles in the vicinity of die wall. Such a die wall effect became less significant with increasing compacting pressure until 250 MPa, as indicated by uniform cell wall microhardness in scaffolds. However, the cell wall microhardness distribution in scaffolds became less homogeneous, as increasing packing coordination and inter-particle friction became dominant when compacting pressure was increased to 350 MPa. Attempts to minimize the variations in pressure and green density in scaffold preforms processed with uniaxial presses have been made by introducing double-action die compaction [12, 29, 33, 42]. With this method, powders or granular materials are compacted from both sides, using two moving punches from the ends of the die. As a consequence, more uniform densification is achieved over cylindrical powder compacts.

A homogeneous distribution of green density in scaffold preforms can also be achieved with isostatic powder compaction. In this method, a flexible mould containing powders or granular materials is pressurized with fluid, e.g., water or oil, to generate a powder compact (see Figure 2.1b). Isostatic compaction can also be used for preparing powder compacts with complex shapes.

Injection moulding is another compaction technique that allows mass production of scaffolds with complex shapes at low production costs [61, 62]. In principle, this technique

combines the versatile plastic injection moulding and conventional powder metallurgy technique for the fabrication of parts from powders (see Figure 2.1c). With this technique, feedstock composed of metal matrix powder and space-holding particles is injected into a mould.

2.5. Space holder removal

Macro-pores in metallic scaffolds prepared with the space holder method are formed, after the removal of space-holding particles. In other words, the removal process determines the geometry of macro-pores, as well as the structural integrity and purity of scaffolds. Complete removal of space-holding particles is desired in order to obtain desired scaffold porosity and to prevent scaffolds from contamination by residual space-holding particles [45]. It is reported that the resulting scaffold porosity is often found to deviate from the designed value due to entrapped space holder residues in scaffold preforms and the collapse of matrix particles during the removal of space-holding particles. In addition, the low structural integrity of scaffold preforms after the removal of space holder causes the distortions of macro-pore geometry and difficulties in handling scaffold preforms prior to sintering [36, 39, 44]. All these problems indicate the importance of this fabrication step for the quality of the final scaffolds. Currently, two techniques for space holder removal are commonly used, i.e., (i) heat treatment and (ii) leaching in liquid.

2.5.1. Space-holder removal through heat treatment

Space holder removal by means of heat treatment is conducted, based on the thermal decomposition and evaporation of space-holding material. Table 2.5 shows a number of common space holders and their decomposition and removal temperatures.

Table 2.5. Examples of space holders and their decomposition and removal temperatures

Space holder material	Decomposition temperature (°C)	Removal temperature (°C)	References
Ammonium hydrogen carbonate	60	150-175	[44, 45]
Carbamide	133	>600	[45]
Tapioca starch	n/a	450	[41]

As shown in Table 2.5, the removal of space holder takes place at a temperature higher than the decomposition temperature of this particular space holder material. At the removal temperature, the space holder evaporates and escape from scaffold preforms along with flushing gas that leaves the furnace [6, 66]. The removal temperature where a space holding material can be eliminated completely is often determined from thermal analysis.

Both the decomposition and removal temperatures of a particular space hold material can be determined by means of thermal analysis [44, 45]. The results obtained from thermo-gravimetric (TG) analysis revealed weight losses due to the escape of ammonium hydrogen carbonate that was used as the space holder in the study of Laptev and his co-workers [44]. In this study, the space holder material was heated at a rate of 5 K min^{-1}. The weight loss of space holder material upon heating started at a temperature of 60 – 80 °C and proceeded more intensively as a result of water evaporation when temperature increased to 100 °C and higher. The weight of ammonium hydrogen carbonate then decreased rapidly, resulting in its complete removal at a temperature of higher than 150 °C. Based on the TG results, the removal of ammonium hydrogen carbonate from scaffold preforms was recommended to be carried out at 150 °C. Similarly, the thermal analysis conducted by Dizlek et al. [45] showed that the decomposition of ammonium hydrogen carbonate (or ammonium bicarbonate) started at about 50 °C and the reaction continued until this space holder material was completely removed at 175 °C. Weight reduction of another space holder, carbamide or urea, started at a temperature above 200 °C but it could not be removed completely until 600°C. In addition, complete removal of binder material, polyvinyl alcohol solution (PVA), occurred at about 480°C.

In practice, the removal of space holder material from scaffold preforms runs more slowly during the real process than during TG analysis [44]. This can be attributed to the time required for the diffusion of removal products through tortuous channels in the interior of scaffold preforms. In order to facilitate the total elimination of space holder, dwelling at a removal temperature for several hours [44], ranging from 1 to 21 h [6, 26, 27, 52, 58, 60], is needed. Macro-pore interconnections in scaffold preforms contribute to speeding up the removal process, i.e. by providing access for the diffusion of removal products. With more interconnected macro-pores in scaffold preforms, space holder removal can be completed within a shorter time [70]. After the process, macro-pores are formed in scaffold preforms with a morphology replicating space-holding particles [6] and surrounded by matrix particles [44].

There are two problems recognized in association with space holder removal through heat treatment, i.e., (i) low green strength and (ii) contamination to porous scaffold preforms. Laptev et al. indicated that after the removal of space-holding particles, scaffold preforms were very weak, because green strength relied only on the mechanical interlocking of irregularly shaped titanium particles [44]. To prevent porous scaffold preforms from collapsing, it should be handled with care during transporting and sintering.

Contamination to scaffolds by the decomposition products of space-holding particles has been reported. Reactions between titanium matrix powder and decomposition products of space-holding particles may occur at temperatures between 300 - 600°C and result in a detrimental effect on the ductility of titanium scaffolds due to the increases in carbon (C), oxygen (O) and nitrogen (N) contents in scaffolds [45]. To prevent scaffolds from contamination, the removal of space-holding particles was conducted in vacuum or under flushing argon gas [6, 12, 27, 42, 60]. For instance, thermal removal of carbamide space-holding particles was carried out in vacuum [27, 60] to prevent the formation of unacceptable biuret in scaffold products [40]. On the other hand, heat treatment for the removal of ammonium hydrogen carbonate can be

performed in atmospheric air without inducing contamination [44, 52]. The use of biocompatible, food-grade particles such as magnesium and tapioca starch has been recognized as an alternative way to preventing contamination [12, 32, 33, 41, 42].

2.5.2. Space-holder removal through leaching

The removal of space-holding particles from scaffold preforms with liquid leaching is performed, based on the dissolution of space holder material in certain liquid. In this method, scaffold preforms are immersed in liquid to allow the dissolution and leaching of space-holding particles from compacts. This technique is often preferred, considering its low environmental impact [29], as compared with heat treatment discussed in Subsection 2.5.1. Water has been chosen as a leaching medium for many space-holders, such as carbamide [22, 29, 47, 63, 71], sodium chloride [14, 15, 36], saccharose [39] and corn starch dextrin [40]. However, other leaching media such as NaOH [22], hydrochloric acid [35], acetic acid [43] and ethanol [35] have also been used, mainly for the removal of space holders that are not dissolvable in water, such as magnesium [35] and stainless steel [43]. Table 2.6 shows a few examples of space holders and solvents for leaching.

In principle, leaching of space-holding particles from scaffold preforms is similar to the solvent debinding process for injection-moulded metallic parts [46, 73, 74]. Dissolution and diffusion are the main mechanisms that govern the leaching process. Once scaffold preforms are immersed in a solvent, space-holding particles at the surface dissolve immediately, forming openings and interconnected pores that allow the liquid to penetrate into the interior of scaffold preforms. The removal process is then governed by the simultaneous dissolution of space-holding particles in the interior of scaffold preforms and by the diffusion of fresh solvent and dissolution products through macro-pore interconnections [46].

Table 2.6. Examples of space holders and solvents used for water leaching

Space holder material	Solvent	References
Carbamide	Water, NaOH	[22, 29, 47, 63]
Sodium chloride	Water	[14, 15, 36]
Corn starch dextrin	Water	[40]
Saccharose	Water	[39]
Magnesium	HCl	[35]
Stainless steel	Acetic acid	[43]

The solubility of space holder material in a particulate solvent is considered of critical importance, determining the resulting structure of scaffold preforms after leaching. The structural integrity of scaffold preforms could be deteriorated and the matrix framework of scaffolds could be oxidized due to a too long immersion time [22, 36]. On the other hand, a short leaching time may lead to incomplete removal of space holder and consequently contamination to scaffold preforms. A highly soluble space holder material in a leaching medium is therefore a preferred choice to ensure a quick dissolution process and complete removal of space-holding particles. In addition, leaching medium should be chosen appropriately. A solvent with a low concentration of HCl, for example, could induce cracks in resulting porous titanium scaffold preforms, while an excessive HCl concentration could chemically deteriorate scaffold preforms [35].

Leaching rate of space-holding particles in a given solvent increases with increasing space holder content in scaffolds [36, 75] (see also Chapters 4 and 5). With a greater space holder content, more interconnected macro-pores may be formed, providing greater access for the diffusion of dissolved products from the interior of scaffold preforms. Leaching rate is also enhanced by micro-pores that are formed in the matrix framework of scaffolds [36] and the shape of space-holding particles. Bekoz and Oktay [47] showed that immersion in water for 150 min could remove 97% of irregularly shaped carbamide particles from scaffold preforms. However, a longer time was required to remove 93% spherical carbamide particles from scaffold preforms [47]. This finding indicates that in scaffold preforms prepared from irregular carbamide particles, the number of isolated space-holding particles was reduced, leading to faster removal of these particles [47]. Recently, the leaching process has been conducted in water and other liquid media at elevated temperatures to increase the dissolution rate of space-holding particles [36, 39, 40, 47, 71]. Torres et al. [36] reported faster dissolution of NaCl space holder in water at 50 - 60°C than at room temperature. Gulsoy and German [71] also showed that the removal rate of carbamide space holder increased with water temperature. Furthermore, Gligor et al. [40] and Jakubowicz et al. [39] performed water leaching at 80°C with magnetic stirring to speed up the leaching of corn starch and sugar particles from titanium scaffold preforms, respectively. Moreover, the use of agitated liquid medium [36, 39] and electrolytic process [43] has been reported to increase the removal rate during leaching. To facilitate the removal of steel space holder through leaching, Kwok et al. [43] utilized an electrolytic cell in a 10 vol.% acetic acid aqueous solution with titanium sheet and titanium-steel compact as the cathode and anode, respectively.

Contamination to scaffold framework in association with residual space-holding particles after the leaching process is rarely reported. Using x-ray diffraction (XRD) and energy-dispersive x-ray spectroscopy (EDS) analysis, Kim et al. showed no peaks of magnesium, which indicated no residuals from magnesium space holder in porous titanium framework after the leaching process [35]. In this study, magnesium space-holding particles were removed from titanium scaffold preforms by dipping alternatively in 2 N hydrochloric acid (HCl) and ethanol for 24 h. After leaching, porous scaffold preforms were cleaned with ethanol and dried in an oven at 60 °C. Peaks that indicate the presence of TiH_2 were however seen in porous titanium framework

due to its reactions with the HCl solvent. Nevertheless, these peaks disappeared after sintering, as a result of the transformation of TiH_2 to pure titanium through thermal decomposition.

2.6. Sintering

Sintering is performed at high temperatures where bonding between metal matrix particles in scaffold preforms takes place. Bonded matrix particles build up the framework of the porous structure of scaffolds. Through sintering, the final structure of metallic scaffolds can be achieved. Stages involved in the sintering of metallic powders are clearly described in the literature [26]. At the beginning, inter-particle bonds and necks are formed at powder particle contact points. Atoms of powder particles are thermally activated, leading to mass diffusion and neck growth at inter-particle contact points. As sintering proceeds, voids at powder particle interstices are rounded, along with densification and grain growth that occur simultaneously. Towards the end of sintering, powder densification keeps occurring but at a slower rate than the earlier stage of the densification process.

2.6.1. Effect of sintering process parameters on densification and porosity

Densification of matrix powder during sintering leads to the increases in the microhardness of scaffold cell wall [65]. As a consequence, the mechanical properties of scaffolds are enhanced. Incomplete sintering, as a result of insufficient diffusion in inter-particle contact area, leads to the formation of micro-pores [66]. Micro-pores are not desired for the mechanical properties of scaffolds, as they reduce the load-bearing cross-sectional area of cell wall and consequently deteriorate the compressive strength of scaffolds [58, 59, 66]. However, several researchers argued that the presence of micro-pores with sizes ranging from 5 to 20 μm could increase the total porosity and osteoinductvity of scaffolds [26, 42].

Micro-porosity of sintered scaffolds can be controlled by adjusting the parameters applied to the sintering process, such as (i) temperature [12, 45, 76], (ii) time [56, 65] and (iii) pressure [76]. Oh et al. [76] reported that the porosity of sintered titanium scaffolds decreased as sintering temperature increased from 900 to 1300 °C. Similarly, the porosity of Ti-6Al-4V scaffolds prepared from loose powder decreased linearly with increasing sintering temperature [12]. This finding corresponds to the increases in the number of inter-particle contacts and enhanced growth of sintering necks that eventually lead to densification and the reduction of micro-pore sizes as sintering temperature increases [35]. A too high sintering temperature is however not preferred, as it may lead to the evaporation of certain alloying elements in matrix powder and induce excessive partial melting [47]. Densification of metal matrix powders in scaffolds also occurs with increasing sintering time. To indicate enhanced densification of matrix powder with prolonged sintering time, Li et al. [65] and Sharma et al. [56] showed significant increases in microhardness at scaffold cell wall and reductions in pore size, as sintering time was extended. Scaffold porosity also decreased, due to the increases in inter-particle contact, if pressure was applied to scaffold preforms during the sintering process (pressure-assisted sintering) [76].

Macro-pores in sintered scaffolds are formed from the space occupied by removed space-holding particles. Using the space holder method, scaffold porosity increases to a certain level

controlled by the volume fraction of the space holder added to the metal matrix powder [22, 52]. Although a number of reports claimed that macro-pores present in sintered scaffolds were similar to space-holding particles [22, 40], the porous structure of the resulting scaffolds was indeed rather difficult to control. Wang et al. [26] reported the deviations of macro-pore sizes in sintered porous Ti-Nb-Zr alloy scaffolds, i.e. 300 - 800 μm, from the initial sizes of space-holding particles used in scaffold fabrication, i.e. 500 - 800 μm. Bram et al. [9] and Li et al. [6] showed smaller macro-pores in sintered scaffolds than the sizes of the space holder particles used in scaffold processing, although this reduction was insignificant [9]. In addition, macro-pore surfaces of sintered scaffolds were rough, containing micro-pores and did not reflect the surfaces of space-holding particles [19, 22]. This characteristic could be observed in scaffolds prepared with small matrix powder particles [40]. However, Bram et al. [9] indicated that the use of small matrix powder particles could lead to fully densified framework without micro-pores.

As discussed earlier, the presence of micro-pores leads to the deviations of the porosity of sintered scaffolds from the designed value. With the space holder method, micro-pores can hardly be avoided. The number of micro-pores can however be reduced by increasing space holder content. With a greater space holder content, the thickness of scaffold framework or cell wall decreases [32, 37], limiting the chance of micro-pore formation in the framework. Accordingly, the difference between the resulting scaffold porosity level and the content of space holder added to the mixture decreases [36]. Aydogmus et al. [32] showed the decreases in micro-porosity down to 1% with an addition of 80 vol.% magnesium space-holding particles. On the other hand, Smorygo et al. [63] and Amigo et al. [52] argued that both total porosity and interconnected porosity were lower than the space holder content mixed with matrix powder, due to the shrinkage of metallic framework during sintering.

The shrinkage of powder compact during sintering occurs as a result of inter-particle neck growth and mass diffusion that lead to the elimination of micro-pores and densification [32, 44]. Laptev et al. [44] noticed axial and radial shrinkages of cylindrical titanium scaffolds prepared with 0 - 70 vol.% space holder contents and with 100 – 450 MPa compaction pressures by 9 - 14% and 10 - 15%, respectively, after sintering at temperatures of 1200 – 1300 °C for 1 – 3 h. Similarly, Aydogmus and Bor [32] revealed the shrinkages of NiTi scaffolds processed with 80 vol.% magnesium space holder by <2.5% in height and <3.5% in diameter after sintering at 1100 °C for 1 h. Shrinkage has to be controlled; otherwise it may ruin the porous structure of scaffolds. In addition to the control of sintering temperature and time [44], the shrinkage of scaffolds can be controlled through compaction prior to sintering [44] and the addition of a specific amount of space holder [14]. A higher green density produced by compaction reduces the shrinkage of sintered scaffolds. Since space-holding particles reduce green density, shrinkage increases with increasing space holder content [44]. Space-holding particles serve as the bridges between matrix particles, which obstruct the effective pressure transmission to matrix particles during compaction. Esen and Bor [42] showed that a critical volume fraction of magnesium space holder that could be mixed with matrix particles was limited to 55 - 60%, above which compacts shrank significantly during sintering. With a lower magnesium content, shrinkage was insignificant, but porosity was higher than the volume fraction of magnesium added, due to the

formation of micro-pores in scaffold framework [42]. However, shrinkage rate decreased in high-porosity scaffolds, as a result of thinner cell wall subjected to densification [65]. It has also been reported that cell reorientation occurs due to shrinkage during sintering. Jha et al. [37] showed the formation of nearly spherical cells having an aspect ratio of 0.98 in sintered titanium scaffolds processed with cubical NaCl space-holding particles.

Sintering may be performed in a single cycle together with heat treatment for the thermal removal of space-holding particles [10, 19, 41, 77]. Mansourighasri et al. [41] performed heat treatment at 450 °C for 2 h to remove tapioca starch from titanium scaffold preforms, followed by sintering at a temperature of 1200 °C for 3 h. Additional thermal processing may also be conducted to ensure complete removal of residues from scaffold preforms. A heat treatment at 850 °C for 1 h was conducted by Bhattarai et al. [27] to allow surface oxides, water molecules and contaminants to volatilize off from scaffold preforms. Sintering was then performed by raising furnace temperature to 1200 °C and holding scaffold preforms at this temperature for 2 h. Sintering may also be performed in a separate furnace with which space holder removal is performed. Amigo et al. [52] conducted heat treatment at a temperature of 80 °C for 21 h in atmospheric air to remove ammonium hydrogen carbonate space holder before sintering. Sintering was then performed in a vacuum furnace at 1300 °C for 2 h.

2.6.2. Contamination induced during sintering

Contamination due to sintering is critical, as it potentially deteriorates the properties of metallic scaffolds. Contamination of titanium scaffolds during sintering can be induced by (i) residual space holder in the scaffold preform, (ii) contaminants in the sintering furnace and (iii) exposure to atmospheric air during sintering. Reactions between residual space-holding particles and the matrix framework of scaffolds during sintering, lead to increased unacceptable impurities in scaffolds [39, 40, 68]. Impurities in sintered scaffolds also increase due to residual contaminants in the sintering furnace that may react with scaffold framework during sintering. Bhattarai et al. [27] noticed no significant increases in C, N and O contents after the removal of carbamide space-holding particles from Ti-6Al-4V scaffolds. However, the concentrations of C, N and O increased slightly after sintering. As the sintering process was carried out in vacuum (2×10^{-3} torr), this might indicate that the increased concentrations of C, N and O impurities in sintered scaffolds could be attributed to the contaminants that were present in the furnace used [27]. A number of studies on titanium scaffold contamination due to sintering have been conducted. Despite its excellent mechanical properties and biocompatibility, titanium has extreme affinity to oxygen and nitrogen when processed at high temperatures. Oxygen and nitrogen can dissolve rapidly in titanium at temperatures above 400 °C [3]. Kim et al. [35] showed an increased oxygen content from 0.297 to 1.118 wt.% in titanium scaffolds after sintering. Sintered titanium exhibits brittle behaviour, once the oxygen content exceeds a critical level for retaining ductility. Therefore, attempts have been made to prevent titanium scaffolds from contamination during sintering by, for instance, introducing vacuum environment [27, 41] and flushing argon gas [12, 42] into the sintering furnace.

The importance of controlled sintering atmosphere was also noticed in a study conducted by Krug and Zachmann [78], which indicated that the injection moulded 316L stainless steel powders sintered under nitrogen (N_2) atmosphere possessed higher tensile strength but lower ductility than those sintered under argon (Ar) and hydrogen (H_2) atmospheres. Exposure to atmospheric air during the sintering process may lead to contamination to scaffolds and deteriorate their mechanical properties. With porosities larger than 79% and elastic moduli in a range of bone tissue (0.1 – 30 GPa), titanium scaffolds processed by means of single-step sintering in air possessed a lower compressive strength of (6 – 9 MPa) [79] than the scaffolds with a porosity of about 70% sintered in vacuum (50 – 100 MPa) [35] and with flushing high-purity argon gas (15 MPa) [42]. As a consequence, the load bearing capability of titanium scaffolds sintered in air would be quite limited. The importance of furnace construction on the sintering results has also been reported. During sintering, furnace may interact with the sintering atmosphere and consequently influence the sintering results. Krug and Zachmann [78] revealed that by using a molybdenum furnace the carbon content in sintered 316L stainless steel powder could be reduced more than by using a graphite furnace, when a hydrogen atmosphere was used during sintering. In addition, a retort is devised in the furnace design to let it act as a separating chamber to prevent the sintered compacts from contamination during heat treatment or sintering [80].

2.6.3. Determination of appropriate sintering temperatures

Considering the importance of sintering parameters, especially sintering temperature, for the final form and performance of metallic scaffolds, attempts have been made by several researchers to determine appropriate sintering temperatures for scaffold fabrication. Several techniques have been used for the evaluation of optimum sintering temperatures for scaffold fabrication with the space holder method, i.e., (i) compression testing, (ii) observation of inter-particle neck growth and (iii) microstructural analysis. In compression testing, the peak compressive stresses of scaffolds sintered at various temperatures may be used as the basis for evaluation. Hao and co-workers [22] showed that an optimum sintering temperature for magnesium foams was found within a range of 610 to 630 ºC. Magnesium foams with relatively high peak compressive stresses could be made, if sintering took place in this temperature range. However, magnesium foams exhibited low compressive strength due to poor inter-particle bonding, resulting from sintering at temperatures below this critical value. On the other hand, sintering at higher temperatures could distort resulting pore sizes and pore shape due to partial melting. Esen and Bor [12] introduced a technique by observing the neck growth in sintered scaffolds to determine an optimum sintering temperature. In this study, the average neck size or bond diameter formed during sintering (X), relative to the average diameter of neighbouring particles (D) was determined and the results were reproducible. The determination of an optimum sintering temperature based on microstructural observation was introduced by Seyedraoufi and Mirdamadi [23]. In their study, Mg-Zn scaffolds were sintered at temperatures of 500, 550, 565 and 580 °C. Optical microscopic analysis was then performed to examine grain sizes. With this method, it was found that an optimum sintering temperature for Mg-Zn

scaffolds was 550 °C. Higher sintering temperatures resulted in grain growth, which would lead to the degradation of scaffolds in mechanical properties [23].

2.7. Concluding remarks

The space holder method has become a promising one for the fabrication of metallic biomedical scaffolds, owing to its ability to produce a wide range of porosity levels and controllable pore geometry in scaffolds. In principle, four processing steps are involved in this method, i.e., (i) mixing of metal matrix powder and space-holding particles, (ii) compaction of granular materials resulting from the mixing process, (iii) removal of space-holding particles and (iv) sintering of scaffold preform. Prior to mixing, powders must be appropriately selected and prepared. Geometrical and dimensional characteristics, mechanical properties and biocompatibility of powders used in scaffold fabrication are among the critically important parameters of powdered materials that must be considered in scaffold fabrication. During the mixing process, the homogeneity of space-holding particles in the mixture containing metal matrix powder determines the pore distribution and mechanical properties of the resultant scaffolds. Compaction is conducted to achieve an appropriate green strength and improve the sinterability of scaffold preforms. At this step, compacting pressure must be optimized in order to reach a balance between the green strength achieved in scaffold preform and the shape of compacted space-holding particles. Several compaction techniques have been used for scaffold fabrication with the space holder method, such as uniaxial die pressing, isostatic pressing and injection moulding. Macro-pores in scaffolds are formed after the removal of space-holding particles, either through heat treatment or leaching in liquid. As the space holder removal process determines the porous structure, green strength and purity of scaffolds, it must be handled carefully. Sintering determines the final form as well as the final porous structure and mechanical properties of scaffolds. With the space holder method, two types of pore are formed in scaffolds, i.e., (i) macro-pores that are formed from the space occupied by space-holding particles and (ii) micro-pores that result from the voids at the interstices of matrix powder particles in scaffold framework. Sintering temperature and time are among the important technical parameters. Contamination and uncontrolled shrinkage remain the challenges in the sintering process for the fabrication of metallic biomedical scaffolds.

References

[1] G. Ryan, A. Pandit and D. P. Apatsidis, "Fabrication methods of porous metals for use in orthopaedic applications," *Biomaterials,* vol. 27, pp. 2651-2670, 2006.

[2] R. Singh, P. D. Lee, R. J. Dashwood and T. C. Lindley, "Titanium foams for biomedical applications: A review," *Materials Technology,* vol. 25, pp. 127-136, 2010.

[3] D. Dunand, "Processing of titanium foams," *Advanced Engineering Materials,* vol. 6, pp. 369-376, 2004.

[4] A. Bansiddhi, T. D. Sargeant, S. I. Stupp and D. C. Dunand, "Porous NiTi for bone implants: A review," *Acta Biomaterialia,* vol. 4, pp. 773-782, 2008.

[5] M. Guden, E. Celik, A. Hizal, M. Altindis and S. Cetiner, "Effects of compaction pressure and particle shape on the porosity and compression mechanical properties of sintered Ti6Al4V powder compacts for hard tissue implantation," *Journal of Biomedical Materials Research B: Applied Biomaterials,* vol. 85, pp. 547-555, 2008.

[6] D. S. Li, Y. P. Zhang, X. Ma and X. P. Zhang, "Space-holder engineered porous NiTi shape memory alloys with improved pore characteristics and mechanical properties," *Journal of Alloys and Compounds,* vol. 474, pp. L1-L5, 2009.

[7] N. Tuncer, G. Arslan, E. Maire and L. Salvo, "Investigation of spacer size effect on architecture and mechanical properties of porous titanium," *Materials Science and Engineering A,* vol. 530, pp. 633-642, 2011.

[8] X. B. Chen, Y. C. Li, P. D. Hodgson and C. Wen, "The importance of particle size in porous titanium and nonporous counterparts for surface energy and its impact on apatite formation," *Acta Biomaterialia,* vol. 5, pp. 2290-2302, 2009.

[9] M. Bram, C. Stiller, H. P. Buchkremer, D. Stover and H. Baur, "High-porosity titanium, stainless steel and superalloy parts," *Advanced Engineering Materials,* vol. 2, pp. 196-199, 2000.

[10] C. E. Wen, M. Mabuchi, Y. Yamada, K. Shimojima, Y. Chino and T. Asahina, "Processing of biocompatible porous Ti and Mg," *Scripta Materialia,* vol. 45, pp. 1147-1153, 2001.

[11] C. E. Wen, Y. Yamada, K. Shimojima, Y. Chino, T. Asahina and M. Mabuchi, "Processing and mechanical properties of autogenous titanium implant materials," *Journal of Materials Science: Materials in Medicine,* vol. 13, pp. 397-401, 2002.

[12] Z. Esen and S. Bor, "Characterization of Ti–6Al–4V alloy foams synthesized by space holder technique," *Materials Science and Engineering A,* vol. 528, pp. 3200-3209, 2011.

[13] L. Reig, V. Amigó, D. Busquets and J. A. Calero, "Stiffness variation of porous titanium developed using space holder method," *Powder Metallurgy,* vol. 54, pp. 389-392, 2011.

[14] X. Zhao, H. Sun, L. Lan, J. Huang, H. Zhang and Y. Wang, "Pore structures of high-porosity NiTi alloys made from elemental powders with NaCl temporary space-holders," *Materials Letters,* vol. 63, pp. 2402-2404, 2009.

[15] A. Bansiddhi and D. C. Dunand, "Shape-memory NiTi foams produced by replication of NaCl space-holders," *Acta Biomaterialia,* vol. 4, pp. 1996-2007, 2008.

[16] A. Ghasemi, S. R. Hosseini and S. K. Sadrnezhaad, "Pore control in SMA NiTi scaffolds via space holder usage," *Materials Science and Engineering C,* vol. 32, pp. 1266-1270, 2012.

[17] Y. Li, J. Xiong, C. S. Wong, P. Hodgson and C. Wen, "Ti6Ta4Sn alloy and subsequent scaffolding for bone tissue engineering," *Tissue Engineering Part A,* vol. 15, pp. 3151-3159, 2009.

[18] A. Ibrahim, F. Zhang, E. Otterstein and E. Burkel, "Processing of porous Ti and Ti5Mn foams by spark plasma sintering," *Materials and Design,* vol. 32, pp. 146-153, 2011.

[19] H. -C. Hsu, S. -C. Wu, S. -K. Hsu, M. -S. Tsai, T. -Y. Chang and W. -F. Ho, "Processing and mechanical properties of porous Ti-7.5Mo alloy," *Materials and Design,* vol. 47, pp. 21-26, 2013.

[20] H. -S. Hsu, S. -C. Wu, T. -Y. Hsu, T. -Y. Chang and W. -F. Ho, "Effect of ball milling on properties of porous Ti–7.5Mo alloy for biomedical applications," *Journal of Alloys and Compounds,* vol. 582 , pp. 793-801, 2014.

[21] Z. Gao, Q. Li, F. He, Y. Huang and Y. Wan, "Mechanical modulation and bioactive surface modification of porous Ti-10Mo alloy for bone implants," *Materials and Design,* vol. 42, pp. 13-20, 2012.

[22] G. Hao, F. Han and W. Li, "Processing and mechanical properties of magnesium foams," *Journal of Porous Materials,* vol. 16, pp. 251-256, 2008.

[23] Z. Seyedraoufi and S. Mirdamadi, "Synthesis, microstructure and mechanical properties of porous Mg-Zn scaffolds," *Journal of the Mechanical Behavior of Biomedical Materials,* vol. 21, pp. 1-8, 2013.

[24] F. Froes, S. Mashl, V. Moxson, J. Hebeisen and V. Duz, "The Technologies of Titanium Powder Metallurgy," *JOM,* vol. 56, pp. 46-48, 2004.

[25] M. Niinomi, "Recent research and development in titanium alloys for biomedical applications and healthcare goods," *Science and Technology of Advanced Materials,* vol. 4, pp. 445-454, 2003.

[26] X. Wang, Y. Li, J. Xiong, P. D. Hodgson and C. Wen, "Porous TiNbZr alloy scaffolds for biomedical applications," *Acta biomaterialia,* vol. 5, pp. 3616-3624, 2009.

[27] S. R. Bhattarai, K. A. Khalil, M. Dewidar, P. H. Hwang, H. K. Yi and H. Y. Kim, "Novel production method and in-vitro cell compatibility of porous Ti-6Al-4V alloy disk for hard tissue engineering," *Journal of Biomedical Materials Research A,* vol. 86, pp. 289-299, 2008.

[28] A. Nouri, P. Hodgson and C. Wen, "Effect of ball-milling time on the structural characteristics of biomedical porous Ti–Sn–Nb alloy," *Materials Science and Engineering C,* vol. 31, pp. 921-928, 2011.

[29] H. Bakan, "A novel water leaching and sintering process for manufacturing highly porous stainless steel," *Scripta Materialia,* vol. 55, pp. 203-206, 2006.

[30] T. Aydogmus, E. Bor and S. Bor, "Phase transformation behavior of porous TiNi alloys produced by powder metallurgy using magnesium as a space holder," *Metallurgical and Materials Transactions A,* vol. 42, pp. 2547-2555, 2011.

[31] T. Aydogmus and S. Bor, "Superelasticity and compression behavior of porous TiNi alloys produced using Mg spacers, Journal of Mechanical Behavior of Biomedical Materials," *Journal of Mechanical Behavior of Biomedical Materials,* vol. 15, pp. 59-69, 2012.

[32] T. Aydogmus and S. Bor, "Processing of porous TiNi alloys using magnesium as space holder," *Journal of Alloys and Compounds,* vol. 478, pp. 705-710, 2009.

[33] G. Ipek Nakas, A. Dericioglu and S. Bor, "Fatigue behavior of TiNi foams processed by the magnesium space holder technique," *Journal of Mechanical Behavior of Biomedical Materials,* vol. 4, pp. 2017-2023, 2011.

[34] G. Ipek Nakas, A. Dericioglu and S. Bor, "Monotonic and cyclic compressive behavior of superelastic TiNi foams processed by sintering using magnesium space holder technique," *Materials Science and Engineering A,* vol. 582, pp. 140-146, 2013.

[35] S. W. Kim, H. D. Jung, M. H. Kang, H. E. Kim, Y. H. Koh and Y. Estrin, "Fabrication of porous titanium scaffold with controlled porous structure and net-shape using magnesium as spacer," *Materials Science and Engineering C,* vol. 33, pp. 2808-2815, 2013.

[36] Y. Torres, J. J. Pavón and J. A. Rodríguez, "Processing and characterization of porous titanium for implants by using NaCl as space holder," *Journal of Materials Processing Technology,* vol. 212, pp. 1061-1069, 2012.

[37] N. Jha, D. Mondal, J. Dutta Majumdar, A. Badkul, A. Jha and A. Khare, "Highly porous open cell Ti-foam using NaCl as temporary space holder through powder metallurgy route," *Materials and Design,* vol. 47, pp. 810-819, 2013.

[38] B. Ye and D. Dunand, "Titanium foams produced by solid-state replication of NaCl powders," *Materials Science and Engineering A,* vol. 528, pp. 691-697, 2010.

[39] J. Jakubowicz, G. Adamek and M. Dewidar, "Titanium foam made with saccharose as a space holder," *Journal of Porous Materials,* vol. 20, pp. 1137-1141, 2013.

[40] I. Gligor, O. Soritau, M. Todea, C. Berce, A. Vulpoi, T. Marcu, V. Cernea, S. Simon and C. Popa, "Porous c.p. titanium using dextrin as space holder for endosseous implants," *Particulate Science and Technology,* vol. 31, pp. 357-365, 2013.

[41] A. Mansourighasri, N. Muhamad and A. B. Sulong, "Processing titanium foams using tapioca starch as a space holder," *Journal of Materials Processing Technology,* vol. 212, pp. 83-89, 2012.

[42] Z. Esen and S. Bor, "Processing of titanium foams using magnesium spacer particles," *Scripta Materialia,* vol. 56, pp. 341-344, 2007.

[43] P. J. Kwok, S. M. Oppenheimer and D. C. Dunand, "Porous titanium by electro-chemical dissolution of steel space-holders," *Advanced Engineering Materials,* vol. 10, pp. 820-825, 2008.

[44] A. Laptev, M. Bram, H. P. Buchkremer and D. Stöver, "Study of production route for titanium parts combining very high porosity and complex shape," *Powder Metallurgy,* vol. 47, pp. 85-92, 2004.

[45] M. Dizlek, M. Guden, U. Turkan and A. Tasdemirci, "Processing and compression testing of Ti6Al4V foams for biomedical applications," *Journal of Materials Science,* vol. 44, pp. 1512-1519, 2008.

[46] B. Arifvianto, M. Leeflang and J. Zhou, "A new technique for the characterization of the water leaching behavior of space holding particles in the preparation of biomedical titanium scaffolds," *Materials Letters,* vol. 120, pp. 204-207, 2014.

[47] N. Bekoz and E. Oktay, "Effects of carbamide shape and content on processing and properties of steel foams," *Journal of Materials Processing Technology,* vol. 212, pp. 2109-2116, 2012.

[48] J. Zhang, L. Wu, D. Jing and J. Ding, "A comparative study of porous scaffolds with cubic and spherical macropores," *Polymer,* vol. 46, pp. 4979-4985, 2005.

[49] B. Dabrowski, W. Swieszkowski, D. Godlinski and K. J. Kurzydlowski, "Highly porous titanium scaffolds for orthopaedic applications," *Journal of Biomedical Materials Research B: Applied Biomaterials,* vol. 95, pp. 53-61, 2010.

[50] C. Wen, Y. Yamada, K. Shimojima, Y. Chino, H. Hosokawa and M. Mabuchi, "Compressibility of porous magnesium foam: dependency on porosity and pore size," *Materials Letters,* vol. 58, pp. 357-360, 2004.

[51] M. Sharma, G. Gupta, O. Modi and B. Prasad, "PM processed titanium foam: Influence of morphology and content of space holder on microstructure and mechanical properties," *Powder Metallurgy,* vol. 56, pp. 55-60, 2013.

[52] V. Amigó, L. Reig, D. Busquets, J. Ortiz and J. Calero, "Analysis of bending strength of porous titanium processed by space holder method," *Powder Metallurgy,* vol. 54, pp. 67-70, 2011.

[53] W. Niu, S. Gill, H. Dong and C. Bai, "A two-scale model for predicting elastic properties of porous titanium formed with space-holders," *Computational Materials Science,* vol. 50, pp. 172-178, 2010.

[54] N. Jain, J. Ottino and R. Lueptow, "Regimes of segregation and mixing in combined size and density granular systems: An experimental study," *Granular Matter,* vol. 7, pp. 69-81, 2005.

[55] P. Tang and V. Puri, "Methods for minimizing segregation: A review," *Particulate Science and Technology,* vol. 22, pp. 321-337, 2004.

[56] M. Sharma, G. Gupta, O. Modi, B. Prasad and A. Gupta, "Titanium foam through powder metallurgy route using acicular urea particles as space holder," *Materials Letters,* vol. 65, pp. 3199-3201, 2011.

[57] T. Shimizu, K. Matsuzaki, H. Nagai and N. Kanetake, "Production of high porosity metal foams using EPS beads as space holders," *Materials Science and Engineering A,* vol. 558, pp. 343-348, 2012.

[58] W. Niu, C. Bai, G. Qiu and Q. Wang, "Processing and properties of porous titanium using space holder technique," *Materials Science and Engineering A,* vol. 506, pp. 148-151, 2009.

[59] I. Mutlu and E. Oktay, "Processing and properties of highly porous 17-4 PH stainless steel," *Powder Metallurgy and Metal Ceramics,* vol. 50, pp. 73-82, 2011.

[60] M. Dewidar, H. Mohamed and J.-K. Lim, "A new approach for manufacturing a high porosity Ti-6Al-4V scaffolds for biomedical applications," *Journal of Materials Science and Technology,* vol. 24, pp. 931-935, 2008.

[61] L. Chen, T. Li, Y. Li, H. He and Y. Hu, "Porous titanium implants fabricated by metal injection molding," *Transactions of Nonferrous Metals Society of China,* vol. 19, pp. 1174-1179, 2009.

[62] G. Engin, B. Aydemir and H. Gülsoy, "Injection molding of micro-porous titanium alloy with space holder technique," *Rare Metals,* vol. 30, pp. 565-571, 2011.

[63] O. Smorygo, A. Marukovich, V. Mikutski, A. A. Gokhale, G. J. Reddy and J. V. Kumar, "High-porosity titanium foams by powder coated space holder compaction method," *Materials Letters,* vol. 83, pp. 17-19, 2012.

[64] J. Banhart, "Manufacture, characterisation and application of cellular metals and metal foams," *Progress in Materials Science,* vol. 46, p. 559–632, 2001.

[65] C. F. Li, Z. G. Zhu and T. Liu, "Microhardness of pore walls in porous titanium prepared with novel powder metallurgy," *Powder Metallurgy,* vol. 48, pp. 237-240, 2005.

[66] G. Kotan and A. S. Bor, "Production and characterization of high porosity Ti-6Al-4V foam by space holder technique powder metallurgy," *Turkish Journal of Engineering and Environmental Science,* vol. 31, pp. 149-156, 2007.

[67] W. Niu, C. Bai, G. Qiu, Q. Wang, L. Wen, D. Chen and L. Dong, "Preparation and characterization of porous titanium using space-holder technique," *Rare Metals,* vol. 28, pp. 338-342, 2009.

[68] D. Mondal, J. Datta Majumder, N. Jha, A. Badkul, S. Das, A. Patel and G. Gupta, "Titanium-cenosphere syntactic foam made through powder metallurgy route," *Materials and Design,* vol. 34, pp. 82-89, 2012.

[69] N. Ozkan and B. Briscoe, "Characterization of die-pressed green compacts," *Journal of European Ceramics Society,* vol. 17, pp. 697-711, 1997.

[70] Y. Torres, J. Rodríguez, S. Arias, M. Echeverry, S. Robledo, V. Amigo and J. Pavón, "Processing, characterization and biological testing of porous titanium obtained by space-holder technique," *Journal of Materials Science,* vol. 47, pp. 6565-6576, 2012.

[71] H. Gülsoy and R. German, "Sintered foams from precipitation hardened stainless steel powder," *Powder Metallurgy,* vol. 51, pp. 350-353, 2013.

[72] A. Manonukul, N. Muenya, F. Léaux and S. Amaranan, "Effects of replacing metal powder with powder space holder on metal foam produced by metal injection moulding," *Journal of Materials Processing Technology,* vol. 210, pp. 529-535, 2010.

[73] K. Hwang and Y. Hsieh, "Comparative study of pore structure evolution during solvent and thermal debinding of powder injection molded parts," *Metallurgical and Materials Transactions A,* vol. 27, pp. 245-253, 1996.

[74] W. Yang, K. Yang, M. Wang and M. Hon, "Solvent debinding mechanism for alumina injection molded compacts with water-soluble binders," *Ceramics International,* vol. 29, pp. 745-756, 2003.

[75] B. Arifvianto, M. Leeflang, J. Duszczyk and J. Zhou, "Characterisation of space holder removal through water leaching for preparation of biomedical titanium scaffolds," *Powder Metallurgy,* vol. 57, pp. 9-12, 2014.

[76] I. -H. Oh, N. Nomura, N. Masahashi and S. Hanada, "Microstructures and mechanical properties of porous titanium compacts prepared by powder sintering," *Materials Transactions,* vol. 43, pp. 443-446, 2002.

[77] L. M. de Vasconcellos, F. N. Oliveira, O. de Leite, L. G. de Vasconcellos, R. F. do Prado, C. J. Ramos, M. L. Graca, C. A. Cairo and Y. R. Carvalho, "Novel production method of porous surface Ti samples for biomedical application," *Journal of Materials Science: Materials in Medicine,* vol. 23, pp. 357-364, 2012.

[78] S. Krug and S. Zachmann, "Influence of sintering conditions and furnace technology on chemical and mechanical properties of injection moulded 316L," *Powder Injection Moulding International,* vol. 3, pp. 66-70, 2009.

[79] H.-C. Hsu, S.-K. Hsu, S.-C. Wu, P.-H. Wang and W.-F. Ho, "Design and characterization of highly porous titanium foams with bioactive surface sintering in air," *Journal of Alloys and Compounds,* vol. 575, p. 326–332, 2013.

[80] S. Robinson and M. Paul, "Debinding and sintering solutions for metals and ceramics," *Metal Powder Report,* vol. 56, pp. 24-34, 2001.

Chapter 3

The compression behaviours of titanium/carbamide powder mixtures in the preparation of biomedical titanium scaffolds with the space holder method

This chapter is adapted from:
The compression behaviours of titanium/carbamide powder mixtures in the preparation of biomedical titanium scaffolds with the space holder method
B. Arifvianto, M.A. Leeflang and J. Zhou, Powder Technology, Vol. 284, 2015, pp. 112-121.

3.1. Introduction

As discussed in Chapter 2, compaction of titanium and space holder mixture plays an important role in determining the porous architecture of titanium scaffold. At this step, the mixture of titanium matrix powder and space holding particles is compacted under a certain compressive pressure to produce a green body of the scaffold. A relatively high compacting pressure is usually applied to produce a scaffold preform in order to obtain a sufficient green strength that keeps the scaffold preform intact at the subsequent processing steps, e.g., during the removal of space-holding particles [1]. However, the geometry of space-holding particles may markedly change under a compacting pressure that exceeds their yield strength or even ultimate strength. As a consequence, the pore shape and sizes of the scaffold will deviate significantly from the initial shape and sizes of space-holding particles [2]. Therefore, a critical compacting pressure that results in geometrical deformation of carbamide space holder needs to be determined to avoid such an undesirable situation.

Recently, a number of ways to determine an appropriate compacting pressure in scaffold fabrication with the space holder method have been reported, for example, by means of visual inspection [3] or evaluation of the mechanical properties [3] and shrinkage percentage [4] of the scaffold. However, there is no information in the open literature on the methods based on powder behaviours under compressive stresses for the determination of appropriate compacting pressures in the preparation of titanium scaffolds with the space holder method.

In this chapter, compression behaviours of the mixtures of titanium matrix powder and carbamide space-holding particles are discussed. Critical compacting pressures that lead to severe deformation of carbamide powder in the mixtures are also determined based on the yield strengths of the monolithic titanium and carbamide powders. To serve this purpose, several compression parameters in the compaction of titanium/carbamide powders are determined with the aid of an instrumented uniaxial powder press, as described in Section 3.2. The specific net energy of compaction, at-pressure relative density and yield pressure of titanium powder, carbamide particles and their mixtures are presented in Section 3.3 and then analyzed in Section 3.4 to determine their behaviours under the compressive stresses applied. In addition, the critical compacting pressures that may result in geometrical changes of carbamide space holding particles in titanium scaffold preform are also determined in this section. Finally, conclusions of this research are given in Section 3.5.

3.2. Materials and methods

3.2.1. Powder mixture preparation

A gas-atomized grade 1 titanium powder (TLS Technik GmbH & Co., Germany) with a spherical particle shape (Figs. 3.1a) and a cubical carbamide powder (Merck, Germany) (Fig. 3.1b) were chosen as the matrix and space holder materials, respectively. Particle sizes of both powders were analyzed using a Mastersizer X (Malvern, UK). With this technique, the volume mean diameters D_m of titanium and carbamide powder particles were determined to be 72.46 ± 1.81 μm and 417.80 ± 5.64 μm, respectively, and their median diameters D_{50} were 70.32 ± 1.61 μm and 399.23 ± 4.85 μm, respectively.

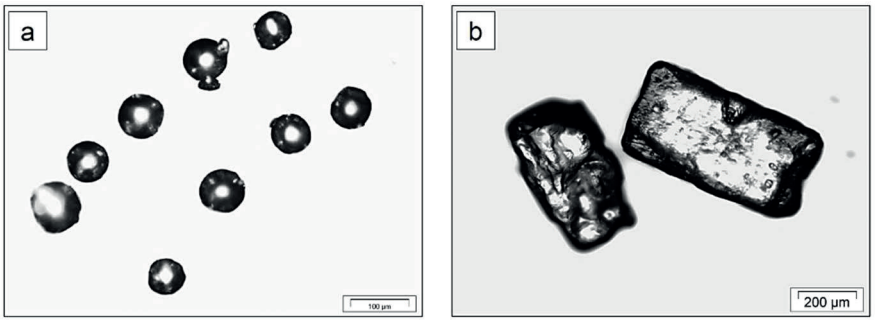

Fig. 3.1. (a) Titanium powder and (b) carbamide powder (Reprinted with permission from Elsevier)

In order to prevent titanium/carbamide powder mixture from segregating, a binder solution prepared from polyvinyl-alcohol (PVA) powder (Alfa Aesar GmbH & Co KG, Germany) dissolved in tap water was added to the titanium powder and mixed for 1 h, prior to mixing with the carbamide powder. The amount of the PVA binder solution added was 3% of the volume of titanium powder in the mixing container. A 20 g wet titanium powder was then put together with 2.52, 5.88, and 13.72 g dry carbamide powder for 3 h mixing in a cylindrical roller mixer

(CAT, Germany) in order to obtain titanium/carbamide powder mixtures with carbamide volume fractions x of 30, 50 and 70%, respectively.

3.2.2. Powder compaction

Titanium/carbamide powder mixtures were cold-compacted in a die with a diameter of 13 mm. Prior to powder filling, a zinc stearate powder was applied to the die inner surface for lubrication. A powder mixture of 1.3 g was poured into the die cavity, tapped manually and pressed at room temperature by using an instrumented Instron 4505 compression tester (Instron, USA). With this tester, precise loads exerted by the upper punch during a powder compression cycle could be registered. The punch speed applied during powder compression and decompression was set at 2 mm/min. Prior to compaction, the powder mixture was pre-compressed at a load of 50 N to level off the powder bed surface. The load-displacement plots obtained from the powder compression cycles were first corrected for the deformation of the machine and punches by using the plot obtained from a dry run without powder mixture and then used for the analysis of powder compression behaviours. The compaction of each of the powder mixtures was conducted in triplicate.

3.2.3. Analysis

The compression behaviours of titanium powder, carbamide powder and their mixtures were analyzed on the basis of the load-displacement plots obtained from the powder compression cycles. A schematic load-displacement plot from Fig. 1 of the Heckel's work [5] was adapted to this study. In this plot, the correlation between the punch position in the die cavity and the load exerted by the upper punch during a single powder compression cycle is illustrated.

a. Specific net energy of powder compression

Specific net energy of powder compression ($E_{sp,net}$) was used to indicate the amount of the energy required to induce plastic deformation of powders during the compression process. The $E_{sp,net}$ could be determined by subtracting the specific energy released due to the punch retraction during the decompression stage ($E_{sp,ep}$) from the specific energy required to compress a powder ($E_{sp,cp}$), as expressed in Eq. (3.1).

$$E_{sp,net} = E_{sp,cp} - E_{sp,ep} \tag{3.1}$$

In this research, both $E_{sp,cp}$ and $E_{sp,ep}$ were first calculated from the area under the loading and unloading curve of the compression cycle, respectively, by using the trapezoidal rule.

b. Elastic recovery

At the decompression stage, the compacted powder bed tends to expand to some extent as the compressive stress is released. To assess this behaviour, elastic recovery ER can be determined, as expressed by Eq. 3.2:

$$ER = \frac{t_0 - t_{\min}}{t_{\min}} \times 100\% \tag{3.2}$$

where t_{min} is the minimum thickness of the powder bed in the die cavity or at the maximum compressive pressure, as determined with the in-die method [6].

c. Powder compaction models

In this study, the compression behaviours of the titanium powder, carbamide powder and their mixtures were also characterized by means of the classic powder compaction models, i.e., the Heckel model and the Kawakita model.

The Heckel compaction model

The Heckel model was developed, based on a number of experiments with metallic powders. In this model, it is assumed that the kinetics of pore reduction in a powder bed during compression is analogous to the first order of chemical reaction [5]. The final form of this model is expressed by Eq. 3.3:

$$-\ln(1-D) = KP + A \tag{3.3}$$

where P is the compacting pressure applied. The constant A is theoretically corresponding to the initial porosity of the powder bed. The relative density of a compacted powder mixture or a component powder D can be determined as the ratio of the density of powder compact to the density of powdered material in the solid form. In this case, $D = 1 - \varepsilon$, where ε is the porosity of the powder bed. The linear region of the Heckel plot is of importance in the analysis of powder compaction. The inverse of the slope K is defined as the yield pressure P_y of the powdered material. Based on the yield pressure P_y, a critical pressure that may result in plastic deformation of the compressed powder could be predicted [6]. To reduce the sensitivity of the P_y value to the accuracy of the slope K, corrections were introduced by Sonnergaard [7], as expressed by Eq. 3.4:

$$P_y = R^2 / K \tag{3.4}$$

where R^2 and K are the correlation coefficient and the slope of the linearly regressed plot with the Heckel model, respectively [7]. Furthermore, Heckel indicated an empirical correlation between the slope K and the yield strength P_y of the powder. Combined with Eq. 3.4, the empirical relationship between the yield pressure and the yield strength of the powder [8] can be written as Eq. 3.5:

$$P_y = 3\sigma_y \tag{3.5}$$

The Kawakita compaction model

The Kawakita model, as expressed by Eq. 3.6, was claimed to be best applicable to the compression analysis of soft fluffy pharmaceutical powders [9]. Therefore, this model was also selected in the present study, considering the use of the organic carbamide powder as the space holder:

$$\frac{P}{C} = \frac{P}{a} + \frac{1}{ab} \tag{3.6}$$

where,

$$C = \frac{V_0 - V}{V_0} \tag{3.7}$$

With this model, the initial volume V_0 of the powder bed needs to be determined. In this study, V_0 was determined by calculating the distance between the upper punch at the onset of loading curve and the point where unloading curve approached zero-load in the load-displacement plot. The constants *a* and *b* derived from the Kawakita plot are of importance. The constant *a* equals to the initial porosity of the powder bed [9], although Denny [10] argued that the derived a value does not always agree well with the measured initial porosity value due to the non-linearity of the plot. The reciprocal value of the constant *b* is interpreted as the yield strength of the powder [11].

d. Optical microscopy

Particle arrangements in the compacted powder were revealed by observing the cross-sectional areas of powder compacts, using a VHX-5000 digital microscope (Keyence, USA). The powder compact was first mounted in acrylic resin (Struers, Germany), ground and polished to expose a cross-sectional area. A manual dry grinding and polishing procedure was followed in order to avoid any damage to the sample and prevent the carbamide powder from dissolution in water-containing liquid. The sample was finally cleaned by flushing the polished surface with compressed air prior to microscopic observation.

3.3. Results

3.3.1. Load-displacement plots

Fig. 3.2 shows the load-displacement plots generated from the compaction cycles of the titanium powder, carbamide powder and their mixtures. All the load-displacement plots generated from the compaction of titanium/carbamide mixtures showed intermediate behaviours between the monolithic titanium and carbamide powders.

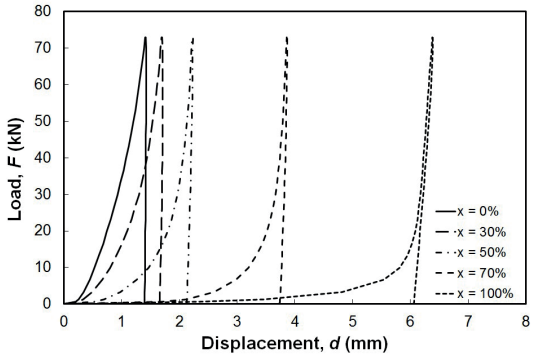

Fig. 3.2. Load-displacement plots of titanium/carbamide powder mixtures
(Reprinted with permission from Elsevier)

3.3.2. Specific net energy in powder compaction cycle

As shown in Fig. 3.3a, the $E_{sp,net}$ values of the titanium powder and titanium/carbamide mixture at x = 30% increased linearly with increasing compacting pressure, except the region of low compacting pressures (P = 0 - 200 MPa). With increasing volume fraction of carbamide in the mixture, however, such a linear behaviour did not hold. In the case of the compaction of the carbamide powder, the $E_{sp,net}$ values remained almost unchanged at P = 200 - 400 MPa. The comparison of the experimental data with the estimated $E_{sp,net}$ values based on Eq. 3.1 is shown in Fig. 3.3b. The rule of mixtures, as expressed in Eq. (3.8), yielded increased $E_{sp,net}$ values at P = 0 - 200 MPa but decreased $E_{sp,net}$ values when higher compacting pressures were applied.

$$\left(E_{sp,net}\right)_{mix} = (1-x)\left(E_{sp,net}\right)_{Ti} + x\left(E_{sp,net}\right)_{Carb.} \tag{3.8}$$

Similar to the case of $E_{sp,cp}$, the experimental data of $E_{sp,net}$ were not comparable to the estimated trend at x > 50% and P > 300 MPa.

3.3.3. Elastic recovery

Fig. 3.4 shows the elastic recovery ER values of titanium/carbamide powder compacts during the decompression stage in the compaction cycle. Carbamide powder compact exhibited higher elastic properties than titanium powder compact and the addition of the former powder increased the elasticity of titanium/carbamide powder mixture compacts.

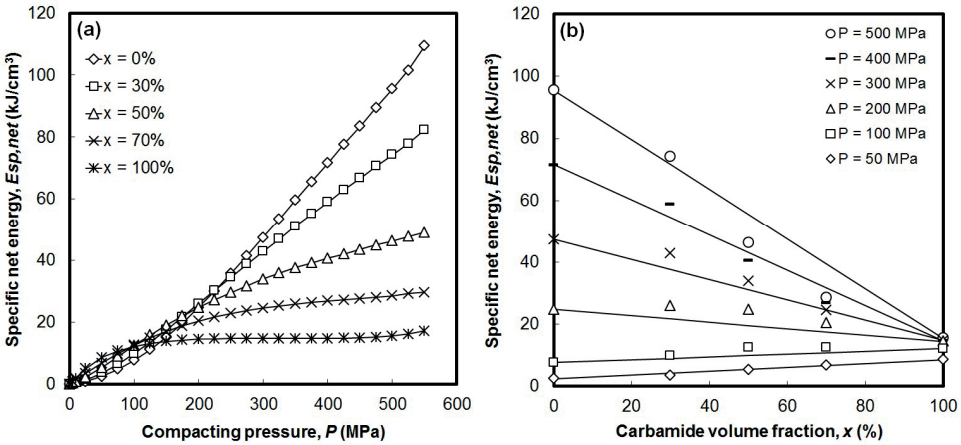

Fig. 3.3. Specific net energies ($E_{sp,net}$) for the compaction of titanium/carbamide powder mixtures (Reprinted with permission from Elsevier)

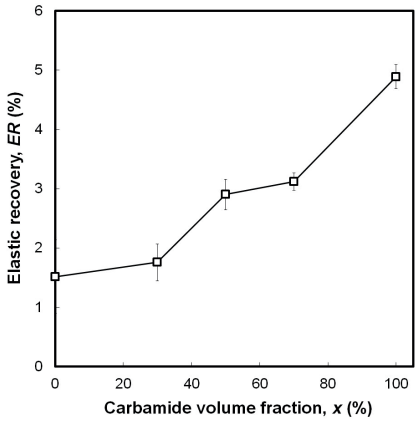

Fig. 3.4. Elastic recovery of titanium/carbamide powder compacts
(Reprinted with permission from Elsevier)

3.3.4. Relative density

The experimental data of the at-pressure relative density D were plotted against the compacting pressure P applied on each sample in order to indicate the variations between materials, which was found to be critical in the analysis with the powder compaction models described in Subsection 3.3.5. The densification characteristics of the titanium powder, carbamide powder and their mixtures are shown in Fig. 3.5. It can clearly be seen in this figure that the densification characteristics of titanium/carbamide powder mixtures lay between those of the titanium and carbamide powders. The densification capacity of the titanium/carbamide powder mixture increased with increasing volume fraction of carbamide in the mixture.

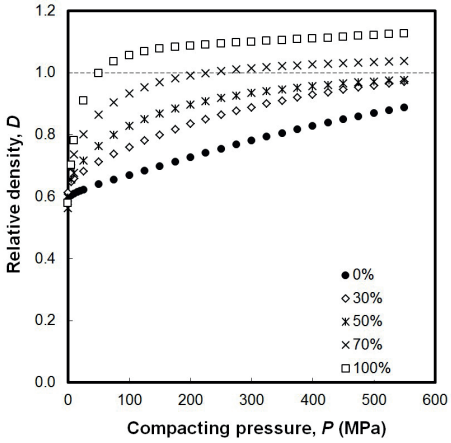

Fig. 3.5. At-pressure relative density of titanium/carbamide powder mixtures
(Reprinted with permission from Elsevier)

3.3.5. Application of the powder compacting models

Fitting of the experimental data into the Heckel powder compaction model and the Kawakita model appeared to be meaningful. Figs. 3.6 and 3.7 show the examples of the results obtained from fitting the experimental data into the models. Additional information on the experimental data fitted into the Heckel and Kawakita models is given in Tables 3.1 and 3.2, respectively.

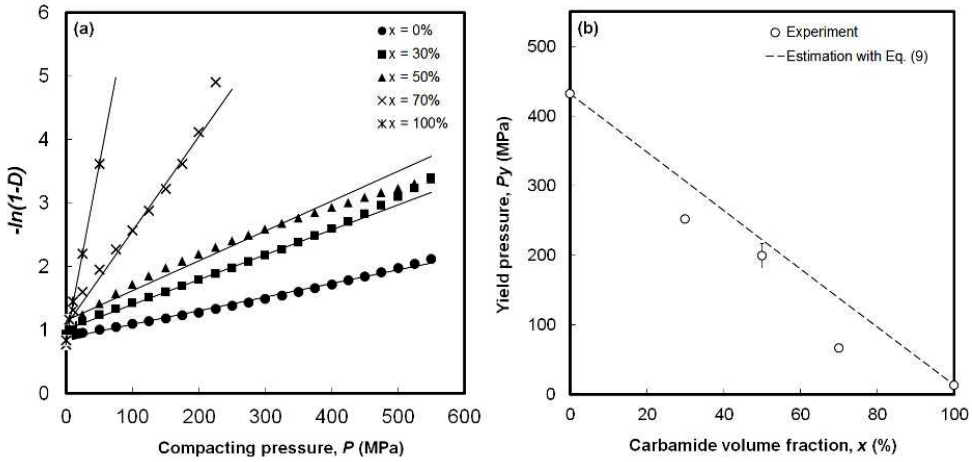

Fig. 3.6. (a) Fitting of data plots into the Heckel compacting model and (b) the relationship between carbamide volume fraction and yield pressure (Reprinted with permission from Elsevier)

Fitting into the Heckel model resulted in a plot having a curved profile at low compacting pressures and a linear profile at higher pressures. Fig. 3.6a shows an example of fitting the data plot of titanium/carbamide powder mixture with various carbamide volume fractions into the Heckel model. The linear regions of the Heckel plot are of importance in the analysis of powder compression. In the case of the compression of the monolithic titanium powder, a linear region occurred over almost the whole range of the compacting pressures applied, except a very small region at $P < 10$ MPa. However, the linear region in the Heckel plot in the case of the compression of the carbamide powder could only be discerned over $P = 0$ to 50 MPa, as a consequence of full densification that occurred at higher pressures. For the mixture at $x = 50\%$, the linear region of the Heckel plot was hard to recognize, as indicated by the values of the coefficient of correlation R^2 that were found to be slightly lower than those of the mixtures with other volume fractions of carbamide (Table 3.1). Moreover, the slope of the linear region in the Heckel plot of the titanium powder was apparently lower than the slopes of titanium/carbamide powder mixtures, resulting in lower Py values of the latter. The influence of the volume fraction of carbamide x on the slope K and thus on the P_y values was determined. It was found that the slope of the linear region in the plot increased as the carbamide content in the mixture increased.

Fig. 3.6b shows a plot depicting the relationship between the yield pressure P_y and the volume fraction of carbamide in the mixture x. The average experimental P_y values of the mixtures were

dependent on the experimental P_y values of the component powders, i.e., the titanium and carbamide powders.

Table 3.1. Summary of the Heckel plot for the analysis of the compression behaviours of titanium/carbamide mixtures (Reprinted with permission from Elsevier)

Carbamide volume fraction, x (%)	Minimum pressure range covered by the Heckel's model (MPa)	Minimum pressure range in the linear region of the Heckel's plot (MPa)	Coefficient of correlation, R^2	Yield pressure, P_y (MPa)
0	0 – 550	10 – 550	0.9915 – 0.9944	432.1 ± 19.5
30	0 – 550	5 – 425	0.9980 – 0.9998	251.8 ± 3.9
50	0 – 550	5 – 425	0.9816 – 0.9939	198.8 ± 17.5
70	0 – 200	10 – 150	0.9952 – 0.9991	66.4 ± 4.1
100	0 – 25	0 – 25	0.9778 – 0.9865	12.9 ± 1.6

Accordingly, the experimental yield pressures of titanium/carbamide powder mixtures P_y decreased with increasing volume fraction of carbamide. However, the experimental P_y values of powder mixtures were always lower than those derived from the rule of mixtures, as expressed by Eq. 3.9.

$$\left(P_y\right)_{mix} = \left(1-x\right)\left(P_y\right)_{Ti} + x\left(P_y\right)_{Carb} \tag{3.9}$$

Similar to Eq. 3.8, Eq. 3.9 would be expected to be applicable to the corresponding properties of powder mixtures.

Fitting of the experimental data into the Kawakita model resulted in the plots as shown in Fig. 3.7. Fig. 3.7a shows an example of fitting the data plot of titanium/carbamide powder with various carbamide volume fractions into the Kawakita model. The Kawakita plot for the carbamide powder appeared to show a linear relationship over the whole range of the compacting pressures applied (P = 0 – 550 MPa). Fitting of the experimental data obtained from the compaction of the carbamide powder into the Kawakita model resulted in a more accurate plot, as indicated by the higher R^2 values of the plot (Table 3.2), than that into the Heckel model. The constant b^{-1} of the Kawakita plot of the carbamide powder could easily be derived due to a broader range of minimum pressures covered by the model (Table 3.2). The Kawakita plot of the compressed titanium powder yielded a curved profile at P = 0 - 100 MPa and a linear region at higher compacting pressures. The constants a and b of the plot were determined through linear regressions of the data plots over the range of P = 100 – 550 MPa. In the case of the compression of titanium/carbamide powder mixtures, the curved region at low compacting pressures in the Kawakita plot gradually diminished along with the increases in the volume fraction of carbamide in the mixture.

Fig. 3.7b shows the plot indicating the relationship between the constant b^{-1} derived from the fitting of the experimental data into the Kawakita model and the volume fraction of the carbamide powder. Similar to the case with the Heckel plot, the dependency of the constant b^{-1} derived from the Kawakita plots of titanium/carbamide powder mixtures on the corresponding

constants of the component powders was indicated. The values of the constant b^{-1} were also plotted on the basis of the rule of mixtures (Eq. 3.10) and then compared with those derived from the experimental work.

$$\left(b^{-1}\right)_{mix} = (1-x)\left(b^{-1}\right)_{Ti} + x\left(b^{-1}\right)_{Carb} \tag{3.10}$$

Similar to the trend found for the P_y values, the experimental b^{-1} values of titanium/carbamide powder mixtures were lower than those predicted with the rule of mixtures.

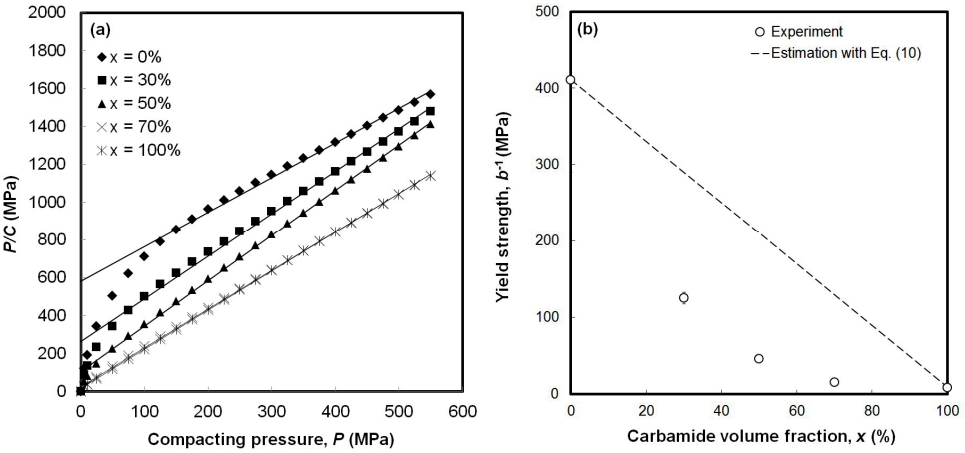

Fig. 3.7. Fitting of data plots into the Kawakita compacting model (Reprinted with permission from Elsevier)

Table 3.2. Summary of the Kawakita plot for the analysis of the compression behaviours of titanium/carbamide mixtures (Reprinted with permission from Elsevier)

Carbamide volume fraction, x (%)	Minimum pressure range covered by the Kawakita model (MPa)	Minimum pressure range in the linear region of the Kawakita plot (MPa)	Coefficient of correlation, R^2	Constant b^{-1} (MPa)
0	0 – 550	100 – 550	0.9949 – 0.9993	410.8 ± 121.0
30	0 – 550	25 – 550	0.9944 – 0.9952	125.1 ± 7.8
50	0 – 550	10 – 550	0.9989 – 0.9990	45.7 ± 2.2
70	0 – 550	5 – 550	0.9997 – 0.9998	15.3 ± 0.4
100	0 – 550	0 – 550	0.9998	8.5 ± 0.3

3.3.6. Particle rearrangement

Fig. 3.8 shows particle rearrangement on the cross sections of powder compacts, as observed by using the optical microscope. It was clear that the white spherical particles clustered on the polished surface represented the titanium powder, while the dark regions corresponded to the carbamide powder. Being spherical, some of titanium particles were only partially polished. Some

of other particles were not exposed to the polished surface but recognizable, such as those located behind the polished carbamide powder particles, as indicated in Figs. 3.8a and 3.8d.

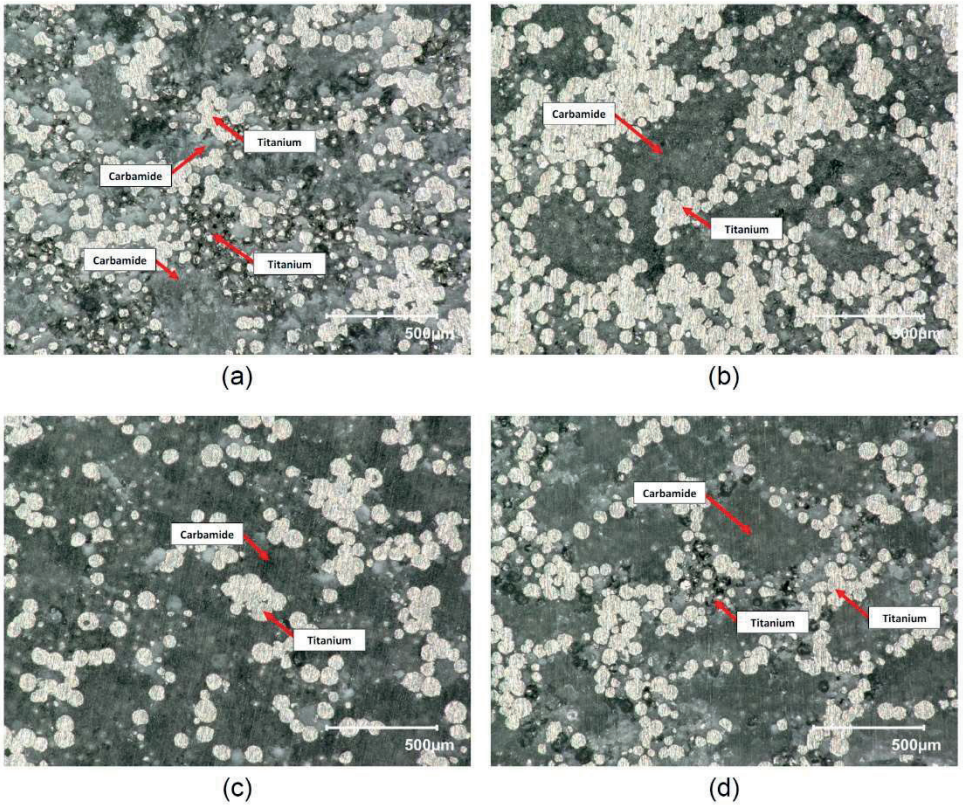

Fig. 3.8. Rearrangement of titanium/carbamide powder particles in the mixtures with various volume fractions of carbamide, as observed on the fracture surfaces of the powder compacts: (a) x = 30%, P = 550 MPa; (b) x = 50%, P = 550 MPa; (c) x = 70%, P = 550 MPa; (d) x = 50%, P = 200 MPa (Reprinted with permission from Elsevier)

From the micrographs, as those shown in Figs. 3.8a – 3.8c, it was clear that powder particle rearrangement in the compacts was affected by the volume fraction of the carbamide powder. In the case of the powder mixture with x = 30% and compressed at P = 550 MPa, titanium powder particles were rearranged, becoming spread around the deformed carbamide particles (Fig. 3.8a). As the volume fraction of carbamide increased to x = 50%, clusters of titanium powder particles were formed, separated by carbamide powder particles (Fig. 3.8b). With a further increase in carbamide volume fraction to x = 70%, more titanium particles were isolated by carbamide particles. As shown in Fig. 3.8c, both individual and clustered titanium particles were surrounded by carbamide powder particles.

To indicate the deformation of carbamide powder particles as a result of the compacting pressure applied, titanium/carbamide powder compacts with 50% carbamide were compressed at P = 550 and 200 MPa, as shown in Figs. 3.8b and 3.8d, respectively. Under a compressive stress of P = 550 MPa, the carbamide powder was no longer intact. As shown in Fig. 3.8b, under such a high compacting stress, titanium powder particles were seen intruding into carbamide powder particles, even breaking up them and resulting in irregular morphologies of carbamide powder particles. In addition, carbamide powder particles became coalesced, thereby forming interconnections between powder particles, as clearly visible in the linked dark area (Fig. 3.8b). By contrast, under a pressure of P = 200 MPa, carbamide powder particles, surrounded by smaller titanium powder particles in the mixture, remained intact (Fig. 3.8d). Some titanium powder particles were located behind carbamide powder particles, but still clearly seen linking with other titanium particles to form boundaries around the intact carbamide particles.

3.4. Discussion

In this research, the compression behaviours of titanium/carbamide powder mixtures were characterized, thereby laying a solid foundation for determining critical compacting pressures that resulted in pore distortions due to geometrical changes or fragmentation of carbamide space-holding particles in titanium scaffold preform. The compression behaviours of the monolithic titanium and carbamide powders were first characterized to aid in the analysis of the compression of titanium/carbamide powder mixtures.

3.4.1. Compression mechanisms

a. Titanium powder

The compaction mechanisms of the titanium powder in the present study was governed mainly by plastic deformation, as implied from a linear increase of $E_{sp,net}$ of this powder over a compressive stress range of P = 200 – 550 MPa. Fitted into the Heckel plot, the experimental data of the titanium powder in the present study also suggested a compression mechanism by plastic deformation at P = 10 – 550 MPa, as indicated by the linear plots over this range of compressive stresses. In a previous study, it was confirmed that uniaxial compression of plastically flowing metallic powders, such as iron, nickel, copper and tungsten powders, resulted in linear plots at the compressive stresses applied (P = 137 – 550 MPa) [5]. In another study, uniaxial compression of atomized aluminium and lead powders yielded linear Heckel plots over the compressive stresses applied, i.e., P = 300 – 800 MPa and P = 100 – 200 MPa, respectively, and moreover the compressive stresses turned toward infinity as the powder bed almost reached full density or the zero porosity state [12]. In the present case, however, the trend of the Heckel plot towards infinity was not visible over the compressive stresses applied to the titanium powder bed.

The present study also confirmed the involvement of particle rearrangement in the densification mechanism of the titanium powder at low pressures. There were several findings that indicated this mechanism. Firstly, an inward curve was observed in the $E_{sp,net}$ plot of the titanium powder over P = 0 to 200 MPa (Fig. 3.3a), demonstrating lower energy required for

plastic deformation. Secondly, a curved region of the Heckel plot of the titanium powder at low compressive pressures, i.e., $P < 10$ MPa (Fig. 3.3a), implied extensive densification of the powder by particle rearrangement [13]. In addition, the ability of spherical titanium particles to maintain their individuality at such low compacting pressures also confirmed the densification mechanisms of this powder by particle rearrangement, as in the case of other powdered metallic materials [12] and plastic flowing pharmaceutical powders [13].

Duberg and Nystrom proposed three different stages during the compression of brittle metallic powder [14], i.e., (i) elastic deformation (*E*), (ii) plastic deformation (*P*) and (iii) powder fragmentation (*F*). Considering the results from the analysis of the energetic parameters, the at-pressure relative density of powder compact and yield pressures derived from the Heckel and Kawakita plots, it could be concluded that the compression mechanisms of the titanium powder under the compressive stresses applied in the present study were governed by elastic (*E*) and plastic (*P*) deformation of the powder, in addition to particle rearrangement at the very beginning of the compaction process. The fragmentation of titanium powder particles may not have occurred under the compressive stresses applied due to their ductile behaviour and strength.

It is important to note that the P_y value of the titanium powder in the present study seemed to be acceptable when compared to the theoretical yield strength values of bulk titanium. By using Eq. 3.5, the yield strength σ_y of the titanium powder derived from the yield pressure P_y was 144.03 ± 6.48 MPa, which was below the range of the typical σ_y values of ASTM grade 1 pure bulk titanium, i.e., 170 - 310 MPa [15]. The application of the Kawakita model for the analysis of the compression of the titanium powder resulted in b^{-1} value of 410.77 ± 121.04 MPa, being much higher than the yield strength σ_y of ASTM grade 1 pure bulk titanium (170 – 310 MPa). This discrepancy clearly indicates the inappropriateness of the Kawakita model to be used for the analysis of the compression behaviour of a ductile metallic powder, such as the titanium powder in the present study, which is very different from soft and fluffy organic powders [10].

b. Carbamide powder

In contrast to the titanium powder, the compaction of the carbamide powder under given compressive pressures ($P = 0 – 550$ MPa) involved more complex mechanisms. The $E_{sp,net}$ plot of the carbamide powder showed three distinct regions, representing a series of powder compression mechanisms involved (Fig. 3.3a). The first region occurred at $P = 0$ - 200 MPa, characterized by steep increases in $E_{sp,net}$ value with increasing compacting pressure. As such, the compression process to realize carbamide powder compacts might occur through plastic deformation at low pressures ($P = 0$ - 200 MPa). Moreover, since the $E_{sp,net}$ values increased steadily without showing a curved region over this pressure range, powder particle rearrangement might not be a dominant mechanism during the compression process of the carbamide powder. The second region in the $E_{sp,net}$ plot of the carbamide powder occurred at $P = 200$ - 400 MPa and it was characterized by the zero slope. As implied in Eq. 3.1, the constant $E_{sp,net}$ values meant no increases in the energy expended to deform the powder plastically with increasing compressive stresses. The compacting energy was then stored in the carbamide powder bed and would be released during the decompression stage. In other words, the

compression mechanism of the carbamide powder over a pressure range of P = 200 to 400 MPa was governed by the elastic behaviour of this material. The $E_{sp,net}$ value slightly increased in the last region of this plot, indicating advanced plastic deformation at P > 400 MPa.

The calculated at-pressure relative density D showed a critical compacting pressure for the carbamide powder at $P \approx 50$ MPa, where a full density compact was achieved. It is revealed in the previous study that full densification of their carbamide powder at a compacting pressure of $P \approx 150$ MPa [16]. Bakan [2] also produced several carbamide powder compacts having green densities of around 1.3 g cm^{-3}, or $D \approx 1$, with a double-action uniaxial press and at compressive stresses of P = 100 – 500 MPa. Interestingly, the relative density of the carbamide powder compact in the present study increased slightly even after full densification had been reached. A similar compression behaviour was observed in the case of the compression of a polyethylene-glycol (PEG) powder [17].

Fitting the experimental data of the carbamide powder into the Heckel model was only applicable at P < 50 MPa. With the Heckel plot, the yield strength σ_y of the carbamide powder was found to be 4.31 ± 0.55 MPa. Comparison of the σ_y value with the typical value of bulk carbamide was however not possible due to the absence of the information on the mechanical properties of carbamide in the open literature. Several authors have revealed the limitations of the Heckel model in describing the powder compression behaviour at zero porosity [12], where the plot reaches infinity. In addition, the linear region of the Heckel plot was hardly recognizable in some cases, causing difficulties in determining the yield pressures of powders [7]. To turn away from these limitations, the Kawakita model was applied. The application of this model resulted in the plots having better accuracies and recognizable linearity over the compressive stresses applied. The prominence of the Kawakita model was obvious in the case of the carbamide powder, confirming the appropriateness of this model for the compression analysis of soft and fluffy organic powders [10]. On the basis of the Kawakita plot, the carbamide powder possessed a lower b^{-1} value than the titanium powder. Moreover, the derived b^{-1} value of the carbamide powder, i.e., 8.49 ± 0.29 MPa, was higher than the yield strength σ_y of the carbamide powder derived from the Heckel plot and Eq. 3.11, i.e., 4.31 ± 0.55 MPa. Considering the better fitting of the experimental data into the Kawakita model, the yield strength σ_y of the carbamide powder, about 8.5 MPa, was considered more trustworthy.

From the results of the analysis using the energetic parameters, the at-pressure relative density and the compacting models, it can be deduced that the compression mechanism of the carbamide powder was mainly governed by plastic deformation and fragmentation prior to the realization of powder compact. Duberg and Nystrom [14] proposed a general sequence of stages during the compaction of organic compound powders, namely (i) elastic deformation of the initial particles (E_1), (ii) plastic deformation of the initial particles (P_1), (iii) fragmentation of the initial particles into smaller particles (F_1), (iv) elastic deformation of the smaller particles (E_2), (v) plastic deformation of the smaller particles (P_2) and (vi) fragmentation of the smaller particles (F_2). However, only F_1, E_2 and P_2 could be observed during the compression of some of organic compound powders, such as paracetamol and aspirin [14]. In the present study, the compression

mechanisms of the carbamide powder might follow the sequence proposed by Duberg and Nystrom [14], i.e., F_1-E_2-P_2, but only under the compressive pressures below the critical stress reaching the full densification of this powder. Further study to distinguish these stages, for instance by applying the Heckel plot at the decompression stage prior to the onset of the full densification of the powder, is needed [18]. The final sequence of the compression process for the carbamide powder was marked by the realization of powder compacts at $P \approx 50$ MPa, as confirmed from the plots of powder compact relative density (Fig. 3.5). Further compression at higher pressures would lead to elastic deformation and plastic deformation of carbamide powder compacts.

c. Titanium/carbamide powder mixtures

Obviously, the compaction of titanium/carbamide powder mixtures involved two types of powder particles having distinctly dissimilar compression behaviours and mechanical properties, as discussed in Subsections 3.1.1 and 3.1.2.

Titanium/carbamide powder mixtures exhibited the intermediate compression behaviours of the titanium and carbamide component powders. A similar trend could be found in the previous work with pharmaceutical powders [19]. The compression behaviours of powder mixtures could in general be predicted based on this trend. The rule of mixtures, for instance, is one of the theoretical approaches that have been widely used for predicting the properties of powder mixtures based on the properties of their component powders. Recently, the rule of mixtures has been applied to determine the appropriate compaction pressures in the preparation of titanium scaffolds with the space holder method [20]. By using this approach, the strengths of component powders, i.e., titanium and cenosphere powders, were used as the references to determine the pressures required to compact titanium/cenosphere powder mixtures [20]. Titanium/cenosphere powder mixtures were then compacted under the pressures lower than the critical stresses predicted by using the rule of mixtures.

The relationships between the volume fraction of a space holder and the compaction parameters studied, i.e., $E_{sp,net}$, P_y and b^1, were however not linear (Figs. 3.3, 3.6 and 3.7, respectively). In the case of powder compression at $P > 300$ MPa and $x \geq 50\%$, the experimental $E_{sp,net}$ values deviated considerably from the values determined by the rule of mixtures. This phenomenon might be attributed to extensive deformation or fragmentation of carbamide powder particles under compressive stresses of $P > 300$ MPa. Based on the Kawakita plot, the yield strength of the carbamide powder was estimated to be about 8.5 MPa. The compression of powder mixtures at $P > 300$ MPa would therefore lead to the fragmentation of carbamide powder particles. With this phenomenon taken into consideration, it is interesting to discuss the possible densification mechanisms of titanium/carbamide powder mixtures by considering the influence of the yield strengths of the component powders and the mixing ratios.

Bouvard [18] proposed three distinct densification mechanisms of powder mixtures consisting of soft and hard particles with various mixing ratios, i.e., (i) isolated inclusion, (ii) aggregation and (iii) percolation. According to him, the isolated inclusion occurs when a mixture is composed of a large volume fraction of soft particles. Under a given compressive pressure, the hard particles hinder the densification of the soft particles. On the other hand, the soft

particles in the mixture are extensively deformed, even broken, under high compacting pressures and tend to fill the voids at the interstices of the hard particles. The densification mechanism by percolation occurs as the volume fraction of the hard particles in the mixture is higher than the soft ones. Since the hard particles are more resistant to deformation, the densification mechanism of the powder mixture is largely controlled by the rearrangement of the hard particles, although deformation of the soft particles occurs once their critical strengths are exceeded. The densification mechanism by aggregation occurs at the intermediate between the isolated inclusion and percolation and is marked by the filling of pores at the interstices of the hard particles by the soft particles.

By considering the densification mechanisms proposed by Bouvard [18], the compression of titanium/carbamide powder mixtures having $x > 50\%$ in the present case might be governed by the isolated inclusion mechanism. This behaviour could explain the deviations of the experimental $E_{sp,net}$ values from the values predicted by using the rule of mixtures at high compacting pressures. Furthermore, the deviations of the experimental $E_{sp,net}$ values from the predicted values were apparently smaller at lower compacting pressures ($P \leq 300$ MPa), indicating that the compression mechanisms were still controlled mainly by the deformation of powder particles in the mixture. All these mechanisms were confirmed by a series of micrographs shown in Fig. 3.8, which depicted powder particle rearrangement viewed on the cross sections of titanium/carbamide powder compacts. The application of a high compacting pressure (P = 550 MPa) would result in severe deformation and even breakage of carbamide powder particles, which eventually caused distortions of pore geometry in the scaffold product. In the case of the titanium/carbamide powder mixture with $x = 50\%$, the carbamide powder apparently remained intact when the mixture was compacted at P = 200 MPa, as predicted by the Heckel plot and the rule of mixtures (Fig. 3.6). It is also revealed that pore geometry in sintered titanium scaffolds distorted as a result of the deformation of carbamide space-holding particles under a compressive stress of P = 500 MPa, exceeding the critical compressive stress of this powder [21].

3.4.2. Prediction of critical pressures for the compression of titanium/carbamide powder mixtures

By considering P_y and b^{-1} values acquired from the Heckel and Kawakita plots, the critical compacting pressures that led to geometrical deformation of carbamide space holder in the titanium/carbamide powder compacts could be determined and used in the preparation of titanium scaffolds with the space holder method. It is clearly shown that both the P_y and b^{-1} values of titanium/carbamide powder mixtures decreased with increasing volume fraction of carbamide in the mixture. Considering the micrographs in Fig. 3.8, however, the Heckel plot was preferable compared to the Kawakita plot in determining the maximum compacting pressure for the titanium/carbamide powder mixture with $x = 50\%$. For instance, a compaction pressure of P = 200 MPa, being about the same as the yield pressure for $x = 50\%$ (Fig. 3.6b), could not deform and break the carbamide powder in the mixture (Fig. 3.8d). When the compressive pressure was increased to P = 550 MPa, the carbamide powder in the mixture was severely deformed or even broken (Fig. 3.8b). It means that although the b-1 constant derived

from the Kawakita plot appeared to be meaningful for estimating the yield strength of the carbamide powder (Subsection 3.1.2), it could not be used directly as a criterion in determining the compacting pressures for titanium/carbamide powder mixtures.

The rule of mixtures could be used to predict the critical compacting pressures for the deformation of space-holding particles. However, both the experimental P_y and b^{-1} values obtained in this study were lower than those predicted by using the rule of mixtures. Iikka and Paronen recorded a similar finding when compression was performed on pharmaceutical powder mixtures consisting of powders with plastic and fragmenting behaviours [13]. Therefore, the rule of mixtures should be applied with caution. Systematic experimental work is still needed to aid in the compression analysis of powder mixtures consisting of a metal matrix powder and softer space-holding particles.

The critical compacting pressures proposed in the current study must also be determined with caution with regard to the strength or structural integrity of the scaffold preform. It has been reported that a minimum compacting pressure was required to prevent the scaffold preform from collapsing during the handling or during the removal of the space holder. A scaffold preform composed of a Ti-6Al-4V powder and a carbamide space holder could not maintain its structural integrity when prepared under compacting pressures below 300 MPa [22]. Torres et al. [1] also showed collapsed titanium scaffold preforms prepared under a compacting pressure of 200 MPa during removing a NaCl space holder through water leaching. A follow-up study to investigate the minimum compressive pressures for the compaction of the mixtures of titanium and space-holding particles has been planned for the determination of appropriate compacting pressures in order to control the porous structure of titanium scaffolds prepared with the space holder method.

Distortions of pore geometry may adversely affect the mechanical properties of the scaffold produced [23]. It has been already reported that porosity, pore sizes (i.e., 200 – 500 μm) [24] and pore interconnections [25] are critically important factors that determine bone cell activities in the scaffold. Distorted pore geometry and poorly interconnected pores may disrupt the activities and growth of bone cells in the scaffold. Therefore, every step in scaffold fabrication must be carefully controlled to ensure porosity, pore sizes and pore interconnections.

3.5. Conclusions

In this study, a series of experiments were performed to characterize the compression behaviours of titanium/carbamide powder mixtures with various volume fractions of carbamide space-holding particles. Several compression parameters, i.e., (i) the specific energy expended during powder compression, (ii) the at-pressure relative density of powder compacts and (iii) the yield pressures of the compacted powder mixtures, were analysed to establish possible compression mechanisms and determine appropriate compaction pressures that could be used in the preparation of titanium scaffolds with the space holder method. The results of this study have led to the following conclusions.

a. The titanium and carbamide powders exhibited dissimilar compression behaviours under the compressive stresses (P = 0 – 550 MPa) applied in the present study. The compression of

the titanium powder was mainly governed by plastic deformation. At low compressive pressures ($P < 10$ MPa), however, the densification of titanium powder bed occurred mainly through particle rearrangement. The carbamide powder experienced plastic deformation and fragmentation prior to full densification and compact realization at $P \approx 50$ MPa. Once full densification was achieved, further compression resulted in elastic deformation and plastic deformation of carbamide powder compact. Titanium/carbamide powder mixtures exhibited intermediate compression behaviours of the monolithic titanium and carbamide powders, with compression mechanisms depending on the volume fraction of carbamide in the mixture.

b. The critical pressures for the titanium powder, carbamide powder and their mixtures could be determined from the yield pressures P_y obtained from the Heckel plots. The rule of mixtures could be applied with cautions to predict the compressive stresses in the preparation of titanium scaffolds with carbamide as the space holder. However, the limitations of this model were recognized when the compacting pressure was high ($P > 300$ MPa) and the volume fraction of carbamide in the mixture was large ($x > 50\%$). In addition, in the case of titanium/carbamide powder mixtures, systematic experimental research would still be needed since the experimental yield pressures obtained were lower than the values determined by using the rule of mixtures. Nevertheless, this study clearly showed a similar trend between the experimental and estimated P_y values as determined by using the rule of mixture.

References

[1] Y. Torres, J. J. Pavón and J. A. Rodríguez, "Processing and characterization of porous titanium for implants by using NaCl as space holder," *Journal of Materials Processing Technology,* vol. 212, pp. 1061-1069, 2012.

[2] H. Bakan, "A novel water leaching and sintering process for manufacturing highly porous stainless steel," *Scripta Materialia,* vol. 55, pp. 203-206, 2006.

[3] C. F. Li, Z. G. Zhu and T. Liu, "Microhardness of pore walls in porous titanium prepared with novel powder metallurgy," *Powder Metallurgy,* vol. 48, pp. 237-240, 2005.

[4] W. Niu, C. Bai, G. Qiu, Q. Wang, L. Wen, D. Chen and L. Dong, "Preparation and characterization of porous titanium using space-holder technique," *Rare Metals,* vol. 28, pp. 338-342, 2009.

[5] R. Heckel, "Density-pressure relationships in powder compaction," *Transactions of Metallurgical Society AIME,* vol. 221, pp. 671-675, 1961.

[6] J. Geoffroy and J. Carstensen, "Effects of measurement method on the property of materials," *Powder Technology,* vol. 68, pp. 91-96, 1991.

[7] J. Sonnergaard, "A critical evaluation of the Heckel equation," *International Journal of Pharmaceutics,* vol. 193, pp. 63-71, 1999.

[8] R. Heckel, "A normalized density-pressure curve for powder compaction," *Transactions of the Metallurgical Society of AIME,* vol. 22, pp. 1073-1074, 1962.

[9] K. Kawakita and K.-H. Ludde, "Some considerations on powder compresion equations," *Powder Technology,* vol. 4, pp. 61-68, 1971.

[10] P. Denny, "Compaction equations: A comparison of the Heckel and Kawakita equations," *Powder Technology,* vol. 127, pp. 162-172, 2002.

[11] F. Nicklasson and G. Alderborn, "Analysis of the compression mechanics of pharmaceutical agglomerates of different porosity and composition using the Adams and Kawakita equations," *Pharmaceutical Research,* vol. 17, pp. 949-954, 2000.

[12] N. Page and M. Warpenius, "Loading relations for metal powders pressed to high density," *Powder Technology,* vol. 61, pp. 87-94, 1990.

[13] J. Iikka and P. Paronen, "Prediction of the compression behaviour of powder mixtures by the Heckel equation," *International Journal of Pharmaceutics,* vol. 94, pp. 181-187, 1993.

[14] M. Duberg and C. Nystrom, "Studies on direct compression of tablets XVII. Porosity-pressure curves for the characterization of volume reduction mechanisms in powder compression," *Powder Technology,* vol. 46, pp. 67-75, 1986.

[15] M. Donachie Jr., Titanium: A technical guide, Ohio: ASM International, The Materials Information, 2000.

[16] N. Tuncer, M. Bram, A. Laptev, T. Beck, A. Moser and H. Buchkremer, "Study of metal injection molding of highly porous titanium by physical modeling and direct experiments," *Journal of Materials Processing Technology,* vol. 214, pp. 1352-1360, 2014.

[17] A. Adolfsson and C. Nystrom, "Tablet strength, porosity, elasticity and solid state structure of tablets compressed at high loads," *International Journal of Pharmaceutics,* vol. 132, pp. 95-106, 1996.

[18] D. Bouvard, "Densification behaviour of mixtures of hard and soft powders under pressure," *Powder Technology,* vol. 111, pp. 231-239, 2000.

[19] V. Busignies, B. Leclerc, P. Porion, P. Evesque, G. Couarraze and P. Tchoreloff, "Compaction behaviour and new predictive approach to the compressibility of binary mixtures of pharmaceutical excipients," *European Journal of Pharmaceutics and Biopharmaceutics,* vol. 64, pp. 66-74, 2006.

[20] D. Mondal, J. Datta Majumder, N. Jha, A. Badkul, S. Das, A. Patel and G. Gupta, "Titanium-cenosphere syntactic foam made through powder metallurgy route," *Materials and Design,* vol. 34, pp. 82-89, 2012.

[21] O. Smorygo, A. Marukovich, V. Mikutski, A. A. Gokhale, G. J. Reddy and J. V. Kumar, "High-porosity titanium foams by powder coated space holder compaction method," *Materials Letters,* vol. 83, pp. 17-19, 2012.

[22] G. Kotan and A. S. Bor, "Production and characterization of high porosity Ti-6Al-4V foam by space holder technique powder metallurgy," *Turkish Journal of Engineering and Environmental Science,* vol. 31, pp. 149-156, 2007.

[23] S. W. Kim, H. D. Jung, M. H. Kang, H. E. Kim, Y. H. Koh and Y. Estrin, "Fabrication of porous titanium scaffold with controlled porous structure and net-shape using magnesium as spacer," *Materials Science and Engineering C,* vol. 33, pp. 2808-2815, 2013.

[24] C. E. Wen, M. Mabuchi, Y. Yamada, K. Shimojima, Y. Chino and T. Asahina, "Processing of biocompatible porous Ti and Mg," *Scripta Materialia,* vol. 45, pp. 1147-1153, 2001.

[25] B. Otsuki, M. Takemoto, S. Fujibayashi, M. Neo, T. Kokubo and T. Nakamura, "Pore throat size and connectivity determine bone and tissue ingrowth into porous implants: Three-dimensional micro-CT based structural analyses of porous bioactive titanium implants," *Biomaterials,* p. 27, 2006.

[26] R. Heckel, "Density-pressure relationships in powder compaction," *Transactions of the Metallurgical Society of AIME,* vol. 221, pp. 671-675, 1961.

Chapter 4

Characterization of space holder removal through water leaching method for preparation of biomedical titanium scaffold

This chapter is adapted from:

- A new technique for the characterization of the water leaching behavior of space holding particles in the preparation of biomedical titanium scaffolds
  B. Arifvianto, M.A. Leeflang and J. Zhou, Materials Letters, (2014) Vol. 120, pp. 204–207.
- Characterization of space holder removal through water leaching method for preparation of biomedical titanium scaffold
  B. Arifvianto, M.A. Leeflang, J. Duszczyk and J. Zhou, Powder Metallurgy, (2014) Vol. 57, pp. 9-12.

4.1. Introduction

In the space holder method, porous structure of metallic scaffolds can be achieved after the removal of space holding particles from the scaffold preform. As discussed in Chapter 2, the removal of space holding particles largely governs the final pore characteristics, structural integrity and purity of the scaffold. Water leaching is a preferred choice for removing the space holding particles from the scaffold preform, considering environmental effects related to removal products [1, 2]. The use of this method has been reported in the fabrication of several metallic foams and scaffolds prepared with water-dissolvable space holding particles such as carbamide [3, 4, 5, 6], sodium chloride [1, 7, 8] and carbohydrate [9]. However, the studies on the space holder removal by water leaching are scarce in the open literature, largely because the information on the testing procedures and water leaching behavior of space holding particles are considered proprietary.

The objective of the work in this chapter is therefore to understand the water leaching behavior of carbamide space holding particles in the preparation of biomedical titanium scaffolds. Leaching tests were performed using a novel real-time weight measurement technique. The results were then verified with the existing models for the solvent debinding process for powder injection molded parts. This aided in establishing the mechanisms operating during the leaching process and removal of carbamide space holder particles.

This study begins with a description of the method for quantitative characterization of the water leaching behavior, as shown in Section 4.2. The leaching tests are then conducted for titanium scaffold preforms with various volume fractions of carbamide space holder. In Section 4.3, the results are presented and verified with the existing models for the solvent debinding process for powder injection molded parts. This aids in establishing the mechanisms operating during the leaching process and removal of carbamide space holder particles, as discussed in Section 4.4. Finally, conclusions are given in Section 4.5 to summarize all the findings of this study.

4.2. Materials and Methods

4.2.1. Materials preparation

A gas-atomized grade 1 titanium powder (TLS Technik GmbH & Co., Germany) with spherical shape and sizes of 63-90 μm and a carbamide powder (Merck, Germany) a cubical particle shape and particle sizes of 250-710 μm were chosen as the matrix and space holder materials, respectively. Volume fraction of the carbamide space holding particles was varied from 38 to 60%. A binder solution was prepared by dissolving 4 wt% polyvinyl-alcohol (PVA) particles (Alfa Aesar GmbH & Co KG, Germany) in water at 80-90ºC. The titanium and carbamide particles were mixed in a cylinder mixer for 2 h. Stepwise particle filling of a mixing container was conducted with 1 vol.% binder solution. Carbamide particles and granules of carbamide particles surrounded by smaller titanium particles resulting from the mixing were cold-compacted in a single-action uniaxial press (Carver Inc., USA) under a pressure of 400 MPa held at that pressure for 5 min. Carbamide compacts and scaffold preforms with a diameter of 12 mm and a height of 3-5 mm were used for immersion and leaching tests.

4.2.2. Water leaching tests

Fig. 4.1 shows the schematic of the experimental set-up for the leaching tests based on ASTM B963-08 standard. The scaffold preform was immersed in 250 ml distilled water at room temperature (21 ºC), supported by a basket with a mesh structure that allowed carbamide space holding particles to leach out from all the surfaces of the scaffold preform. Non-corrosive wires and frame were used to connect the basket to a weight balance (Denver Instrument, AA-160, USA). The leaching tests were carried out in triplicate for each group of the scaffold preform.

The initial weight of the scaffold preform in water ($W_{0,w}$) was calculated using Eq. (4.1):

$$W_{0,w} = W_{0,a}\left(1 - \frac{\rho_w}{\rho_s}\right) \tag{4.1}$$

where $W_{0,a}$ is the initial weight of scaffold preform in air and ρ_w and ρ_s are the density of water and scaffold preform, respectively. The density of the scaffold preform consisting of titanium matrix particles and space holding particles was calculated using Eq. (4.2):

$$\rho_s = (1-x)\rho_m + x\rho_{sh} \tag{4.2}$$

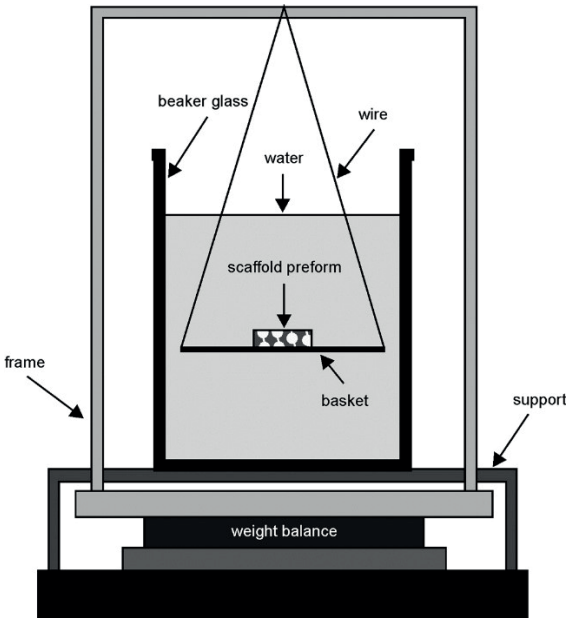

Fig. 4.1. Schematic of the experimental setup (Reprinted with permission from Elsevier)

where ρ_m and ρ_{sh} are the densities of titanium matrix particles (4.5 g cm^{-3}) and carbamide space holding particles (1.32 g cm^{-3}), respectively and x is the space holder volume fraction in the scaffold preform. The space holder removal was quantified by measuring the weight of scaffold preform after certain duration of immersion ($W_{t,w}$). The weight loss at certain immersion period was determined using Eq. (4.3) as percentage of scaffold preform relative weight (W_t*):

$$W_t^* = W_{t,w}/W_{0,w} \tag{4.3}$$

The leaching behaviour of the space holder could also be expressed quantitatively by percentage of removed space holder during immersion (W_d*) such as in Eq. (4.4),

$$W_d^* = \left(\frac{W_{0,w} - W_{t,w}}{W_{0,w} - W_{f,th}} \right) \tag{4.4}$$

where $W_{f,th}$, as defined in Eq. (4.5), is the expected final weight of the scaffold preform after complete removal of the space holder,

$$W_{f,th} = (1-x)\left(\frac{\rho_m}{\rho_s} \right) W_{0,w} \tag{4.5}$$

The space holder removal efficiency was determined from the percentage of removed space holder at saturation.

4.2.3. Mathematical models

The space holder removal process by water leaching is principally similar to the solvent debinding process of powder injection molded parts. Hence, the existing solvent debinding models were applied in this study to evaluate and determine possible mechanisms operating during the leaching process of space holding particles. The existing solvent debinding models used in this study are briefly described in the following.

1. Modified Lin-German model

Lin and German developed a solvent debinding model in Eq. (4.6) based on Fick's law in one dimension [10]:

$$\ln\frac{1}{F} = \frac{D_e \pi^2}{(2L)^2} t \tag{4.6}$$

In this case, F is the fraction of remaining binder or space holder in the component, i.e. $F = 1 - W_d^*$, t and D_e are the debinding or leaching duration and the effective diffusion, respectively and L is the shortest distance travelled by dissolved binder or space holder from the symmetry plane to the surface of the component. This model was modified into Eq. (4.7) by introducing effective length scale (ψ) to replace L for use in three dimensional cases [10]:

$$\ln\frac{1}{F} = \frac{D_e \pi^2}{(2\psi)^2} t \tag{4.7}$$

The effective length scale, ψ, which is the ratio of volume and surface area of the component, is expressed in Eq. (4.8) for cylindrical specimen as in the present case:

$$\psi = \frac{\pi D^2 H/4}{\pi D(H + D/2)} \tag{4.8}$$

where D and H are the diameter and height of the scaffold preform. With this model, the leaching data in $\ln(1/F)$ were plotted against t/ψ^2.

2. Square-root debinding model

Kim et al. [11] indicated that the weight fraction of the removed binder (W_d^*) from powder injected parts was proportional to square-root of debinding times as described in Eq. (4.9):

$$W_d^* = 2\left(\frac{D_e t}{\pi L^2}\right) \tag{4.9}$$

The square-root debinding model was also developed by Krauss et al. [141]. Both models were however developed for one-dimensional condition. In this study, L is therefore replaced by ψ such as seen in Eq. (4.10):

$$W_d^* = 2\left(\frac{D_e t}{\pi \psi^2}\right) \tag{4.10}$$

4.3. Results

4.3.1. Water leaching mechanisms

In this research, the influence of PVA binder solution on the dissolution of carbamide particles was studied through the weight loss measurement of carbamide compacts during the water immersion. Rapid removal of carbamide compacts was clearly seen in Fig. 4.2. However, only small amount of the PVA compacts were dissolved in water over total immersion period of 10 min, leaving about residue with 80 wt.% in water. Obviously, the addition of 4 vol.% PVA binder solution retarded dissolution of the carbamide compact.

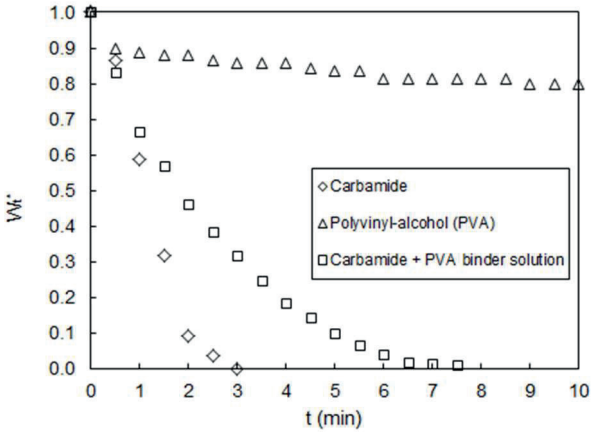

Fig. 4.2. Measured weight losses of carbamide and PVA compacts
(Reprinted with permission from Tandfoline)

Fig. 4.3 shows the continuous plot of weight losses of the scaffold preform prepared with 50.5 vol.% carbamide space holder, indicating reliability and accuracy of the measurements, over a total immersion period of 45 min and the corresponding standard deviations (S.D.) resulting from triplicate measurements. Signal noises of the measured weight in the weighing balance were however observed during the first 15 – 20 s of immersion (data not shown) and the plot was discontinuous when $t < 30$. The weight of the scaffold preform decreased smoothly and decayed at $t \approx 32$ min with $W^* \approx 0.84$. The reproducibility of the data acquired from using this technique was evident, as can be seen from the standard deviation values fluctuating over a range of 0.002 – 0.007.

Fig. 4.4 shows the leaching behavior of the carbamide space holder in terms of the percentage of removed weight fraction. Precision of the novel characterization technique in the current study was demonstrated by comparing with the leaching behavior studied by Bafti and Habibolahzadeh [5].

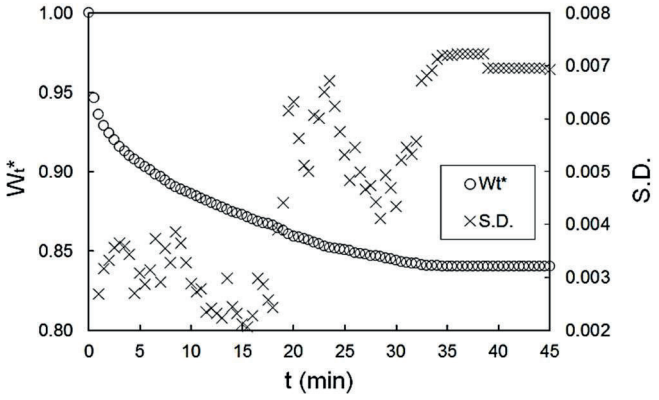

Fig. 4.3. Weight losses of the titanium scaffold preform prepared with 50.5 vol.% carbamide space holder (Reprinted with permission from Elsevier)

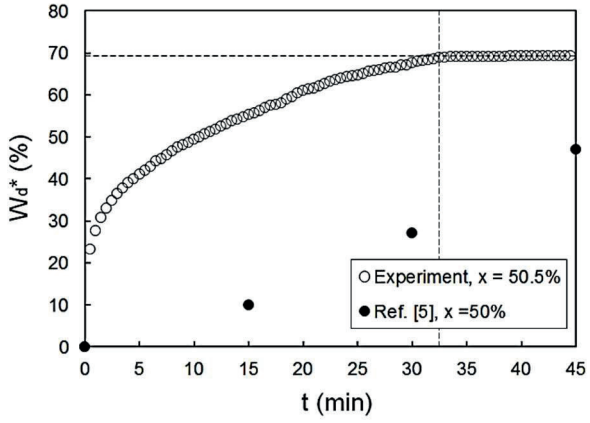

Fig. 4.4. Weight fractions of dissolved carbamide particles during immersion in this study and from the work by Bafti and Habibolahzadeh [5]. (Reprinted with permission from Elsevier)

Fitting the data acquired with the present technique into the existing solvent debinding models (Fig. 4.5) appears to be meaningful. Regression was applied to the plot to get an insight into the leaching process of carbamide particles according to this model. In this study, the regression lines appeared to be acceptable, when a criterion of R^2 value being as close as 1 was fulfilled. Three primary regimes of the space holder leaching process were identified, namely (i) rapid dissolution-controlled regime, (ii) dissolution and diffusion-controlled regime and (iii) saturation regime.

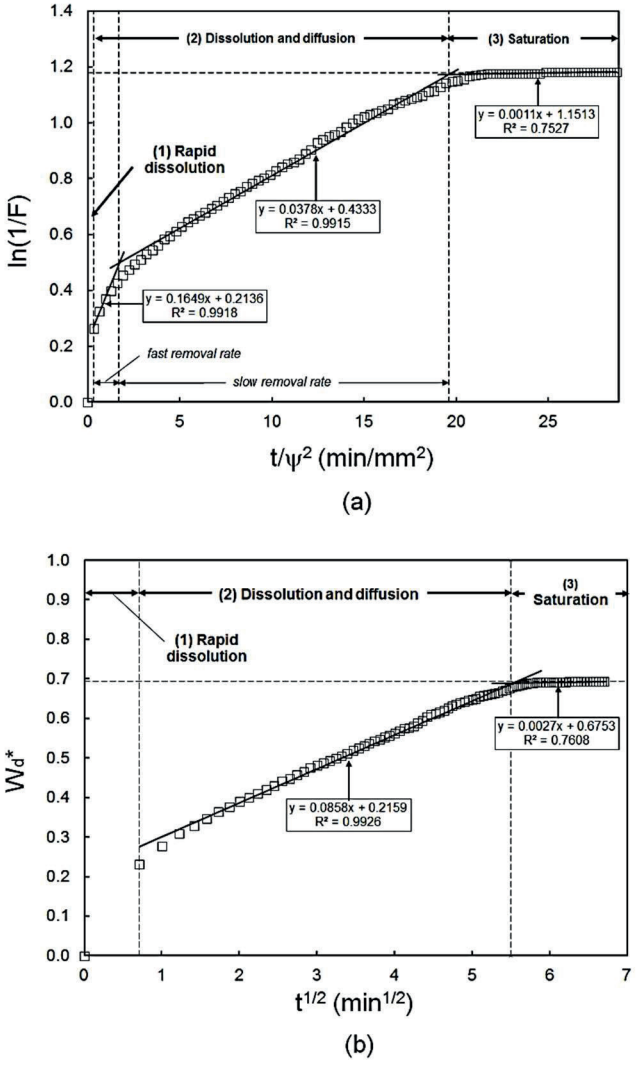

Fig. 4.5. Application of (a) the modified Lin-German model and (b) the square-root model to the water leaching process for the removal of carbamide space holding particles (Reprinted with permission from Elsevier)

The first rapid dissolution-controlled regime was marked by a discontinuous plot corresponding to the first 30 s of immersion. Based on the modified Lin-German model (Fig. 4.5a), the dissolution and diffusion-controlled regime could be subdivided further into regions with fast and slow removal rates. Despite the absence of this transition, the plot with the square-root model confirms the diffusion-controlled regime that occurred after the rapid dissolution process (Fig. 4.5b). In the case of titanium scaffold preform with 50.5 vol.% carbamide content, the

effective diffusion coefficients (D_e) derived from the modified Lin-German are 11.13×10^{-6} and 2.55×10^{-6} cm^2s^{-1} for fast and slow removal rate, respectively. Meanwhile, the D_e value derived from the square-root model is 1.51×10^{-6} cm^2s^{-1}.

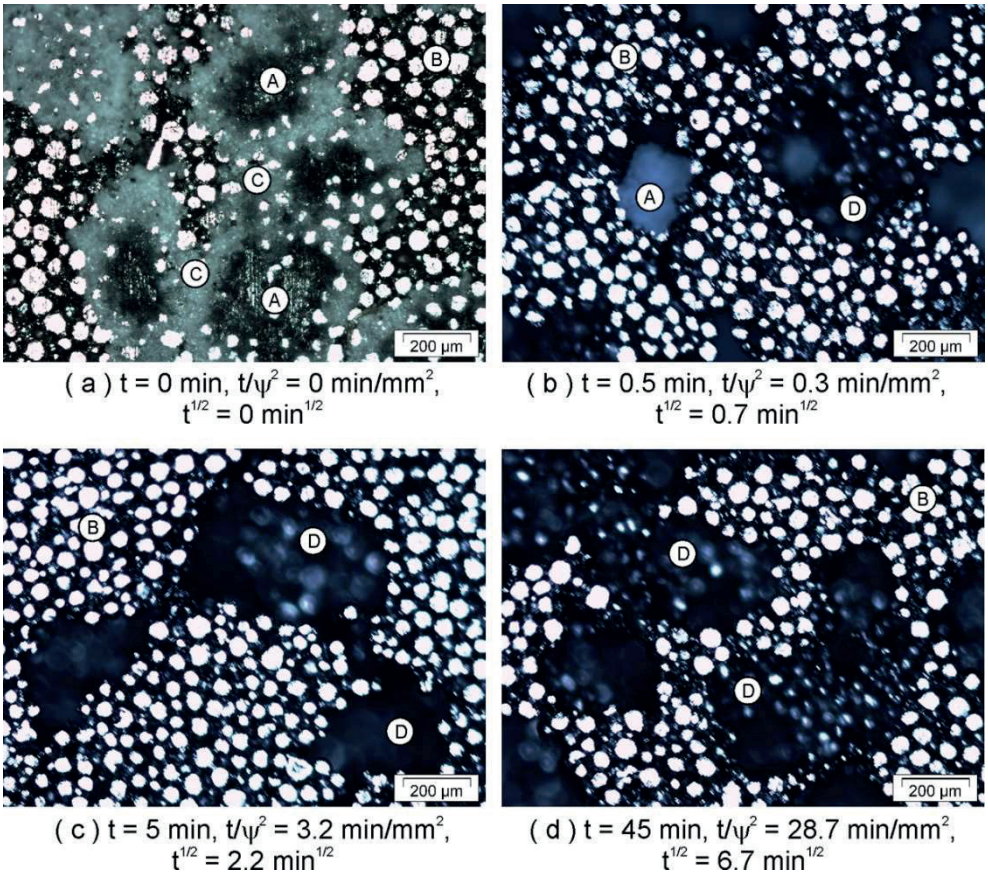

Fig. 4.6. Formation of surface openings and interconnected pores in the scaffold preform during the water leaching process (Reprinted with permission from Elsevier)

A series of micrographs (Fig. 4.6) show the progressive evolution of the porous surface structure of the scaffold preform during the water leaching and space holding particle removal process. It is obvious in Fig. 4.6a that the initial scaffold preform consisted of carbamide space holding particles (A) surrounded by dried binder solution (C) and titanium particles (B). In this study, the dissolution of carbamide particles on the surface of the scaffold preform occurred during the first 30 s of immersion, yielding openings (D) as shown in Fig. 4.6b. However, deeper water penetration through these openings and further dissolution of carbamide space holding particles in the interior of the scaffold were not achieved over this immersion period. This was confirmed by the presence of carbamide particles at the subsurface of the scaffold preform.

Interconnected pores growing into the interior of the scaffold preform were formed after 5 and 45 min of immersion, as shown in Figs. 4.6c and 4.6d, respectively. The larger openings observable on the surface of the scaffold preform after 45 min of immersion might result from the partial collapse of titanium particles around the pores.

4.3.2. The influence of space holder contents on the water leaching behavior

The removal of carbamide particles from titanium scaffold preforms by water leaching is indicated in Fig. 4.7, with characteristics depending on the space holder volume fraction. It is shown that a more weight loss occurred during the immersion of scaffold preforms with a larger space holder volume fraction. With this figure, however, the characteristics of the space holder removal by water leaching were difficult to be analyzed considering the remaining titanium matrix.

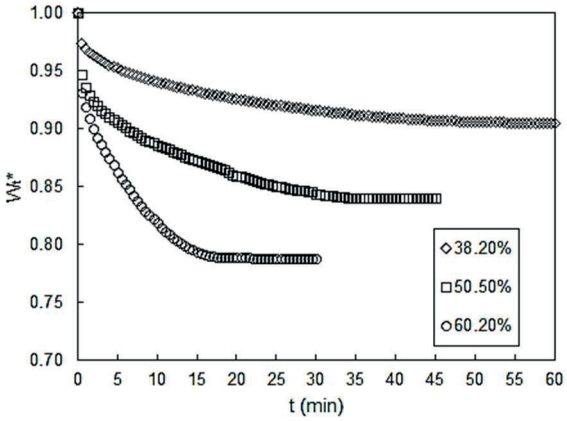

Fig. 4.7. Measured weight losses of titanium scaffold preforms prepared with various space holder volume fractions (Reprinted with permission from Tandfoline)

Plotting the weight loss data of the scaffold preforms based on the modified Lin-German and square-root solvent debinding models resulted in curves as shown in Figs. 4.8. It is obvious in Fig. 4.8 that the space holder removal rates increase with the increasing volume fraction of the space holder in the scaffold preforms. With the plots in Fig. 4.8b, the efficiency of the space holder removal by water leaching (η) could be determined from the maximum fraction of removed carbamide particles from the scaffold preform. The influence of the carbamide volume fraction on the space holder removal efficiencies is indicated in Table 4.1. A higher space holder removal efficiency was also found in the scaffold preforms with a greater space holder volume fraction, although the removal efficiency of the scaffold preforms of 50.5 vol.% space holder was slightly greater than that of 60.2 vol.%. It is however important to note that saturation of the leaching process of the latter scaffold preforms occurred earlier, indicating the lower space holder removal rates of the former scaffold preforms.

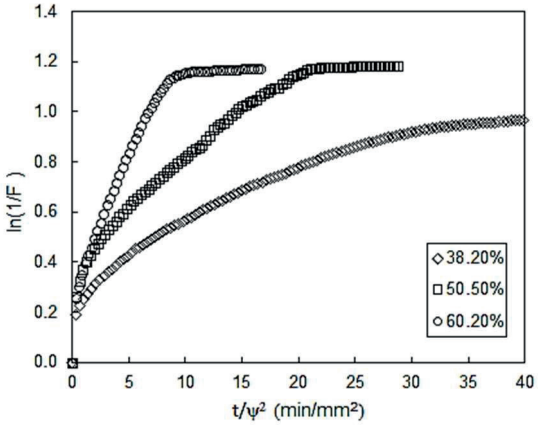

(a)

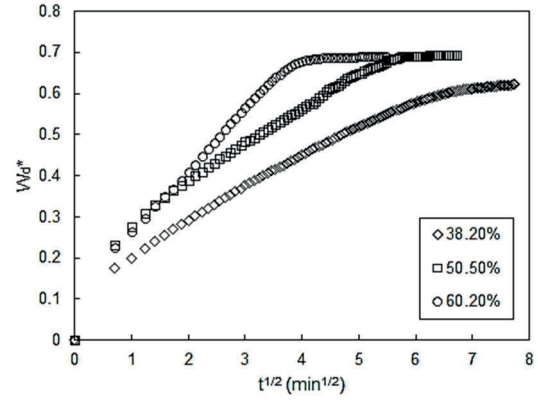

(b)

Fig. 4.8. Plots of the leaching data of the carbamide space holder in the scaffold preform with various space holder volume fraction (a) modified Lin-German model and (b) square-root model (Reprinted with permission from Tandfoline)

With the aid of the solvent debinding models and regression, the effective diffusivities (D_e) in the leaching process of carbamide space holder could also be determined such as seen in Table 4.2. The use of the modified Lin-German model resulted in a slightly higher D_e values than those with the square-root model. However, both models obviously indicated the increasing D_e values with the addition of space holder volume fraction in the scaffold preforms. With the modified Lin-German model, however the transition of regions with the fast and slow removal rates in the scaffold preforms with 60.2 vol% space holder could not be recognized.

Table 4.1. Space holder removal efficiencies

x (%)	η (%)
38.2	62.1
50.5	69.3
60.2	68.9

Table 4.2. Effective diffusivities of carbamide space holding particles in the scaffold preforms during the leaching process

Volume fraction (%)	Modified Lin-German model						Square-root model		
	Fast removal rate			Slow removal rate					
	m	R^2	D_e (x10^{-6} cm s^{-1})	m	R^2	D_e (x10^{-6} cm s^{-1})	m	R^2	D_e (x10^{-6} cm s^{-1})
38.2	0.0718	0.9899	4.85	0.0186	0.9676	1.26	0.0676	0.9850	0.86
50.5	0.1649	0.9918	11.13	0.0378	0.9915	2.55	0.0858	0.9926	1.51
60.2	0.1089	0.9935	7.35	-	-	-	0.1494	0.9991	5.28

m = regression slope

4.4. Discussion

In the current research, the water leaching behavior of in the removal of carbamide space holding particles for the preparation of biomedical titanium scaffolds was studied. A novel real-time weight measurement technique was introduced for a quantitative characterization of the leaching process.

Prior to the water leaching characterization of titanium scaffold preform, it is of importance to investigate the contribution of PVA binder on dissolution of carbamide powder. Since titanium/carbamide powder mixture tended to segregating without binder addition, the water leaching test was then performed in a compacted carbamide powder. As seen in Fig. 4.2, the carbamide compact was dissolved rapidly, indicating high solubility of this material in water as reported by Salman [12]. With the addition of PVA binder solution, dissolution of carbamide compact retarded. In this case, the binder solution coated the surface of the carbamide particles and acted as a barrier that prevents the carbamide particles from direct contact with water.

The earlier investigations into the water leaching behavior of space holder yielded the results of considerably lower accuracy, owing to the handling for weighing and drying scaffold preforms after extraction from water [5]. The weight loss measurement in the previous studies was taken only once every 10 to 30 min [1, 3, 4, 5, 9]. In addition, handling for weighing after extraction from water reduced the structural integrity and even ruined scaffold preforms [1]. Drying of scaffold preforms at temperatures of 40 – 110 ºC for 0.5 to 6 h [1, 3, 5] was time-consuming and might result in the evaporation of residual water together with dissolved space holder and thus

inaccuracy. As a consequence, the measured weight values of scaffold preforms deviated from the actual weight values.

On the basis of this study, the possible mechanism of water leaching for the removal of carbamide space holding particles from the scaffold preform can be proposed. The space holder removal through water leaching commences by the immediate dissolution of space holding particles at the surface of scaffold preform, leading to the rapid dissolution process. Openings are then formed in the surfaces, allowing deeper penetration of water into the interior of scaffold preform. As more interconnected pores are formed in the interior of the scaffold preform, the leaching behavior and space holder removal become controlled by the dissolution and diffusion process. With increasing immersion time, longer channels of interconnected pores are formed and the removal rate decreases, finally leading to the saturation of the leaching process. It is however important to note that the saturation of the leaching process does not always correspond to the complete removal of carbamide particles from scaffold preform. In the case of titanium scaffold preform having 50.5 vol.% space holder fraction, only about 69% of the total carbamide particles could be removed from the scaffold preform, which means that some residual carbamide particles were still present in the scaffold preform.

With the aid of the solvent debinding models and regression, the effective diffusivities (D_e) in the leaching process of scaffold preform with various space holder volume fractions could also be determined such as seen in Table 4.2. The use of the modified Lin-German model resulted in a slightly higher D_e values than those with the square-root model. However, both models obviously indicated the increasing D_e values with the addition of space holder volume fraction in the scaffold preforms. This implies that the more channels and interconnected pores were formed in the scaffold preform with the greater space holder volume fraction, that finally resulted in the increased water diffusivity in the interior of the scaffold preforms. A higher space holder removal efficiency was also found in the scaffold preform with a greater space holder volume fraction, although the removal efficiency of the scaffold preform of 50.5 vol.% space holder was greater than that of 60.2 vol.%. It is however important to note that the saturation of the leaching process of the latter scaffold preform occurred earlier, indicating a lower space holder removal rate of the former scaffold preform.

4.5. Conclusions

Space holder removal by water leaching in the fabrication chain of biomedical titanium scaffold was investigated using a novel and accurate weight measurement technique. With this characterization technique, the scaffold weight losses due to the removal of space holding particles were precisely read. The mechanisms operating in the space holder removal by water leaching were also determined based on the existing solvent debinding models for powder injection moulded parts. Three primary regimes representing the leaching behavior of the carbamide particles in the scaffold preforms were recognized, namely (i) rapid dissolution, (ii) dissolution and diffusion and (iii) saturation. In addition, a higher effective diffusivity values and space holder removal efficiency in the leaching process were found in the scaffold preforms with a greater space holder volume fraction.

References

[1] Y. Torres, J. J. Pavón and J. A. Rodríguez, "Processing and characterization of porous titanium for implants by using NaCl as space holder," *Journal of Materials Processing Technology,* vol. 212, pp. 1061-1069, 2012.

[2] A. Bansiddhi and D. Dunand, "Shape-memory NiTi foams produced by replication of NaCl space-holders," *Acta Biomaterialia,* vol. 4, pp. 1996-2007, 2008.

[3] H. Bakan, "A novel water leaching and sintering process for manufacturing highly porous stainless steel," *Scripta Materialia,* vol. 55, pp. 203-206, 2006.

[4] H. Gülsoy and R. German, "Sintered foams from precipitation hardened stainless steel powder," *Powder Metallurgy,* vol. 51, pp. 350-353, 2013.

[5] H. Bafti and A. Habibolahzadeh, "Production of aluminum foam by spherical carbamide space holder technique," *Materials and Design,* vol. 31, pp. 4122-4129, 2010.

[6] B. Jiang, N. Zhao, C. Shi and J. Li, "Processing of open cell aluminum foams with tailored porous morphology," *Scripta Materialia,* vol. 53, pp. 781-785, 2005.

[7] A. Bansiddhi and D. C. Dunand, "Shape-memory NiTi foams produced by replication of NaCl space-holders," *Acta Biomaterialia,* vol. 4, pp. 1996-2007, 2008.

[8] R. Surace, L. De Filippis, A. Ludovico and G. Boghetich, "Influence of processing parameters on aluminium foam produced by space holder technique," *Materials and Design,* vol. 30, pp. 1878-1885, 2009.

[9] N. Michailidis, F. Stergioudi and A. Tsouknidas, "Deformation and energy absorption properties of powder-metallurgy produced Al foams," *Materials Science and Engineering A,* vol. 528, pp. 7222-7227, 2011.

[10] T. Shivashankar and R. German, "Effective length scale for predicting solvent-debinding times of components produced by powder injection molding," *Journal of the American Ceramics Society,* vol. 82, pp. 1146-1152, 1999.

[11] S. Kim, H. Lee, H. Song and B. Kim, "Pore structure evolution during solvent extraction and wicking," *Ceramics International,* vol. 22, pp. 7-14, 1996.

[12] O. Salman, "Polymer coating on urea prills to reduce dissolution rate," *Journal of Agricultural and Food Chemistry,* vol. 36, pp. 616-621, 1988.

Chapter 5

Characterization of the porous structures of the green body and sintered biomedical titanium scaffolds with micro-computed tomography

This chapter is adapted from:
Characterization of the porous structures of the green body and sintered biomedical titanium scaffolds with micro-computed tomography
B. Arifvianto, M.A. Leeflang and J. Zhou, Materials Characterization (2016), Vol. 121, pp. 48-60.

5.1. Introduction

The space holder method has been considered to be one of the viable techniques for the fabrication of titanium scaffolds. As noted in Chapter 2, however, a number of technological challenges are still being taken up, such as the difficulties in controlling the changing porous structure through a series of fabrication steps involved in this technique. Owing to the limitations inherent to conventional characterization techniques, the knowledge of the transformation of space-holding particles in the green body into macro-pores in the scaffold and the changes of the 3-dimensional (3D) porous structure during scaffold fabrication is lacking. As a consequence, the question remains unanswered as to whether the final porous structure of the scaffold could be controlled from its green structure.

Laptev et al. [1] and Tuncer et al. [2] tried to link the physical properties of the green body with those of the sintered titanium scaffolds prepared with the space holder method. By calculating the relative density, Laptev et al. [1] noticed that the green body was densified to some extent during sintering, as indicated by an increase in the relative density of the scaffold. This result was confirmed by the measured axial and radial shrinkages of the green body during sintering [1]. Owing to the irregular porous structure prepared with the space holder method, however, the work conducted by Laptev and his co-workers [1] did not reveal detailed spatial changes in the interior of the scaffold as a result of sintering. Obviously, to understand the

shrinkage phenomena that occurred during the sintering of titanium scaffolds prepared with the space holder method, 3-dimensional (3D) analysis is needed. Tuncer et al. [2] utilized micro-computed tomography (micro-CT) to analyze the changes of the 3D porous structure from the green body to the titanium scaffold as a result of sintering. In their study, pore wall thickening and slight decreases in the sizes of macro-pores created by the space holder, accompanied by the overall shrinkage of the green body during sintering, were reported [2]. Despite the precise quantitative and qualitative analysis of the 3-dimensional (3D) porous structure of the scaffold [3], the micro-CT study conducted by Tuncer et al. [2] did not provide information on the shrinkage occurring during sintering with representative geometrical parameters, such as pore interconnection and specific surface area both of which are actually of critical importance for the explanation of the shrinkage mechanisms as well as for bone tissue regeneration inside the scaffold [3]. As mentioned earlier, pore interconnection is needed to provide access for the transport of nutrients, oxygen and metabolic waste through the scaffold as well as to facilitate cellular activities, e.g. cell migration, for the growth of new bone tissue [3, 4]. Also needed is a high ratio of surface area to volume to enhance cellular attachments for bone tissue ingrowth [3].

On the basis of the understanding of the structural evolutions throughout the scaffold fabrication with the space holder method, it was hypothesized that the final porous structure of titanium scaffold product prepared with this method could be estimated from the titanium and space-holding powder arrangements in the green body. To test this hypothesis, the porous structures of both the green body and the sintered titanium scaffolds prepared with the space holder method were quantitatively characterized. As described in Section 5.2, micro-CT and image analysis were performed to determine the porosity and geometrical parameters of the green body containing carbamide space-holding particles and the sintered titanium scaffolds in order to establish the mechanisms involved in the structural changes from the green body to the final scaffold products. In this connection, the water leaching process for the complete removal of the space holder material from the green body and the sintering process that resulted in shrinkage were examined. The results are presented in Section 5.3. Then, the mechanisms involved in the structural changes of the porous titanium material due to sintering are proposed in Section 5.4. Finally, the conclusions drawn from this research are given in Section 5.5.

5.2. Materials and methods

5.2.1. Scaffold preparation

Titanium scaffolds were prepared by mixing a spherical grade 1 titanium powder (TLS Technik, Germany) and a cubical carbamide powder (Merck, Germany) as the matrix and space holder materials, respectively. The mean and median diameters of both the powders determined from five samples by using a Mastersizer X laser diffractometer (Malvern, UK) are presented in Table 5.1.

The compositions of the mixtures (x) were established by recalling Eq. 2.1c:

$$x = \frac{m_{sh}/\rho_{sh}}{m_m/\rho_m + m_{sh}/\rho_{sh}} \quad (2.1c)$$

where m_m and m_{sh} are the masses of the titanium powder and carbamide space-holding particles added to the matrix, respectively, and ρ_m and ρ_{sh} are the theoretical densities of titanium (i.e., 4.5 g cm^{-3}) and carbamide (i.e., 1.32 g cm^{-3}), respectively. In this research, m_m and m_{sh} were adjusted to produce titanium scaffold preforms with x = 40, 50, 60, 70 and 80 vol.%. Mixing of the titanium and carbamide powders was carried out with a roller mixer (CAT, Germany) operating at 80 rpm. A dry cylindrical glass bottle having an inner diameter of 40 mm and a length of 52 mm was used as the mixing container. To prevent the mixture from segregating, the titanium powder was first blended with a 6 wt.% polyvinyl-alcohol (PVA) binder solution for 1 h prior to 3 h mixing with the dry carbamide powder. The binder solution was prepared by dissolving 6 wt.% PVA particles (Alfa Aesar, Germany) in water at 80 - 90 ºC.

Table 5.1. Sizes of titanium and carbamide powder particles

Particle size parameter	Titanium	Carbamide
Particle mean diameter, D_m (μm)	71.47 ± 1.47	415.62 ± 5.66
Particle diameter (10 vol.% of the sample particles below this size) D_{10} (μm)	55.28 ± 1.06	285.55 ± 5.42
Particle diameter (50 vol.% of the sample particles below this size, i.e., the median particle diameter), D_{50} (μm)	70.26 ± 1.29	396.94 ± 5.04
Particle diameter (90 vol.% of the sample particles below this size), D_{90} (μm)	89.50 ± 2.69	573.52 ± 9.16

Compaction of titanium/carbamide powder mixtures was conducted with a uniaxial powder press (Carver, USA). At this step, approximately 1.3 g powder mixture was cold-compacted in a 13 mm diameter die (Carver Inc., USA) and at uniaxial compressive pressures of 260, 220, 180, 140 and 100 MPa for preparing titanium scaffold preforms with 40, 50, 60, 70 and 80 vol.% carbamide particles, respectively [5]. The removal of carbamide particles from the scaffold preforms was performed with the water leaching technique. Detailed procedures and methods for characterizing the water leaching behavior of carbamide are presented in Subsection 2.3. The porous green body was then sintered at 1200 ºC for 3 h.

5.2.2. Characterization of porous structure of the green body and sintered scaffolds

3D structures of titanium scaffold preforms and sintered scaffold products were characterized by using X-ray micro-computed tomography (micro-CT) (Nanotom, Phoenix/X-rays, The Netherlands). With this technique, a set of 2-dimensional (2D) radiographs of a projected structure with carbamide particles or a projected porous scaffold with an image

resolution of 10 μm were generated. A 3D model of the structure with dimensions of 2.5 × 2.5 × 2.5 mm was then constructed by cropping a stack of radiographs and analyzed quantitatively by using the open-source ImageJ 1.50i software [6] with BoneJ plugin that was originally intended for the characterization of the trabecular structure of bone tissue [7].

Quantitative analysis was performed by applying auto local thresholding using the Bernsen method (radius = 30). An additional series of image processing steps were followed for the analysis of macro-pores, i.e., median filter application (with a radius of 3 pixels) and purification to eliminate micro-pores and isolated small pores in the 3D model of the scaffold.

Both ImageJ and BoneJ plugin have been used in other studies, for instance, in the investigation of bone histomorphometry [8] and the porous structures of tissue engineering scaffolds [4]. By using BoneJ, a set of structural parameters describing the characteristics of scaffold preforms or scaffolds could be determined, i.e., (i) porosity (p), which is derived from the ratio of the framework volume and the total volume of the 3D model (BV/TV); (ii) the connectivity density of the pores that are formed from the space occupied by space-holding particles (*Conn.D.*); (iii) the specific surface area of the matrix framework (SSA), which is derived from the surface area of the framework (BS) divided by the total volume of the 3D model (iv) the thickness of the matrix framework (*Th.Ti.*) and (v) the spacing of the space occupied by space-holding particles in the scaffold preform (*Th.Sp.*). All these structural parameters were determined in triplicate and plotted against the volume fraction of the carbamide space holder embedded in the titanium matrix.

Observation of the morphologies of macro- and micro-pores in the titanium scaffold was carried out by using a JSM-6500F field emission scanning electron microscope (JEOL, Japan). Prior to the characterization, the sample was first ground to expose the interior of the scaffold and cleaned by sonication for 5 min in ethanol.

5.2.3. Characterization of the water leaching process

The leaching behavior of carbamide space-holding particles was characterized by measuring the real-time weight losses of the scaffold green body during immersion in 250 ml demineralized water, as described in Ref. [9] or Chapter 4. With this method, the fraction of carbamide removed from the scaffold preform was measured over immersion time. The removed carbamide particles from the scaffold green body during the leaching process was quantified by using Eqs. 4.1 – 4.5.

In order to determine the leaching rate, the effective diffusivity of dissolving space-holding particles inside the scaffold preform D_e was determined by fitting the data into the square-root model expressed in Eq. 4.10.

5.2.4. Characterization of space holder residues in the scaffold green body after leaching

To ascertain the complete removal of the carbamide material in the scaffold preforms, X-ray diffraction (XRD) analysis was performed with a Bruker D8 Advance diffractometer (Bruker, The Netherlands). After being taken out of the water bath, the titanium scaffold preform was dried at room temperature for >48 h and then deposited on a Si510 wafer in a polymethyl-

methacrylate (PMMA) sample holder. The measurement was carried out with Cu Kα radiation. The XRD analysis of the initial titanium powder and titanium/carbamide powder compact was also conducted.

5.3. Results

5.3.1. Structures of the green body and sintered titanium scaffolds

Fig 5.1 illustrates a series of typical 2D micro-CT radiographs and 3D models of the green body and the sintered titanium scaffolds prepared with various volume fractions of carbamide. As shown in the left column (Fig. 5.1a), the radiographs displayed the space holder material as dark-colored particles spreading over the brighter titanium matrix in the scaffold preforms due to the lower density of carbamide compared to titanium. It was obvious that the number of isolated carbamide powder particles was lower at a higher x value. Comparison between Fig. 5.1a and Fig. 5.1b showed insignificant differences between the dark-colored carbamide particles in the 2D radiographs or 3D models and the macro-pores (Fig. 5.1b) in the sintered scaffolds.

Unfortunately, samples with x = 80% collapsed during water leaching for the removal of carbamide particles. Therefore, further analysis of the sintered samples could not be performed. Samples having x = 55 and 65% were added for the structural analysis of the green body and the sintered titanium scaffolds.

Fig. 5.2 shows the results obtained from the quantitative analysis of the green body and sintered titanium scaffolds, based on micro-CT radiographs. As clearly visible in Fig. 5.2a, the total porosity p values of both the green body and sintered titanium scaffolds were lower than the space holder volume fractions x designed by making use of Eq. 2.1c. Linear regression analysis of the x against p plot appeared to be acceptable, as indicated by the coefficients of confidence R^2 = 0.986 and 0.996 for the green body and the sintered titanium scaffolds, respectively. Based on this analysis, a linear relationship between x and p for the green body and the sintered scaffolds could be established and expressed mathematically by Eqs. 5.1 and 5.2, respectively:

$$p = 1.145\,x - 15.381 \quad \text{(green body)} \tag{5.1}$$

$$p = 1.070\,x - 13.747 \quad \text{(sintered scaffold)} \tag{5.2}$$

The total porosity values of the sintered samples were 1.2 – 8.4% lower than those of the green body.

It is of critical importance to analyze the influence of the volume fraction of the space holder measured by the micro-CT (x_m) on the macro-porosity of the sintered titanium scaffolds (p_{mac}) in order to determine the accuracy of this fabrication technique in achieving the target porosity of the scaffold from its green structure. Fig. 5.2b demonstrates the relationship between the macro-porosity of the green body and the total and macro-porosity of the sintered titanium scaffold. Since macro-pores were formed from the space occupied by the space holder material, the actual volume fraction of carbamide particles in the powder compact could be taken as the macro-

porosity of the scaffold green body. A linear relationship between the x_m and p_{mac} values of the sintered scaffolds was obtained and expressed in Eq. 5.3:

$$p_{mac} = 1.008x_m - 1.313 \quad (5.3)$$

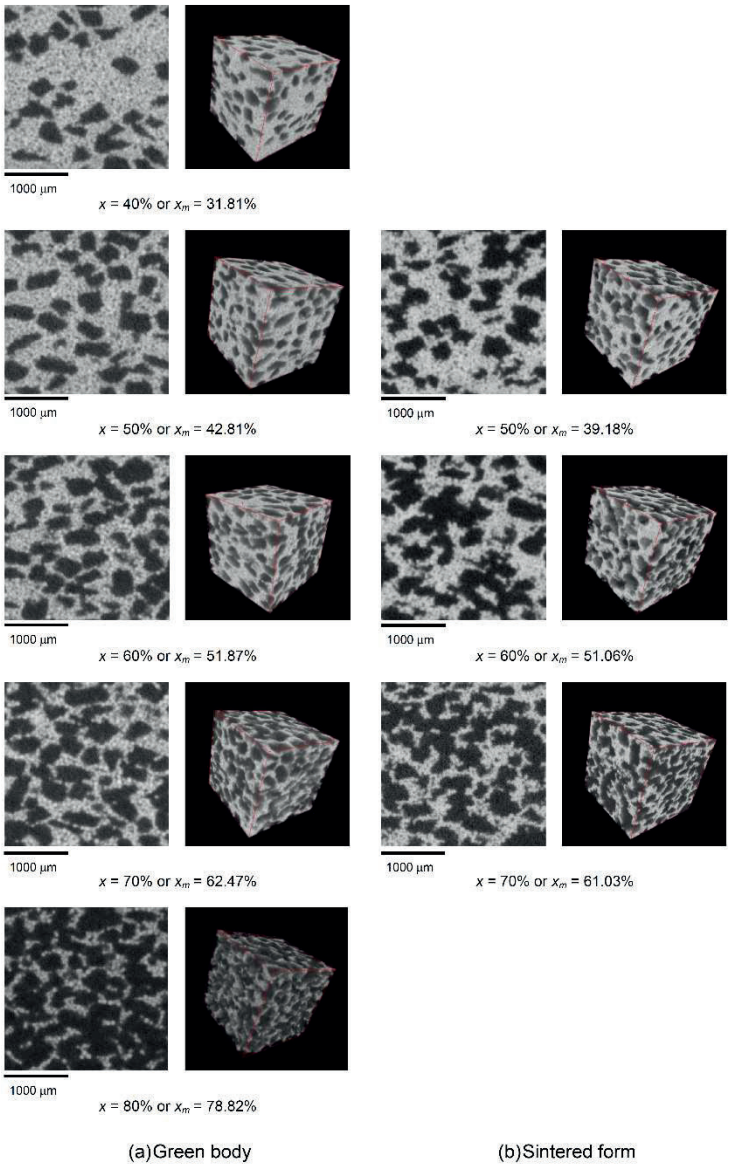

Fig. 5.1. 2D radiographs and 3D models of (a) the green body and (b) sintered titanium scaffolds (Reprinted with permission from Elsevier)

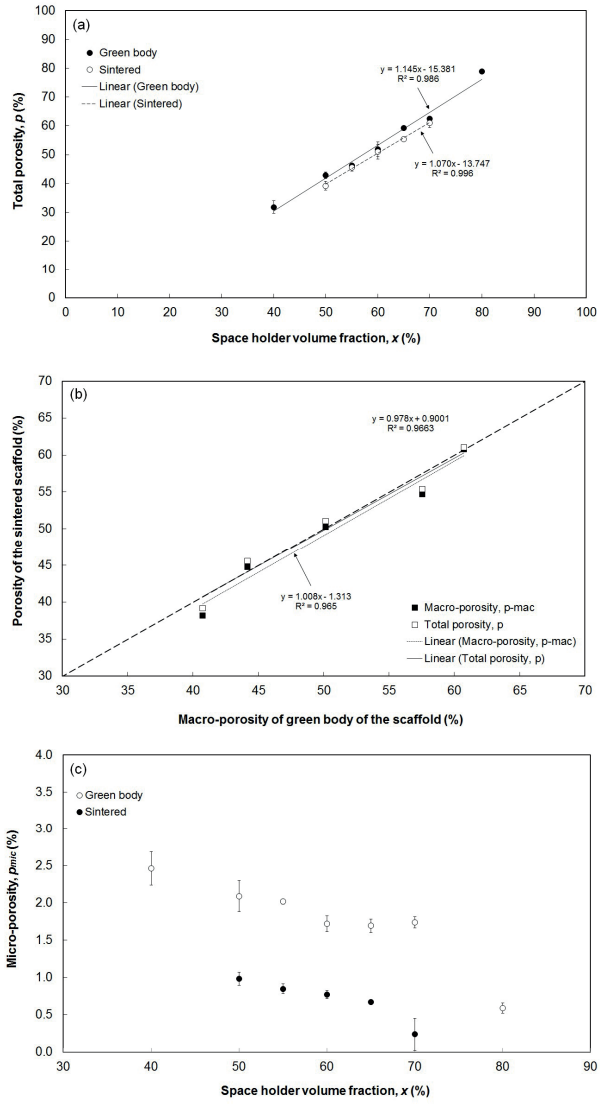

Fig. 5.2. Relationships between (a) the space holder volume fraction (x) and total porosity (p), (b) the macro-porosity of the green body and macro-porosity of the sintered scaffolds (p_{mac}) and (c) the space holder volume fraction (x) and micro-porosity (p_{mic}). (Reprinted with permission from Elsevier)

A linear relationship was obtained when the x_m values were plotted against the total porosity p of the sintered scaffold, as expressed in Eq. 5.4:

$$p = 0.978x_m + 0.9663 \quad (5.4)$$

With the space holder method, macro- and micro-pores are formed from the space occupied by carbamide particles and the interstices between titanium powder particles, respectively. Fig. 5.2c clearly shows that micro-porosity at the titanium framework decreased with increasing space holder volume fraction. After sintering, micro-porosity decreased by 53.11 - 86.37%. Interestingly, the percentage of micro-porosity reduction as a result of sintering increased with rising macro-porosity of the green body.

Figs. 5.3a and 5.3b show the relationships between the space holder volume fraction and the connectivity density determined based on the total porosity (*Conn.D.*$_{total}$) and macro-porosity (*Conn.D.*$_{mac.}$) of the scaffold, respectively. Although the *Conn.D.*$_{total}$ values were generally higher than those of the *Conn.D.*$_{mac.}$ values, both of them increased with rising porosity of the green body or that of the sintered titanium scaffold. Moreover, sintering decreased the pore connectivity at the interior of the scaffolds, except for the sintered samples with x = 70%. With these results, the connectivity density of micro-pores (*Conn.D.*$_{mic.}$) could be determined by subtracting *Conn.D.*$_{mac.}$ from *Conn.D.*$_{total}$. The range of the percentage reductions of *Conn.D.*$_{mic.}$ as a result of sintering was higher than that of *Conn.D.*$_{mac.}$, i.e., 15.05 – 45.04% versus 0.54 – 26.66%.

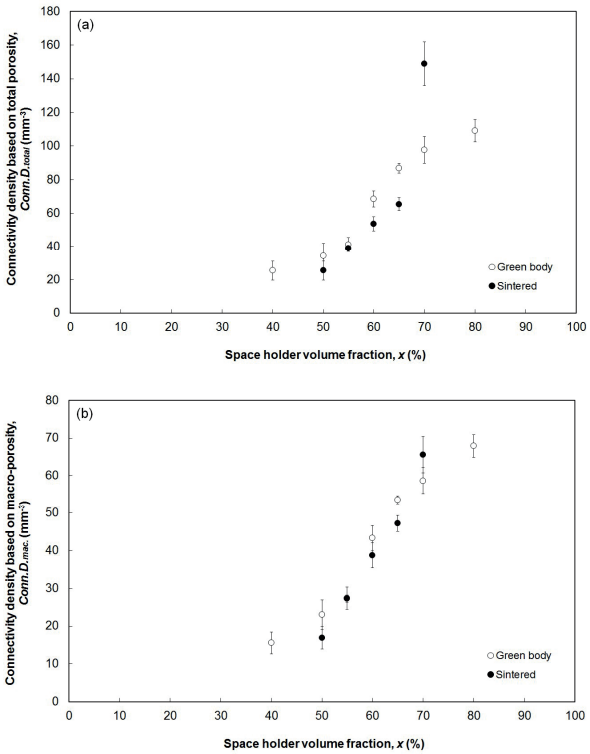

Fig. 5.3. Connectivity density (*Conn.D.*) of the green body and the sintered titanium scaffolds, determined based on (a) the total porosity and (b) the macro-porosity. (Reprinted with permission from Elsevier)

The relationship between the x value and the specific surface area SSA of the green body could be determined by making use of the parabolic plots, as shown in Figs. 5.4a and 5.4b. Based on these plots, a maximum SSA value of the green body could be achieved at x = 60% or x_m = 51.87%. The corresponding SSA values of the sintered scaffolds deviated slightly from those of the green body at x > 60% and a maximum value could be achieved at x = 65% or x_m = 55.38%.

The relationship between the space holder volume fraction x and the mean thickness of the titanium framework in the porous titanium scaffold (*Th.Ti.*) before water leaching and after sintering is displayed in Fig. 5.5a. In general, the *Th.Ti* values of both the green body and sintered scaffolds decreased with increasing x value. The influence of sintering on *Th.Ti* was however unclear, as indicated by small fluctuations of this parameter. The *Th.Ti* values of the green body with x = 55, 60 and 70% decreased slightly by 4.0 – 5.7%, while the *Th.Ti* values of the samples with x = 50 and 65% increased by 8.9 and 2.1%, respectively, as a result of sintering.

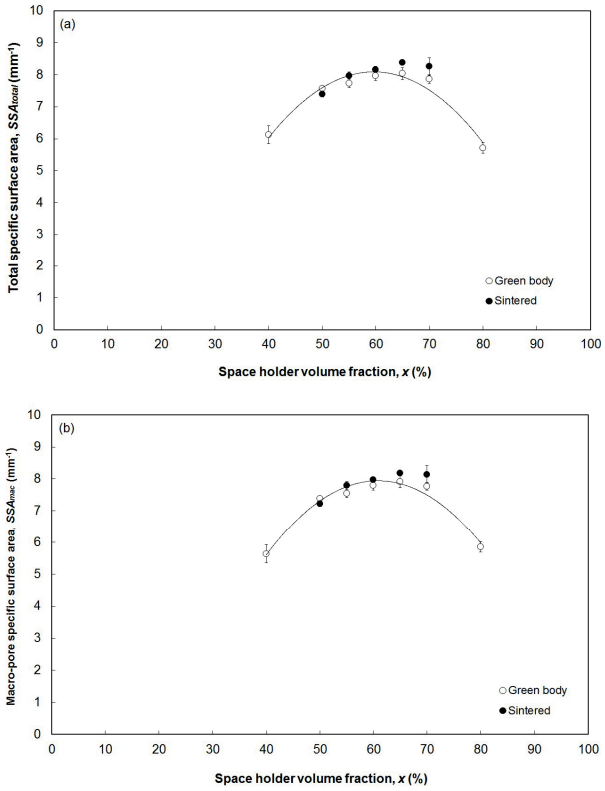

Fig. 5.4. Total and macro-pore specific surface areas (SSA) of the green body and sintered titanium scaffolds. (Reprinted with permission from Elsevier)

Fig. 5.5b shows the relationship between x and the spacing of macro-pores formed by space-holding particles in the green body and sintered titanium scaffolds (*Th.Sp.*). In this research, *Th.Sp.* was intended to be used to indicate the sizes of carbamide space holder particles in the

scaffold preforms after cold compaction and changed macro-pore sizes after sintering. Obviously, the *Th.Sp.* values of both the green body and the sintered scaffolds fluctuated over narrow ranges, i.e., 210-220 μm and 211-218 μm, respectively, over the x range of 40 – 60%. At x > 60%, however, the *Th.Sp.* values of both the green body and sintered scaffolds increased slightly. It was also noted that the *Th.Sp.* values of all sample groups decreased by 0.94 – 4.78% as a result of sintering.

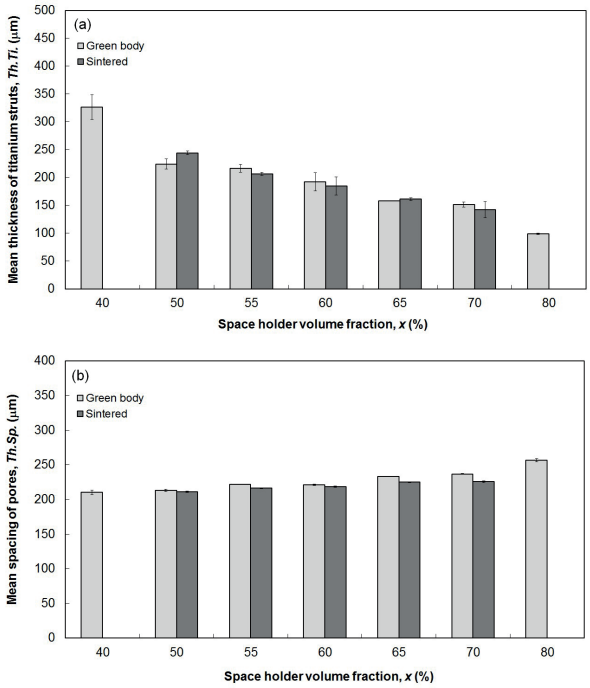

Fig. 5.5. Mean thicknesses of (a) titanium struts (*Th.Ti*) and (b) spacing of macro-pores (*Th.Sp.*) of the green body and sintered titanium scaffolds. (Reprinted with permission from Elsevier)

Fig. 5.6 shows the radial shrinkages of the titanium scaffolds as a result of sintering. The radial shrinkage was determined by using Eq. 5.5:

$$\text{Radial shrinkage} = \frac{D'-D}{D} \times 100\% \tag{5.5}$$

where D' is the diameter of the sintered scaffold. The longitudinal shrinkage could not be measured due to the disintegration of some titanium particles at the bottom part of the green body during water leaching for the removal of carbamide space-holding particles (Section 3.2). The plot in Fig. 5.6 clearly shows that the radial shrinkage of the titanium framework increased from 5.7 to 6.8% with increasing carbamide volume fraction from 50 to 70%.

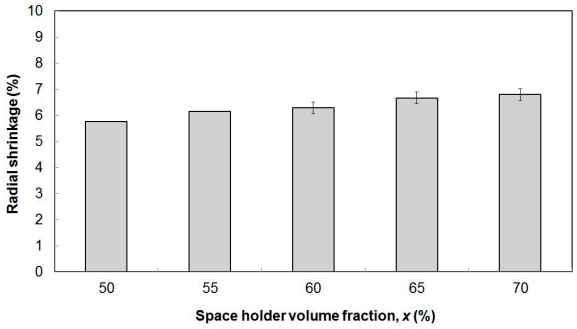

Fig. 5.6. Radial shrinkage of the titanium framework due to sintering at 1200 ºC for 3 h. (Reprinted with permission from Elsevier)

Fig. 5.7 presents a series of micrographs illustrating the porous structures of the sintered titanium scaffolds prepared with x = 50, 60 and 70% space-holding particles. Obviously, sintering at 1200 ºC for 3 h could lead to the bonding between titanium particles and the formation of the scaffold framework. Macro-pores were formed replicating carbamide space-holding particles and had rough surfaces, reflecting the structural characteristics of the sintered spherical titanium powder. As indicated by the red arrows, the struts of the titanium scaffolds contained some micro-pores. The macro-pore interconnections were indicated in this figure by the openings at the pore walls in the interior of the scaffold.

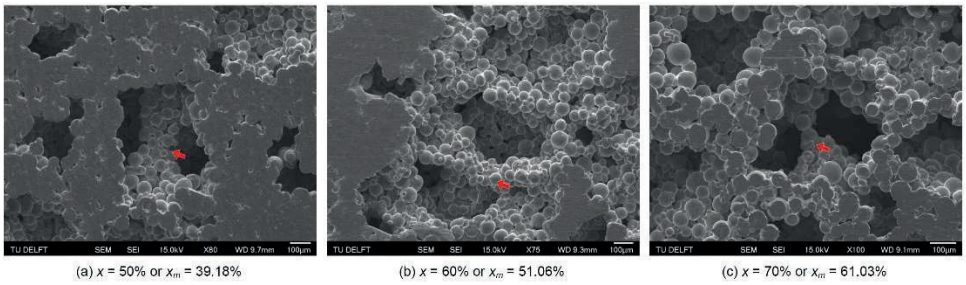

Fig. 5.7. Porous structures of the sintered titanium scaffolds with (a) x = 50%, (b) x = 60% and (c) x = 70%, as observed with scanning electron microscope (SEM). (Reprinted with permission from Elsevier)

5.3.2. Water leaching behavior of space-holding particles

Fig. 5.8a shows the weight losses of titanium scaffold preforms during immersion in water for 60 min to remove carbamide space-holding particles. In general, the weight of the scaffold preform decreased rapidly during the first minutes of immersion, depending on the volume fraction of the space holder added to the scaffold preform. Afterwards, the weight loss decreased slowly and started to decay. As indicated by the arrows, a transition from rapid weight loss to decayed weight loss occurred earlier in the case of the scaffold preform prepared with a larger

volume fraction of the carbamide space holder. The titanium scaffold preform prepared with x = 80% could not retain its shape during leaching for the removal of the carbamide powder. As a consequence, the water leaching behavior of this preform could not be characterized. To gain an accurate understanding of the water leaching behavior, the volume fraction of the space holder x in Eqs. 3 and 6 should be substituted with the measured values from micro-CT (x_m), as shown in Fig. 5.1.

Fig. 5.8b presents a series of plots obtained from fitting the data shown in Fig. 5.8a into the square-root model expressed in Eq. 5.7. By using the plot, with x = 70% or x_m = 60.74% as an example, three primary regimes describing the characteristics of the leaching process could be recognized, i.e., (i) rapid dissolution, (ii) dissolution and diffusion controlled and (iii) saturation. From the slopes in the dissolution regime and diffusion-controlled regime, the effective diffusion rate of the dissolving carbamide powder inside the scaffold preform D_e could be determined.

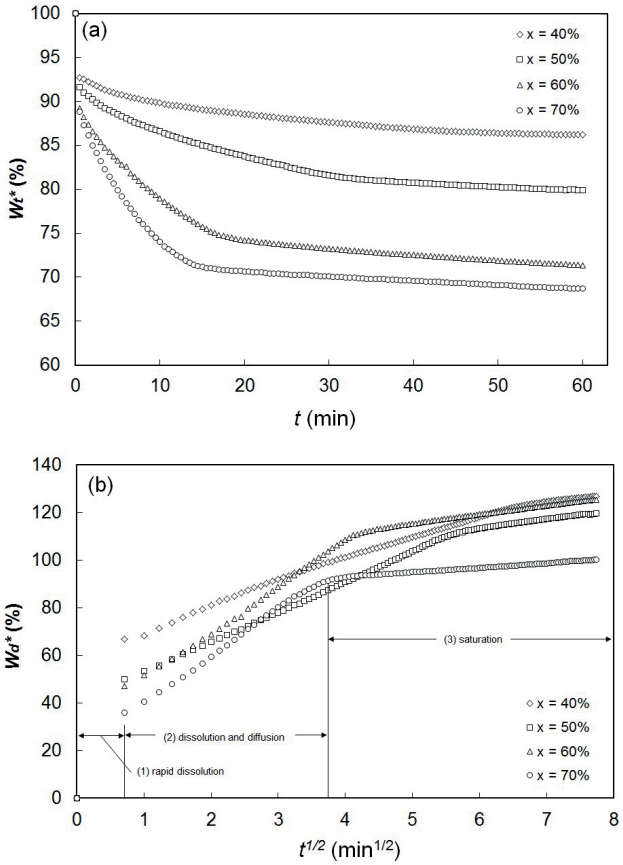

Fig. 5.8. (a) Weight losses of titanium scaffold preforms during water leaching (W_t*) and (b) data fitting into the square-root model to characterize the water leaching process for the removal of the carbamide space holder. (Reprinted with permission from Elsevier)

Fig. 5.9a illustrates the relationship between x and effective diffusivity D_e during the leaching process. Obviously, D_e value increased from 1.56 ± 0.36 × 10^{-6} cm^2s^{-1} to 10.49 ± 1.13 × 10^{-6} cm^2s^{-1} with rising x from 40 to 70% or x_m from 31.81 ± 2.12 % to 60.74 ± 0.79 %.

On the basis of the plots shown in Fig. 5.8a, the time required to achieve the saturation of the leaching process could be determined. Fig. 5.9b shows the relationship between x and the minimum duration required to achieve the saturation of the leaching process (t_{min}). It is clear from this plot that a longer immersion time was required for leaching from a scaffold preform with a lower volume fraction of carbamide. In addition, Fig. 5.9b demonstrates the relationship between x and the weight fraction of removed carbamide powder measured at t_{min} ($W_{d,f}$*). It is obvious that the $W_{d,f}$* values of all samples decreased with rising x and were all above 100%, which suggested that the carbamide material had been removed completely from the scaffold preforms. It is important to note that some titanium particles disintegrated from the circumference of the bottom part of the scaffold preforms and the detached particles at the bottom of the water bath could be observed.

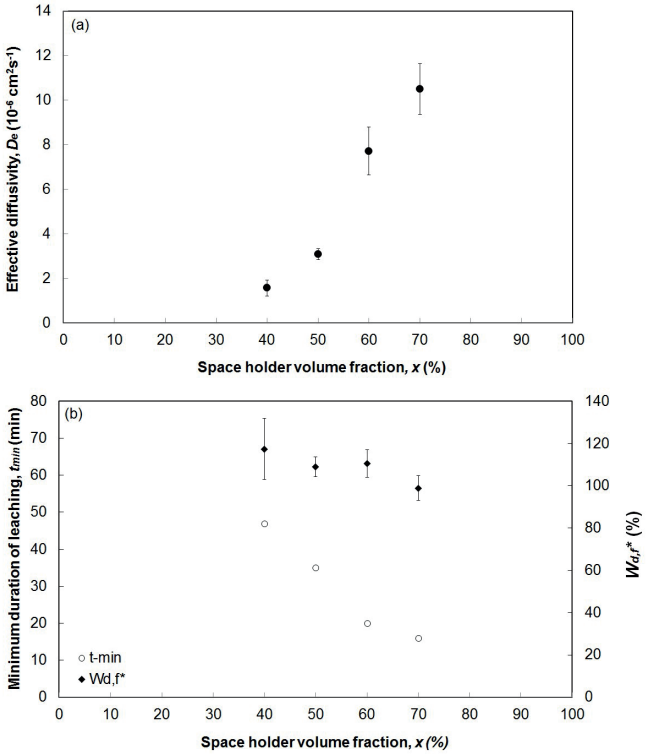

Fig. 5.9. (a) Relationship between the space holder volume fraction (x) and effective diffusivity of dissolving carbamide particles inside the green body (D_e) and (b) the minimum duration to achieve the saturation of the leaching process (t_{min}) and weight fraction of the scaffold preform at tmin ($W_{d,f}$*). (Reprinted with permission from Elsevier)

The results of the XRD analysis of the titanium powder and titanium/carbamide compacts are presented in Figs. 5.10a and b, which were used for the comparative analysis of the XRD patterns of the titanium scaffold preforms after leaching. The presence of the carbamide material in Fig. 5.10b is indicated by black dots at the peaks of the XRD pattern. Figs. 5.10c – f show the XRD patterns of the titanium scaffold preforms taken out of the water-leaching bath at t_{min}. Obviously, all the XRD patterns of titanium scaffold preforms showed no traces of the carbamide material and demonstrated similar patterns to the XRD pattern of the titanium powder shown in Fig. 5.10a.

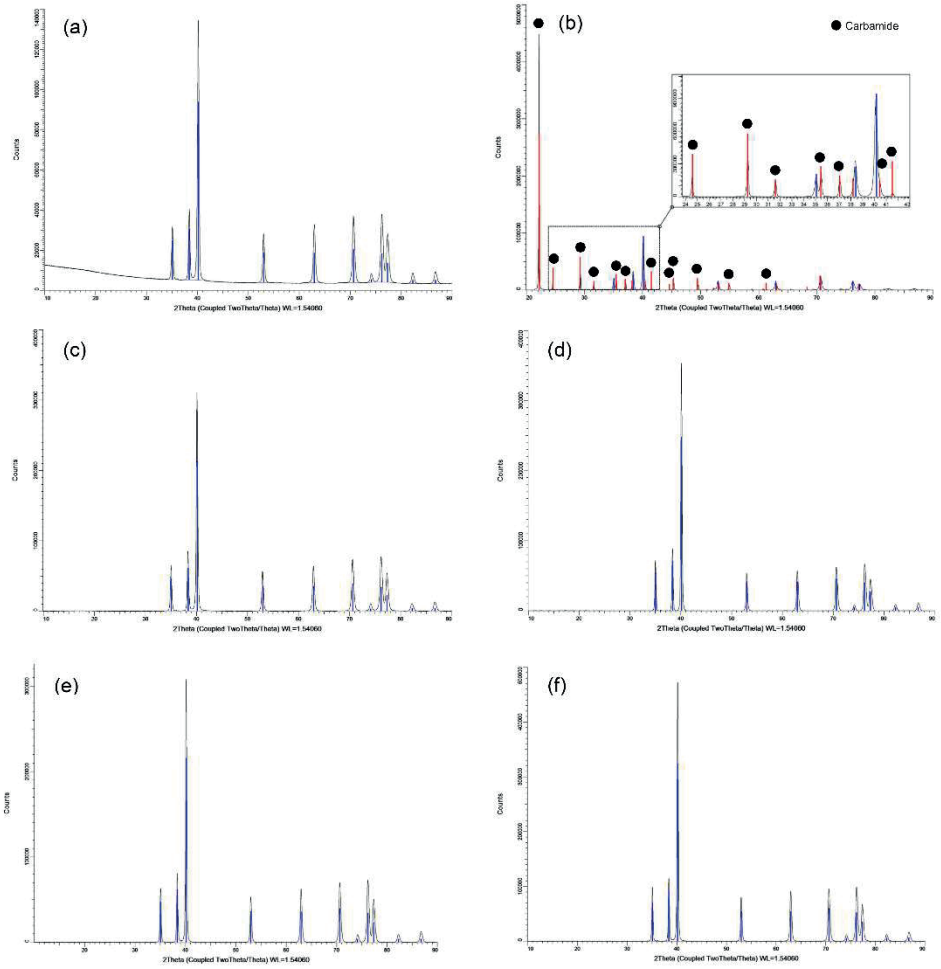

Fig. 5.10. XRD patterns of (a) titanium powder, (b) titanium/carbamide powder compact, titanium scaffold preforms with (c) $x = 40\%$, (d) $x = 50\%$ (e) $x = 60\%$ and (f) $x = 70\%$. (Reprinted with permission from Elsevier)

5.4. Discussion

In this research, the powerful micro-CT technique was used to characterize the 3D structures of the green body and sintered titanium scaffolds prepared with the space holder method. Besides its capability of 3D structure analysis, micro-CT is a non-destructive technique [3] and thus can avoid disruptions of powder packings and arrangements in the low-strength green body.

5.4.1. Porous architecture of the green body

The characterization of the porous structure of the scaffold green body is of fundamental importance, because it is this structure that forms the basis for further structural evolutions at subsequent processing steps. It was considered desirable that the porous structure of the sintered scaffold could be optimized by controlling powder particle arrangement in the green body of the scaffold preform. In this way, the attempt to optimize the final porous structure of the scaffold would become more efficient and less expensive than conducting a series of trial-and-error studies on the sintered titanium scaffolds. Up to now, however, the porous structure of the green body of a titanium scaffold preform prepared with the space holder method has rarely been studied.

In the current study, the relationship between the space holder volume fraction x and the total porosity p of the green body appeared to be linear, as expressed in Eq. 5.1. This result confirmed a linear relationship between x and p of the scaffold that has been reported and recently modeled by Jian et al. [10] in Eq. 5.4:

$$p = ax + b \tag{5.4}$$

where p and x are the scaffold porosity and space holder content, respectively. The constants a and b are related to the volumetric changes of pores that occur during scaffold processing. The decreased micro-porosity with rising volume fraction of the space holder in the green body of the scaffold preform was attributed to the decreased thickness of the titanium framework in the scaffold preform, as confirmed in Fig. 5.5a.

It has been reported that the surface area of a scaffold affects initial cell attachments [11]. A larger surface area is usually preferred for enhanced bone tissue regeneration. The present research showed that a maximum surface area of the titanium scaffold preform could be achieved at x = 60% or x_m = 51.87%. Based on this result, further analysis of the porous structures of the sintered titanium scaffolds was performed over a narrower range of space holder volume fractions, i.e., from x = 50 to 70%.

In the BoneJ plugin software, the interconnectivity of pores is defined as the connectivity density (*Conn.D.*), which is calculated from the connectivity determined based on the Euler characteristic in a network divided by the volume of the sample [7]. *Conn.D.* of the green body increased with increasing x as a result of an increased number of contact points between carbamide particles inside the scaffold preform, as demonstrated in Fig. 5.1a. Part of micro-pores were also interconnected with each other or with macro-pores inside the green body, as reflected by lower $Conn.D._{mac.}$ values than $Conn.D._{total}$ values in Fig. 5.3.

In the preceding research, on the basis of the behaviors of powder mixtures under compressive stresses, an appropriate compacting pressure was determined for the preparation of a titanium scaffold with a given volume fraction of carbamide space-holding particles [5]. In order to avoid extensive deformation and breakage of carbamide particles, a lower compacting pressure was suggested to be applied in the preparation of a titanium scaffold preform with a higher volume fraction of the carbamide space holder. An appropriate compacting pressure P could be estimated by applying the rule of mixtures, as expressed in Eq. 5.5:

$$P = \left(P_y\right)_{mix} = (1-x)(P_y)_{Ti} + x(P_y)_{Carb.} \tag{5.5}$$

where P_y and x are the yield pressure of the compacted powder mixture, as determined by using the Heckel model [12] and the carbamide volume fraction of the scaffold preform, respectively. The subscripts Ti and Carb. correspond to titanium and carbamide, respectively. With the values of $(P_y)_{Ti}$ and $(P_y)_{Carb.}$ being 432.1 and 12.92 MPa, respectively [5], the relationship between $(P_y)_{mix}$ and x could be expressed in Eq. 5.6:

$$P = 432.1 - 419.2x \tag{5.6}$$

In this research, the sizes of macro-pores created by the carbamide space holder in the scaffold green body prepared at the compacting pressures based on Eq. 5.5 were also analysed. In this case, the sizes of macro-pores were represented by mean *Th.Sp.* values. Acceptable *Th.Sp.* values were obtained from the samples prepared with x = 40 - 60% (or x_m = 31.81 - 51.87%). Coalescences and interconnections of carbamide particles at a higher x value indeed led to a larger *Th.Sp.* value. As a consequence, the *Th.Sp.* value might not reflect the sizes of carbamide powder particles in the scaffold preform. As shown in Fig. 5.5b, the mean *Th.Sp.* values of the scaffold preforms prepared with x = 40 - 60% ranged from 210.07 ± 3.41 to 220.93 ± 1.17 μm. These values were lower than the average diameter D_{av} and the median particle diameter D_{50} of the carbamide powder given in Table 5.1, i.e., 415.62 ± 5.66 μm and 396.94 ± 5.04 μm, respectively.

5.4.2. Water leaching behavior and residues of the space holder material

In this research, the water leaching behavior of carbamide space-holding particles was characterized to provide information concerning the porous structures of the green body of the titanium scaffolds prior to sintering. Although having rarely been studied and reported in the open literature, space holder removal is a critical step in the scaffold fabrication. The characterization of leaching for the removal of space-holding particles has so far only been reported only in a few articles. Gulsoy and German reported that the removal rate of the carbamide space holder increased with increasing water temperature [13]. Torres et al. reported the influences of compacting pressure and stirring on the water leaching behavior of the NaCl space holder in titanium scaffold preforms [14]. The influence of the volume fraction of the space holder on the leaching behavior was studied by Bafti and Habibolahzadeh [15]. These researchers however utilized an inaccurate method, owing to the handling for weighing and

drying, to characterize the removed space holder after the sample was taken out of water [9]. Recently, a real-time technique for the characterization of the space holder removal through water leaching has been proposed, based on the Archimedes principle, as reported in Refs. [9, 16] and Chapter 4. However, the capability of this technique to ensure complete removal of space-holding particles has not yet been confirmed.

As demonstrated in Fig. 5.8a, the weight of the titanium scaffold preform decreased rapidly over a certain period of immersion time, i.e., t_{min}, resulting from the dissolution and leaching of carbamide space-holding particles into water. Thereafter, weight loss occurred slowly. Despite the low rates, the weight of the titanium scaffold preform after t_{min} in the current study kept decreasing. Such a phenomenon was not observed in a similar study [16] and could be related to the collapse of titanium particles resulting from a relatively low compacting pressure applied (140 - 260 MPa), compared with those applied in the previous study [16], i.e., 400 MPa. The disintegration of titanium particles occurred mainly at the circumference of the bottom part of the scaffold preform. The study of Özkan and Briscoe [17] confirmed this finding by indicating that the lowest green density at this location as a consequence of pressure variation that occurred in a compacted powder prepared by means of single-action cold compaction.

Similar to the results obtained from a previous study [17], the effective diffusivity D_e of the dissolving carbamide powder in the scaffold preform during leaching increased with rising x. It was attributed to an increased number of pore interconnections formed with rising x. With more pores interconnected, the diffusion rate of dissolving carbamide powder particles inside the scaffold preform increased and the minimum duration to achieve the saturation of the leaching process tmin became shorter (see Fig. 5.9b). The plot of *Conn.D.* of the scaffold green body in Fig. 5.3 confirmed this explanation; a higher volume fraction of carbamide resulted in a larger connectivity density of the scaffold preform.

The mechanisms of the leaching process have been well described in a previous study [9], based on the analysis using the square-root model [18]. Once immersed in water, the carbamide space holder dissolves rapidly, forming openings at the surface of the scaffold preform. These openings allow deeper penetration of water, leading to further dissolution of carbamide particles in the interior of the scaffold preform. Due to the differences in concentration between the fresh penetrating water and the water with rich dissolution products, a diffusive flow occurs through interconnected and tortuous channels that are formed by linked space-holding particles till the saturation of the leaching process.

In the current study, it was of critical importance to examine whether t_{min} obtained from the plots in Fig. 5.8b could indicate if the carbamide space holder had been removed completely from the scaffold preform. As shown in Fig. 5.9b, the $W_{d,f}$* values of all the samples were higher than 100%, which indicated complete removal of the space holder material from the scaffold preforms. Ideally, complete removal should be indicated by $W_{d,f}$* = 100%. In this research, however, higher $W_{d,f}$* values were obtained due to the loss of titanium particles during leaching. Disintegration of titanium powder particles during leaching must have reduced the accuracy of the calculated D_e values in this study. The XRD patterns shown in Fig. 5.10 confirmed that there were no carbamide traces at the titanium scaffold preforms so that tmin determined in Fig. 5.8b

was acceptable to be used to indicate the minimum duration of leaching for the removal of carbamide space-holding particles.

5.4.3. Porous architecture of the sintered titanium scaffolds

A review of the recent studies showed that solid-state sintering for the preparation of titanium scaffolds prepared the space holder method was mostly performed at 1100 – 1300 ºC for 0.5 - 3 h [1, 2, 19, 20, 21, 22, 23, 24, 25, 26, 27]. In this research, sintering was conducted at 1200 ºC for 3 h to achieve the final titanium scaffolds.

Similar to the case of the scaffold green body, a linear relationship between x and p of the sintered titanium scaffold could be recognized in Fig. 5.2a. However, the regression line of the porosity data plots of the sintered samples was slightly below the line of the green body, confirming the shrinkage of the titanium framework during sintering, as demonstrated in Fig. 5.6. Apparently, the parameters used in water leaching and sintering did not cause large deviations of the macro-porosity of the sintered sample from its green structure, as indicated by the slope of the regression line correlating the macro-porosity of the green body to that of the sintered sample ($m_{mac.}$) in Fig. 5.2b. In this case, a small constant in Eq. 5.3, i.e., -1.313, demonstrated a low level of shrinkage that occurred during sintering, as confirmed by the plots in Fig. 5.6. In addition, the slope $m_{mac.}$ was very close to 1, i.e., 1.008, and could be interpreted as homogeneous shrinkage growth of macro-pores over the range of the macro-porosity values studied. The reduction of the spacing created by the space holder due to sintering was also considerably small, i.e., over a range of 0.94 – 4.78%, as indicated in Fig. 5.6b. On the basis of this finding, it could be concluded that water leaching and subsequent sintering at 1200 ºC for 3 h did not result in large changes in macro-porosity and macro-pore sizes in the titanium scaffolds prepared with the space holder method. In addition, the macro-pore sizes in the final titanium scaffolds in this study ranged from 211 to 218 μm, as indicated by the *Th.Sp.* values.

In many reports on the porous structures of scaffolds for bone tissue engineering, pore sizes of 200 – 500 μm are, in general, considered suitable [26]. Hulbert et al., for example, considered pore sizes of 75 - 100 μm as the minimum required for significant ingrowth of bone tissue in scaffold [28]. It can therefore be concluded that the application of the compacting pressures based on Eq. 5.5 could avoid the changes of carbamide particle sizes from ~400 μm to <100 μm in the titanium/carbamide compacts due to either extensive deformation or breakage.

In this research, it was also interesting to investigate the level of micro-pore shrinkage due to sintering. Shrinkage of micro-pores during sintering was confirmed in Fig. 5.2c. The shrinkage growth, as indicated by the percentage of micro-porosity reduction, increased to 86% with rising macro-porosity in the green body. Similar findings were reported by Laptev et al. [1] and Esen and Bor [21]; excessive shrinkage occurred to the titanium-based scaffolds having porosity values higher than 60%. Laptev et al. explained that the increased space-holder volume fraction reduced the densification of the titanium matrix during compaction. As a consequence, a higher shrinkage growth occurred during the sintering of the titanium scaffold with a higher macro-porosity value [1].

As described previously, a higher volume fraction of the space holder resulted in more interconnections between macro-pores within the scaffold. Similar to the case of the green body, both the $Conn.D._{total}$ and $Conn.D._{mac.}$ values of the sintered scaffold increased with rising space holder volume fraction. Shrinkage of the titanium framework during sintering also reduced the pore connectivity density in the scaffolds, except for the samples with x = 70%. As expected, the range of the percentage reductions of $Conn.D._{mic.}$ was higher than that of the $Conn.D._{mac.}$, i.e., 15.05 – 45.04% versus 0.54 – 26.66%, due to smaller sizes of micro-pores than those of macro-pores. During sintering, neck growth between titanium particles might close some interconnected micro-pores and increased the number of isolated micro-pores in the scaffold framework. Despite the shrinkage to some extent, the large sizes of macro-pores could maintain the interconnections of these pores.

Specific surface area *SSA* has been recognized as another critical parameter of bone tissue engineering scaffolds. Murphy et al. [11] reported a significant number of cells in a scaffold having small pores, i.e. <325 μm, in comparison to those growing on larger pore sizes due to a larger *SSA* value for initial cell attachment. As demonstrated in Subsection 5.4.1, a scaffold green body with a maximum SSA could be prepared with an addition of 60 vol.% carbamide particles to the titanium matrix powder. After sintering, a maximum *SSA* value was achieved with a slightly higher carbamide volume fraction, i.e., x = 65%. The contribution of micro-pores to enlarging the *SSA* value was confirmed in this study, as indicated by the higher *SSA* values calculated based on the total porosity than those on the basis of the macro-porosity of the scaffold. Theoretically, the *SSA* value decreased due to the shrinkage of the scaffold framework during sintering, as seen in the samples with x = 50%. However, larger *SSA* values of the sintered titanium scaffolds with x > 50% were seen due to the shrinkage and thus the inclusion of neighboring pores around the confined boundary of the cubical 3D scaffold model into the quantitative analysis. In the case of the samples with x = 50%, this effect was not noticed, possibly due to a different shrinkage mechanism from that of the samples with x > 50%.

Tuncer et al. [2] argued that the overall shrinkage of titanium scaffolds prepared with the space holder method could be attributed to the thickening of struts and slight decreases of macro-pores. In the current study, however, thickening of the titanium framework was only obvious in samples with x = 50%. This phenomenon was not observed in samples with higher x values, except for an negligible *Th.Ti* increase of the samples with x = 65% after sintering. A slight decrease of the macro-porosity of the scaffold was confirmed through the 3D structural analysis, as shown in Fig. 5.5b. On the basis of the results obtained from this research, it can be concluded that the shrinkage mechanism of titanium scaffolds depends on the volume fraction of the space holder material. In the samples with a low space holder volume fraction, i.e., x = 50%, shrinkage occurs mainly due to the reductions of macro- and micro-pore sizes, while the struts of the scaffold framework become slightly thicker. In the samples with x > 50%, however, shrinkage is caused by the reductions of both macro- and micro-pore sizes as well as the thickness of struts.

The results presented above demonstrate that the control of the final porous structure of the titanium scaffold from its green body is indeed feasible as long as appropriate parameters for

removing the space-holding particles and sintering of the porous green body of the titanium scaffold are applied. This presents a convenient and efficient way to realize the desired porous structure of a titanium scaffold by selecting the right space holder volume fraction and ensure homogeneous powder particle distribution, thereby avoiding multiple attempts based on trial and error to realize the desired porous structure. The simplification of the control of the porous structure during scaffold fabrication will surely help to stir up the interest of medical device and implant producers in the space holder method and open up additional perspectives for bone tissue engineering applications.

5.5. Conclusions

In this research, 3D porous structures of the green body and sintered titanium scaffolds were characterized by means of micro-CT. With this characterization technique, detailed information on the changes of 3D porous structure from the green body to the sintered titanium scaffolds due to the space holder removal and sintering was obtained. The shrinkage mechanism during the sintering of the titanium scaffold was established. The results led to the main conclusion that the porous structures of the titanium scaffolds processed through water leaching and sintering at 1200 ºC for 3 h did not deviate significantly from their green structures. A small deviation of the final porous structure from its green body was due to shrinkage during sintering. Thus, the control of the final porous structure of the titanium scaffold from its green body would be feasible. A maximum specific surface area could be produced with an addition of 60-65 vol.% carbamide particles to the matrix powder. For the scaffolds prepared with space-holding volume fractions of >50%, the shrinkage of the titanium scaffolds was caused by the reductions of both macro- and micro-pore sizes and the thickness of struts.

References

[1] A. Laptev, M. Bram, H. P. Buchkremer and D. Stöver, "Study of production route for titanium parts combining very high porosity and complex shape," *Powder Metallurgy,* vol. 47, pp. 85-92, 2004.

[2] N. Tuncer, G. Arslan, E. Maire and L. Salvo, "Investigation of spacer size effect on architecture and mechanical properties of porous titanium," *Materials Science and Engineering A,* vol. 530, pp. 633-642, 2011.

[3] S. Ho and D. Hutmacher, "A comparison of micro CT with other techniques used in the characterization of," *Biomaterials,* vol. 27, pp. 1362-1376, 2006.

[4] T. Fiedler, I. Belova, G. Murch, G. Poologasundarampillai, J. Jones, J. Roether and A. Boccaccini, "A comparative study of oxygen diffusion in tissue engineering scaffolds," *Journal of Materials Science: Materials in Medicine,* vol. 25, pp. 2573-2578, 2014.

[5] B. Arifvianto, M. Leeflang and J. Zhou, "The compression behaviors of titanium/carbamide powder mixtures in the preparation of biomedical titanium scaffolds with the space holder method," *Powder Technology,* vol. 284, pp. 112-121, 2015.

[6] T. Ferreira and W. Rasband, ImageJ User Guide, 2012.

[7] M. Doube, M. Klosowski, I. Arganda-Carreras, F. Cordelieres, R. Dougherty, J. Jackson, B. Schmid, J. Hutchinson and S. Shefelbine, "BoneJ: Free and extensible bone image analysis in ImageJ," *Bone,* vol. 47, pp. 1076-1079, 2010.

[8] M. Doube, M. Klosowski, A. Wiktorowicz-Conroy, J. Hutchinson and S. Shefelbine, "Trabecular bone scales allometrically in mammals and birds," *Proceedings of the Royal Society B,* vol. 278, pp. 3067-3073, 2011.

[9] B. Arifvianto, M. Leeflang and J. Zhou, "A new technique for the characterization of the water leaching behavior of space holding particles in the preparation of biomedical titanium scaffolds," *Materials Letters,* vol. 120, pp. 204-207, 2014.

[10] X. Jian, C. Hao, Q. Guibao, Y. Yang and L. Xuewei, "Investigation on relationship between porosity and spacer content of titanium foams," *Materials and Design,* vol. 88, pp. 132-137, 2015.

[11] C. M. Murphy, M. G. Haugh and F. J. O'Brien, "The effect of mean pore size on cell attachment, proliferation and migration in collagen-glycosaminoglycan scaffolds for bone tissue engineering," *Biomaterials,* vol. 31, pp. 461-466, 2010.

[12] R. Heckel, "Density-pressure relationships in powder compaction," *Transactions of Metallurgical Society AIME,* vol. 221, pp. 671-675, 1961.

[13] H. Gülsoy and R. German, "Sintered foams from precipitation hardened stainless steel powder," *Powder Metallurgy,* vol. 51, pp. 350-353, 2013.

[14] Y. Torres, J. J. Pavón and J. A. Rodríguez, "Processing and characterization of porous titanium for implants by using NaCl as space holder," *Journal of Materials Processing Technology,* vol. 212, pp. 1061-1069, 2012.

[15] H. Bafti and A. Habibolahzadeh, "Production of aluminum foam by spherical carbamide space holder technique," *Materials and Design,* vol. 31, pp. 4122-4129, 2010.

[16] B. Arifvianto, M. Leeflang, J. Duszczyk and J. Zhou, "Characterisation of space holder removal through water leaching for preparation of biomedical titanium scaffolds," *Powder Metallurgy,* vol. 57, pp. 9-12, 2014.

[17] N. Ozkan and B. Briscoe, "Characterization of die-pressed green compacts," *Journal of European Ceramics Society,* vol. 17, pp. 697-711, 1997.

[18] S. Kim, H. Lee, H. Song and B. Kim, "Pore structure evolution during solvent extraction and wicking," *Ceramics International,* vol. 22, pp. 7-14, 1996.

[19] B. Dabrowski, W. Swieszkowski, D. Godlinski and K. J. Kurzydlowski, "Highly porous titanium scaffolds for orthopaedic applications," *Journal of Biomedical Materials Research B: Applied Biomaterials,* vol. 95, pp. 53-61, 2010.

[20] L. M. de Vasconcellos, F. N. Oliveira, O. de Leite, L. G. de Vasconcellos, R. F. do Prado, C. J. Ramos, M. L. Graca, C. A. Cairo and Y. R. Carvalho, "Novel production method of porous surface Ti samples for biomedical application," *Journal of Materials Science: Materials in Medicine,* vol. 23, pp. 357-364, 2012.

[21] Z. Esen and S. Bor, "Processing of titanium foams using magnesium spacer particles," *Scripta Materialia,* vol. 56, pp. 341-344, 2007.

[22] J. Jakubowicz, G. Adamek and M. Dewidar, "Titanium foam made with saccharose as a space holder," *Journal of Porous Materials,* vol. 20, pp. 1137-1141, 2013.

[23] A. Mansourighasri, N. Muhamad and A. B. Sulong, "Processing titanium foams using tapioca starch as a space holder," *Journal of Materials Processing Technology,* vol. 212, pp. 83-89, 2012.

[24] O. Smorygo, A. Marukovich, V. Mikutski, A. A. Gokhale, G. J. Reddy and J. V. Kumar, "High-porosity titanium foams by powder coated space holder compaction method," *Materials Letters,* vol. 83, pp. 17-19, 2012.

[25] D. Mondal, J. Datta Majumder, N. Jha, A. Badkul, S. Das, A. Patel and G. Gupta, "Titanium-cenosphere syntactic foam made through powder metallurgy route," *Materials and Design,* vol. 34, pp. 82-89, 2012.

[26] C. E. Wen, M. Mabuchi, Y. Yamada, K. Shimojima, Y. Chino and T. Asahina, "Processing of biocompatible porous Ti and Mg," *Scripta Materialia,* vol. 45, pp. 1147-1153, 2001.

[27] I. Gligor, O. Soritau, M. Todea, C. Berce, A. Vulpoi, T. Marcu, V. Cernea, S. Simon and C. Popa, "Porous c.p. titanium using dextrin as space holder for endosseous implants," *Particulate Science and Technology,* vol. 31, pp. 357-365, 2013.

[28] S. F. Hulbert, F. A. Young, R. S. Mathews, J. J. Klawitter, C. D. Talbert and F. H. Stelling, "Potential of ceramic materials as permanently implantable skeletal prostheses," *Journal of Biomedical Materials Research,* vol. 4, pp. 433-456, 1970.

Chapter 6

Diametral compression behavior of biomedical titanium scaffolds with open, interconnected pores prepared with the space holder method

This chapter is adapted from:
Diametral compression behavior of biomedical titanium scaffolds with open, interconnected pores prepared with the space holder method
B. Arifvianto, M.A. Leeflang and J. Zhou, Journal of Mechanical Behavior of Biomedical Materials (2017), Vol. 68, pp. 144-154.

6.1. Introduction

As pointed out in Chapter 1, elastic modulus and compressive strength are the critical parameters of the scaffold that must be ensured prior to its clinical use for bone tissue engineering. A scaffold with an elastic modulus higher than that of the host bone tissue may fail to induce bone regeneration due to stress shielding [1, 2]. On the other hand, a scaffold with adequate strength and fracture resistance can aid in the healing of the defect in the load-bearing skeletal tissue [1, 3]. In general, the mechanical properties of a scaffold decrease with increasing porosity [4, 5, 6, 7, 8, 3, 9, 10, 11]. Therefore, it is necessary to search for a trade-off between these two opposite parameters in order to meet the requirements of scaffolds for bone tissue engineering.

In most cases, the elastic modulus and compressive strength of a scaffold material are determined by performing uniaxial compression (UC) tests [8, 12]. In order to obtain comparable results, specimens with standardized dimensions are required, such as those specified in the ISO 13314:2011 standard. According to this standard, the specimen of a porous or cellular metallic material subjected to uniaxial compression tests with a loading direction parallel to its height should have a height-to-diameter ratio (H/D) between 1 and 2. With the space holder method, however, scaffolds with such a high H/D ratio could not be produced without a region with a low green strength [13] that is prone to collapse during the removal of space-holding particles

to create macro-pores in the scaffold green body. In the case of a green body prepared with a single-action die press, its *H/D* ratio must be kept low in order to ensure a homogeneous green density distribution and to minimize the presence of a region with a low green strength, relative to the rest of the powder compact body [13]. Considering this limitation, an alternative method to determine the mechanical properties of disc-shaped scaffolds should be used.

In the last few decades, diametral compression (DC) tests have been applied in a number of studies to determine the mechanical properties of powder compacts or grain compacts with low *H/D* ratios or disc shapes [13, 14, 15, 16]. Although the method was originally used for rock specimens, a standard for the DC tests has been established, such as that specified in ASTM D3967-08. DC tests have also been used to determine the mechanical properties of porous ceramic biomaterials [17, 18]. With increasing use of numerical analysis in recent years, stress distributions inside disc-shaped specimens during DC tests have been revealed [19, 20]. However, the use of DC tests to determine the elastic moduli and compressive strengths of porous titanium scaffolds and sintered metallic materials has rarely been reported in the open literature. In contrast to UC tests [5, 8], it is still not confirmed whether the stress-strain diagrams derived from DC tests are applicable to indicate the deformation behavior and failure of porous metallic materials under compressive loads.

The present research was aimed to establish the correlations between the diametral compression behavior, space-holder volume fraction and geometric parameters of the scaffolds prepared by using the space holder method. Porous structures and open, interconnected pores within the scaffold interior were ascertained by performing micro-computed tomography (micro-CT) analysis and permeability tests, as described in Section 6.2. Also, the elastic moduli and yield strengths of the scaffolds with various porosities were determined from the stress-strain diagrams obtained from the DC tests. In addition, the porous structures of the scaffolds after compression to a number of predetermined strains were characterized in order to establish the deformation and failure mechanisms involved in the DC tests of the porous titanium scaffolds. The results are presented in Section 6.3. In the end, the scaffolds with balanced elastic modulus, yield strength and optimum porosity that could meet the requirements for bone tissue engineering are recommended in Section 6.4. Finally, conclusions are given in Section 6.5 to highlight the important findings of this study.

6.2. Materials and methods

6.2.1. Scaffold preparation

In this research, titanium scaffolds were prepared by mixing a spherical titanium powder (TLS Technik, Germany) with rectangular carbamide particles (Merck, Germany) for 3 h by using a roller mixer (CAT, Germany). The median particle diameters (D_{50}) of the titanium and carbamide powders were 70.32 ± 1.61 μm and 399.23 ± 4.85 μm, respectively, as determined by using a Mastersizer laser diffractometer (Malvern, UK). To produce a set of highly porous titanium scaffolds, carbamide volume fractions in the titanium/carbamide powder mixture were selected to be 50 to 80%. Prior to mixing, a polyvinyl-alcohol (PVA) binder solution was first blended with the titanium powder in order to minimize the segregations of titanium and

carbamide powders due to their dissimilar characteristics. The volume fraction of PVA was 3%. The green bodies of the scaffolds were produced by compacting the titanium/carbamide powder mixtures in a single-action uniaxial die press at pressures of P = 100 – 220 MPa, which were the critical compacting pressures determined in a previous study [21]. To generate macro-pores, carbamide particles in the scaffolds were removed by immersing the green bodies in 250 ml demineralized water for varied periods of time [22]. Finally, the scaffold preforms were sintered in a tube furnace (Carbolite, UK) at 1200 ºC for 3 h under a flowing argon atmosphere, after heating at a rate of 10 ºC/min. By using this procedure, titanium scaffolds with a diameter of 12 mm and a height of 3 – 4 mm were prepared for subsequent characterization. Both the top and bottom surfaces of the sintered disk-shaped samples were ground prior to characterization.

6.2.2. Micro-computed tomography (Micro-CT) analysis

The porous structures of the titanium scaffolds were characterized by using X-ray micro-computed tomography (micro-CT) (Nanotom, Phoenix X-rays, The Netherlands) with an image resolution of 10 μm. In addition, the influence of compressive strain during the DC tests on the porous structure characteristics of the scaffold was investigated. Prior to micro-CT, the sample was first cleaned by sonication in ethanol for 5 min. Quantitative analysis of the porous structure was performed by using the open-source ImageJ 1.50i software [23] with BoneJ plugin [24] on the 3D model of the scaffold with dimensions of 2.5 × 2.5 × 2.5 mm, which was chosen by cropping the volume of interest at the core of the scaffold. Prior to the quantitative analysis, an auto local thresholding using the Bernsen method and a radius of 30 was applied on the 3D model of the scaffold.

By using the BoneJ software, a set of geometrical parameters describing the characteristics of a scaffold could be determined, i.e., (i) porosity (p), (ii) the specific surface area of the matrix framework (SSA), (iii) the connectivity density of pores that are formed from the space previously occupied by space-holding particles ($Conn.D.$), (iv) the thickness of the matrix framework ($Th.Ti$) and (v) the spacing of the space occupied by space-holding particles in the scaffold preform ($Th.Sp.$).

6.2.3. Permeability tests

To ascertain the presence of open, interconnected pores in the scaffolds, gas permeability tests with air as the working fluid were carried out at room temperature. A gas permeameter (Ruska, USA) was used to determine the pressure drop (ΔP) of the air that flew steadily through the scaffold. As shown schematically in Fig. 6.1, a diametrically-sealed sample was placed by press-fitting into a cylindrical rubber holder with its circular area facing the air inflow. The intrinsic permeability constant k was determined by using the modified one-dimensional Darcy's law, as expressed in Eq. 6.1:

$$k = \frac{\mu Q H}{A \Delta P} \tag{6.1}$$

where μ is the air dynamic viscosity (i.e., 1.85×10^{-5} Pa s), Q is the air flow rate, and A and H are the cross-sectional area and height of the scaffold, respectively.

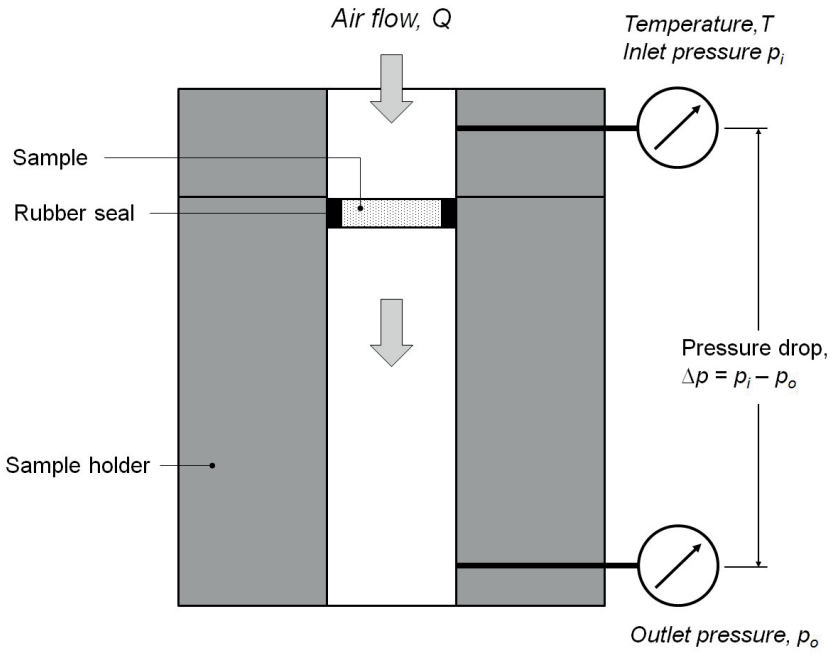

Fig. 6.1. Experimental set-up for air permeability tests. (Reprinted with permission from Elsevier)

6.2.4. Diametral compression (DC) tests

The mechanical properties of the sintered titanium scaffolds were determined by performing diametral compression (DC) tests, considering the low H/D ratios of the specimens, i.e., 0.25 – 0.35. Fig. 6.2 is a schematic illustration of the experimental set-up used for the DC tests.

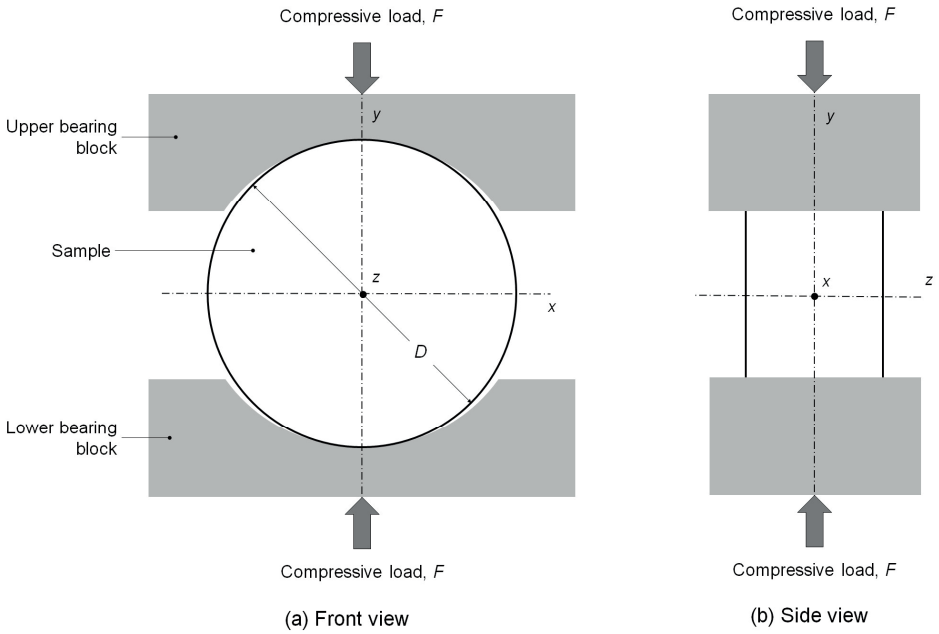

Fig. 6.2. Experimental set-up for diametral compression tests, based on the ASTM D3967-08 standard. (Reprinted with permission from Elsevier)

The specimen loaded laterally in a universal material testing machine (Instron, USA) was tested at a crosshead speed of 0.5 mm/min to a maximum displacement of 4 mm. A pair of curved bearing blocks were designed, according to the ASTM D 3967-08 standard, and used to hold the specimen during loading. A force-displacement plot was obtained and then converted to a stress-strain (σ- ε) diagram.

The maximum diametral compressive stress occurred at the center of the disc (σ_c) and it can be derived from Eq. 6.2 [15, 19]:

$$\sigma_c = \sigma_y(0,0) = -6F/\pi HD_o \tag{6.2}$$

where F and Δd_y are the loading force and crosshead displacement, respectively, and D_O is the initial specimen diameter. The minus sign indicates compression. The compressive strain of the disc specimen can be determined by using Eq. 6.3:

$$\varepsilon_y = \Delta d_y / D_o \tag{6.3}$$

By using Eqs. 6.2 and 6.3, the load-displacement plot could be converted into the stress-strain diagram of the DC test.

6.2.5. Electron microscopy analysis

To aid in establishing the failure mechanisms operating under compressive loads during the DC tests, a series of micrographs showing the changing porous structures of the titanium scaffolds were generated by using a JSM-IT100 scanning electron microscope (SEM) (JEOL Europe, Netherlands). Similar to the procedures used in the preparation for micro-CT analysis, the sample was first cleaned by sonication in ethanol for 5 min prior to observation with SEM.

6.3. Results

6.3.1. Porous structures of the titanium scaffolds

Fig. 6.3 shows the relationship between the nominal volume fraction of the space holder x and the total porosity p of the sintered titanium scaffold, determined from micro-CT. In this research, the titanium scaffolds with total porosities in a range of 31.18 – 61.03%, determined from micro-CT, were prepared by using carbamide particles with nominal volume fractions x ranging from 50 – 70%.

The results of the regression analysis showed a linear relationship between x and p, with a slope $m = 1$ and $R^2 = 0.99$. It is important to note that the titanium/carbamide powder compact with x = 80% could not retain its shape during water leaching to remove carbamide space-holding particles and consequently the characterization of the sintered scaffold could not be performed. Indeed, an increase in total porosity corresponded to an increase in the number of interconnected pores in the scaffold, as indicated by increased connectivity density *Conn.D.*, shown in Fig. 6.4. A larger standard deviation occurred to the scaffold with $p = 61.03\%$.

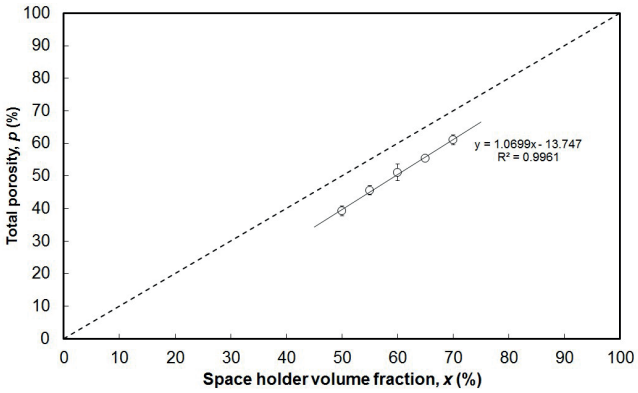

Fig. 6.3. Relationship between the space holder volume fraction (x) and the resulting total porosity (p) of the titanium scaffolds. (Reprinted with permission from Elsevier)

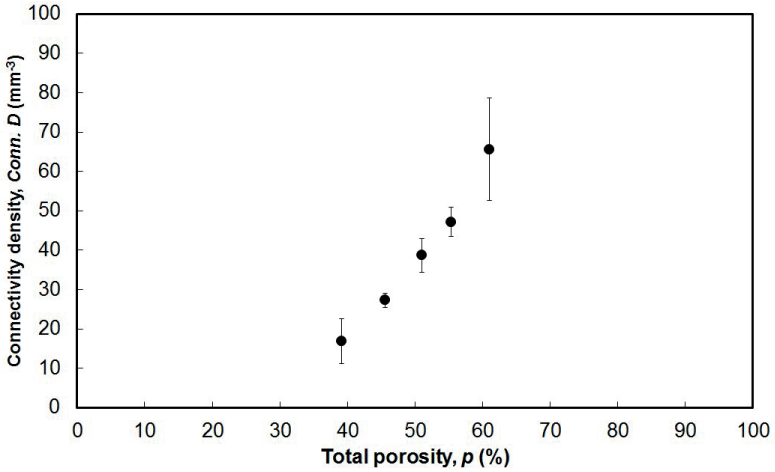

Fig. 6.4. Relationship between the total porosity (*p*) and connectivity density (*Conn.D.*) of the titanium scaffolds. (Reprinted with permission from Elsevier)

Thinner struts in the titanium scaffold framework were formed in a scaffold with a higher porosity, as indicated by a decreased *Th.Ti* value shown in Fig. 6.5. In addition, the mean spacing formed by carbamide space-holding particles (*Th.Sp.*) was relatively stable and only increased slightly at a porosity higher than 50%. In this research, the *Th.Sp.* parameter was intended to be used to represent the mean size of macro-pores in the scaffold.

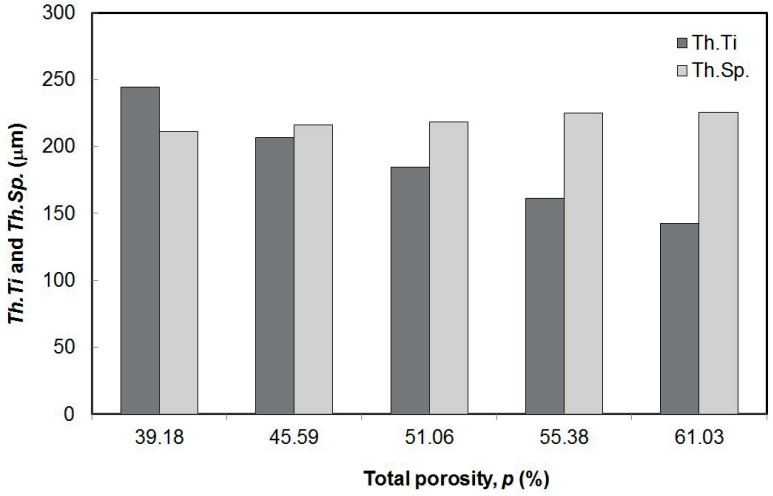

Fig. 6.5. Relationships between the total porosity (*p*) and the thickness of titanium struts (*Th.Ti*) and between the total porosity (*p*) and the space occupied by the space holder (*Th.Sp.*) inside the titanium scaffolds. (Reprinted with permission from Elsevier)

Interestingly, the total specific surface area (*SSA*) of the titanium scaffold reached a maximum at the measured porosities *p* between 50 and 55%, as shown in Fig. 6.6. Similar to the case of *Conn.D.*, the standard deviation of the *SSA* value of the scaffold with *p* = 61.03% was higher than that of the scaffold with a lower porosity.

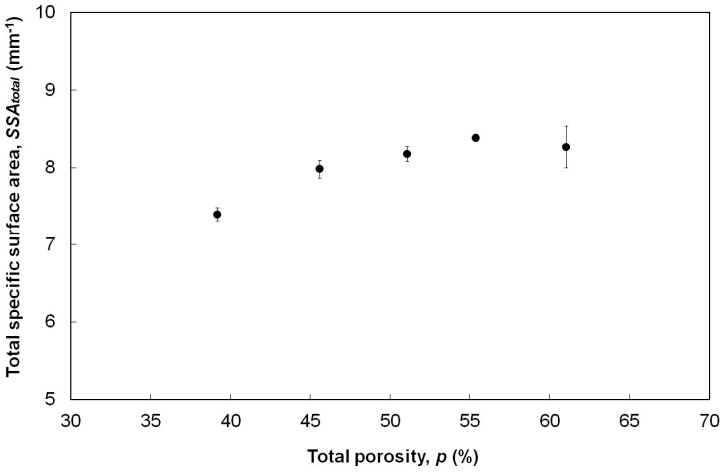

Fig. 6.6. Relationship between the total porosity (*p*) and total specific surface area (*SSA*) of the titanium scaffolds. (Reprinted with permission from Elsevier)

6.3.2. Permeability of the titanium scaffolds

The results of the air permeability tests of the titanium scaffolds with measured porosities *p* in a range of 31.18 – 61.03% are shown in Fig. 6.7.

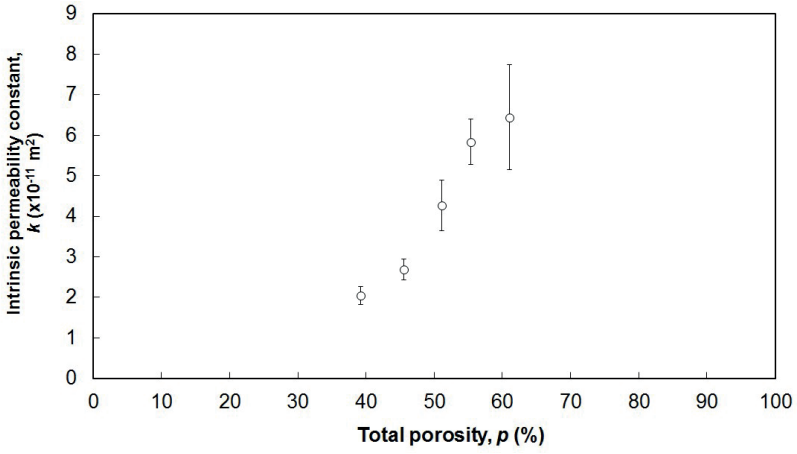

Fig. 6.7. Relationship between the total porosity (*p*) and intrinsic permeability constant (*k*) of the titanium scaffolds. (Reprinted with permission from Elsevier)

The intrinsic permeability constant k increased with rising porosity of the scaffold, with values spanning from $k = 2.04 \pm 0.22 \times 10^{-11}$ to $6.38 \pm 2.95 \times 10^{-11}$ m^2. Again, the standard deviation of the k value for the scaffold with $p = 61.03\%$ was larger than that of the scaffold with a lower porosity. To obtain further characteristics of the porous structures, tortuosity T was determined by using Eq. 6.4 [25]:

$$T = \sqrt{\frac{p^3}{k \cdot SSA^2}} \tag{6.4}$$

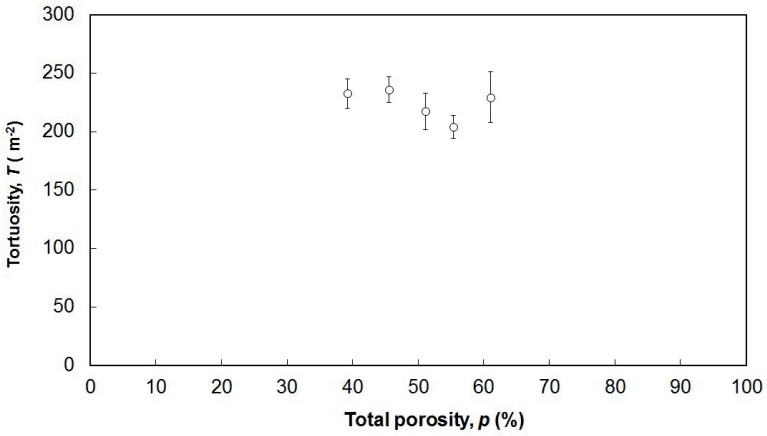

Fig. 6.8. Relationship between the total porosity (p) and tortuosity of interconnected pores (T) within the titanium scaffolds. (Reprinted with permission from Elsevier)

As shown in Fig. 6.8, the tortuosity value of the scaffold decreased with p increasing from 45 to 60%, but increased with p increasing from 60% to 61.03%. The standard deviation of the tortuosity of the scaffold with 61.03% porosity was also larger than that of a scaffold with a lower porosity.

Fig. 6.9 shows a plot comparing the k values obtained in the current research with those reported in the literature. Obviously, over a porosity range from 31 to 61%, the k values of the titanium scaffolds in this study were considerably lower than those of other scaffolds with porosities higher than 70%.

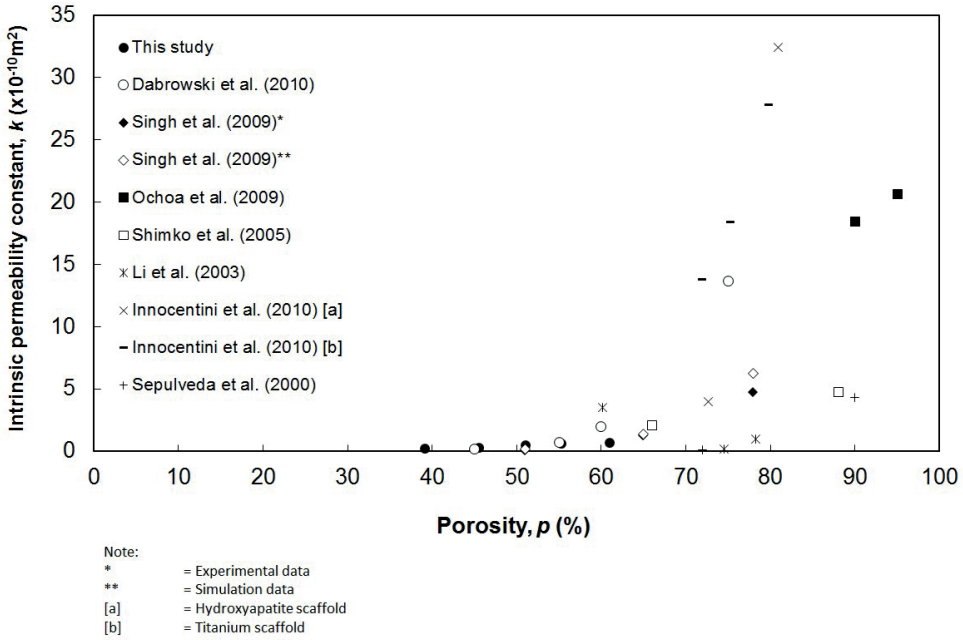

Fig. 6.9. Intrinsic permeability constant (k) of scaffolds for bone tissue engineering. (Reprinted with permission from Elsevier)

6.3.3. Diametral compression behavior of the titanium scaffolds

Fig. 6.10 illustrates a typical stress-strain diagram obtained from the DC test of the titanium scaffold prepared with $x = 60\%$ or $p \approx 50\%$, plotted together with (a) the calculated deformation level of the scaffold, (b) total porosity and (c) the interior parameters of the scaffold, i.e., *Th.Ti* and *Th.Sp.*, after the release of the compressive load at a number of predetermined crosshead displacements.

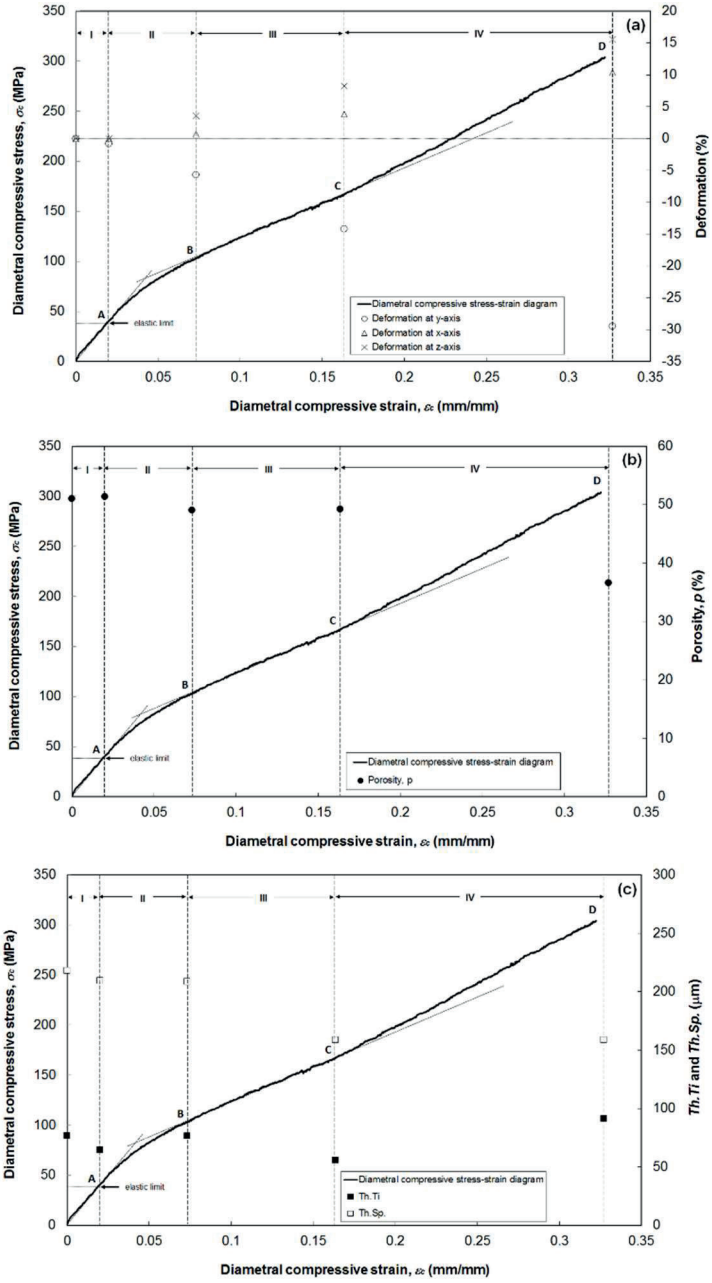

Fig. 6.10. Diametral compressive stress-strain diagram of the titanium scaffold with p = 50%, plotted together with the changes in (a) deformation level, (b) porosity, and (c) thicknesses of titanium struts and spacing between struts in the scaffold with increasing strain during the DC test. (Reprinted with permission from Elsevier)

Apparently, there are four discernible regions in the diagram, namely regions I, II, III and IV. The deformation level of the disc-shaped titanium scaffold was calculated by using Eq. 6.5:

$$R_i = \frac{D_{o,i} - D_i}{D_{o,i}} \times 100\% \tag{6.5}$$

where $D_{o,i}$ and D_i are the initial and final sizes of the disk-shaped specimen. The subscript i can be substituted by x, y and z, according to the direction of deformation (see Fig. 6.2). In the z-direction, for example, the D_o and D values correspond to the initial and final thickness of the scaffold. As shown in Fig. 6.10a, all the R_x, R_y and R_z values at strains ε_c = 0 - 0.02 mm/mm remained unaltered from their initial values. However, R_y decreased and both R_x and R_z increased at ε_c > 0.02 mm/mm.

Fig. 6.10b shows the changes of scaffold porosity along with the progressive diametral compression test of the titanium scaffold prepared with x = 60%. Obviously, the porosity of the scaffold remained unchanged until ε_c = 0.02 mm/mm and then decreased at higher ε_c values. In addition to porosity, the thickness of titanium struts (*Th.Ti*) and the spacing between struts (*Th.Sp.*) in the scaffold interior were also determined by means of micro-CT analysis and then plotted together with the stress-strain diagram obtained from the DC test, as shown in Fig. 6.10c. Clearly, *Th.Sp.* slightly decreased with increasing ε_c up to 0.073 mm/mm. Afterwards, *Th.Sp.* decreased at higher ε_c. On the contrary, the changes in *Th.Ti* were hardly recognizable, due to small fluctuations of this parameter over the range of the diametral compressive strains studied.

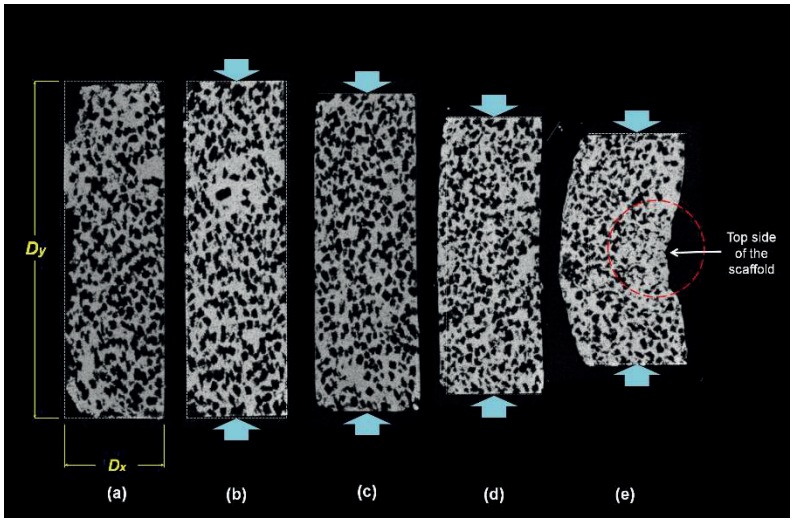

Fig. 6.11. Micro-CT radiographs showing the cross-sections of the titanium scaffolds after a DC test to predetermined strains of: (a) 0 mm/mm, (b) 0.02 mm/mm, (c) 0.073 mm/mm, (d) 0.163 mm/mm and (e) 0.327 mm/mm. (Reprinted with permission from Elsevier)

Fig. 6.11 shows a series of micro-CT radiographs on the longitudinal cross-sections of the titanium scaffold prepared with x = 60% (or $p \approx 50\%$) during the DC test to a number of predetermined compressive strains. Obviously, the diameter of the scaffold parallel to the compressive load applied (D_y) decreased with rising strain ε_c applied during the DC test. At high strains, i.e., ε_c = 0.163 and 0.327 mm/mm, larger deformation occurred on the top side, relative to the bottom side of the disc-shaped scaffold, resulting in buckling along the x-axis of the scaffold. Despite being hard to observe the changes in pore size as a result of compressive load (Fig. 6.11a – 6.11d), it is obvious that collapsed macro-pores, followed by local densification, occurred in the region enclosed with the red circle in Fig. 6.11e, which resulted in the bending of the scaffold once the compressive strain reached ε_c = 0.327 mm/mm.

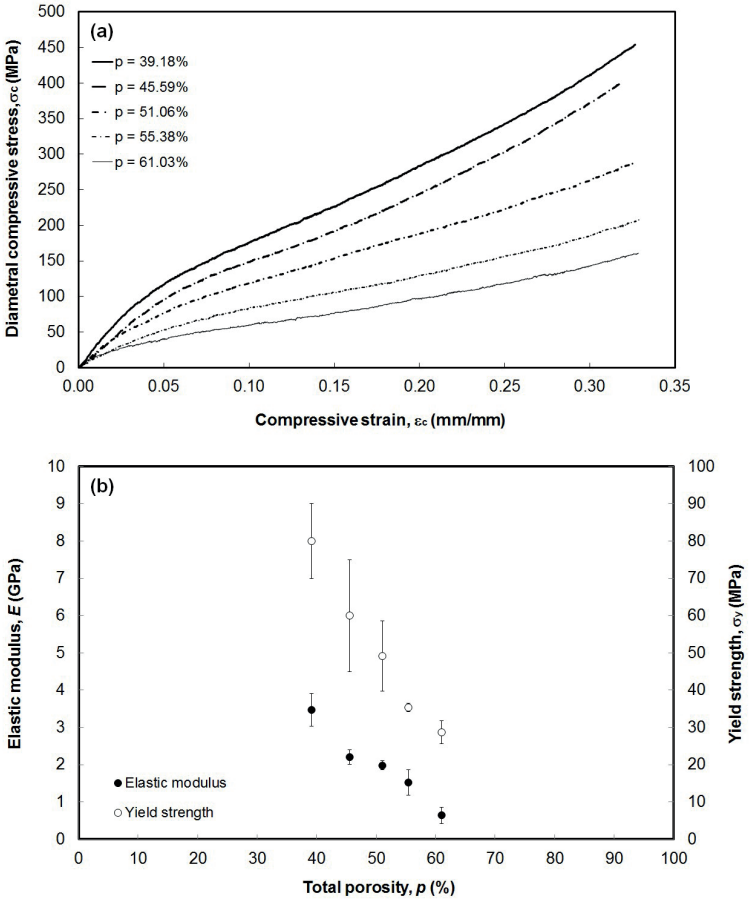

Fig. 6.12. Influence of scaffold porosity on: (a) the diametral compression stress-strain (σ-ε) relationship and (b) the elastic moduli (E)and yield strengths (σ_y) of the titanium scaffolds. (Reprinted with permission from Elsevier)

The influence of scaffold porosity on the diametral stress-strain relationships of the titanium scaffolds is presented in Fig. 6.12a. Based on the analysis of the linear slope in the elastic region of the diagram (see Subsection 6.4.2), the elastic modulus E and yield strength σ_y of the scaffold could be determined, as presented in Fig. 6.12b. In Table 6.1, the E and σ_y values of the scaffolds in the current study are presented together with the values of other titanium scaffolds reported in the literature.

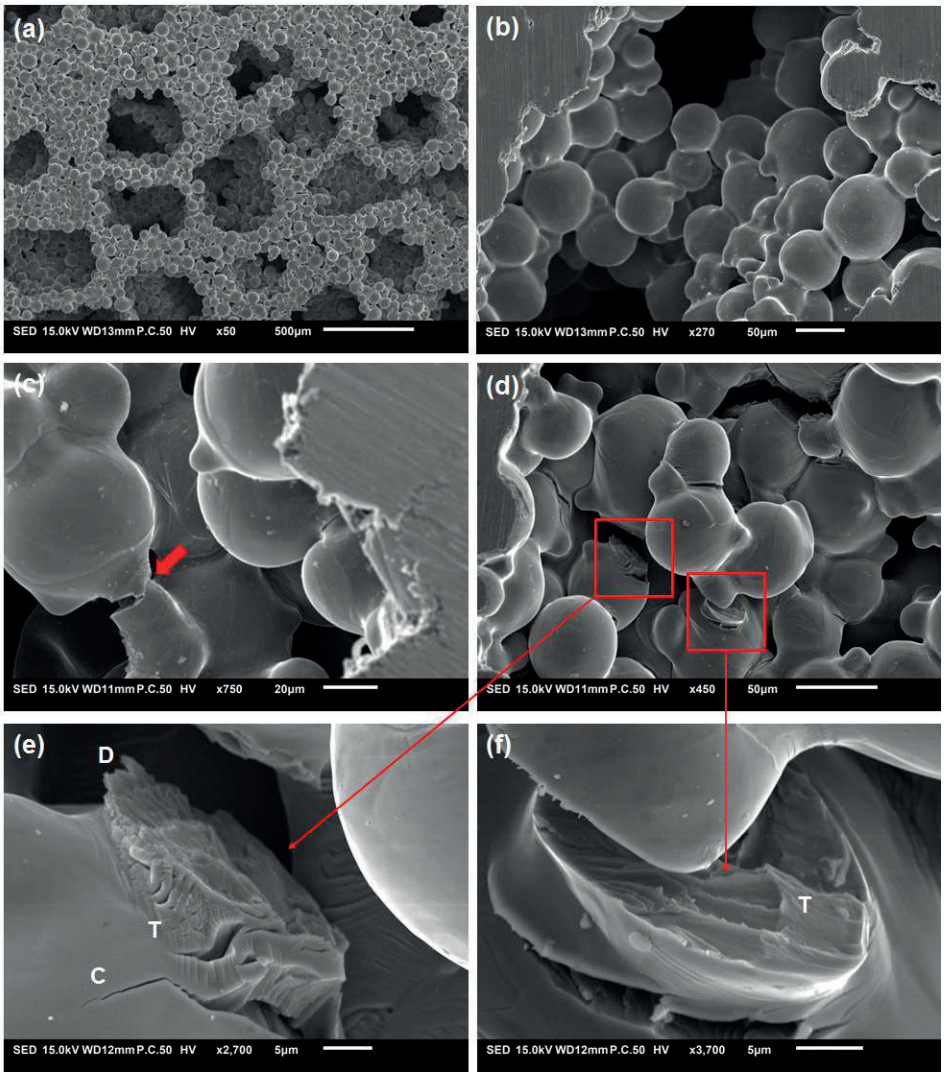

Fig. 6.13. Micrographs of the porous structures of the titanium scaffolds compressed to σ_c = 0 - 0.163 mm/mm, showing that fracture in the struts of the scaffold was initiated by cracks in the necks of sintered titanium powders. (Reprinted with permission from Elsevier)

Table 6.1. Porosities and mechanical properties of the titanium scaffolds prepared with the space holder method

References	Porosities, p (%)	Elastic modulus, E (GPa)	Compressive strength, σ_y (MPa)
This study	31.2 – 61	0.64 – 3.47	28.67 – 80
Esen and Bor [5]	45 – 69.8	0.42 – 8.8	15 – 116
Dabrowski et al. [4]	45 – 75	1 – 8	18 – 121
Torres et al. [26]	42.8 – 45	24.11 – 24.63[a] 9.3 – 10.6[b]	174.5 – 215
Kim et al. [7]	50 – 71	n/a	59 – 280[c] 38 – 111[d]
Gligor et al. [6]	15 – 45	5.6 – 10.1	408 – 969
Mondal et al. [9]	51 – 62	25.05 – 41.4	21.2 – 57.7

a. Based on the ultrasound technique
b. Based on the uniaxial compression test
c. Pores aligned parallel to the direction of compression
d. Pores aligned perpendicular to the direction of compression

Fig. 6.13 shows a series of the micrographs taken in the center of the disc-shaped titanium scaffolds with $p \approx 50\%$ after the DC test to $\varepsilon_c = 0 – 0.163$ mm/mm. In Fig. 6.13a, the presence of macro-pores produced by space-holding particles and micro-pores resulting from incomplete sintering was indicated as well as the channels interconnecting macro-pores inside the scaffold. As shown in Fig. 6.13b, the DC test to $\varepsilon_c = 0.02$ mm/mm did not yield any failure of necks formed during sintering between neighboring titanium powder particles or the overall structure of the titanium matrix. At a higher compressive strain, i.e., $\varepsilon_c = 0.073$ mm/mm, however, fracture of necks occurred, as indicated by the red arrows in Fig. 6.13c. More cracks and fracture at the sintering necks in the scaffold were observed during the DC test to $\varepsilon_c = 0.163$ mm/mm, as visible in Fig. 6.13d. Figs. 6.13e and 6.13f show the fracture surfaces of sintered necks in the scaffold at greater magnifications. Apparently, a terraced pattern was observed in both the fracture surfaces, as marked with T. In Fig. 6.13e, it was observed that a crack from the fractured surface of a titanium particle propagated into its core, as marked with C. In addition, dimples on the fractured surface of titanium necks were found.

To gain a deeper understanding of the failure mechanisms of a porous titanium scaffold occurring during the DC test, the top side and bottom side of the titanium scaffold after a compression test to $\varepsilon_c = 0.327$ mm/mm were examined. Micrographs are shown in Figs. 6.14a and 6.14b. Obviously, the failure was marked by the collision and then slippage of fractured struts on the top surface of the titanium scaffold, as shown in Fig. 6.14a. In addition, cleavages of titanium struts were clearly visible on the bottom side of the scaffold (Fig. 6.14b). Furthermore, cracks that led to the failure of titanium struts in the scaffold were originated from both micro- and macro-pores, as marked by CI and CA in Figs. 6.14c and 6.14d, respectively.

Fig. 6.14c shows a cleavage toward the core of a titanium particle with a terraced pattern on the fractured surface, as seen in Fig. 6.14d.

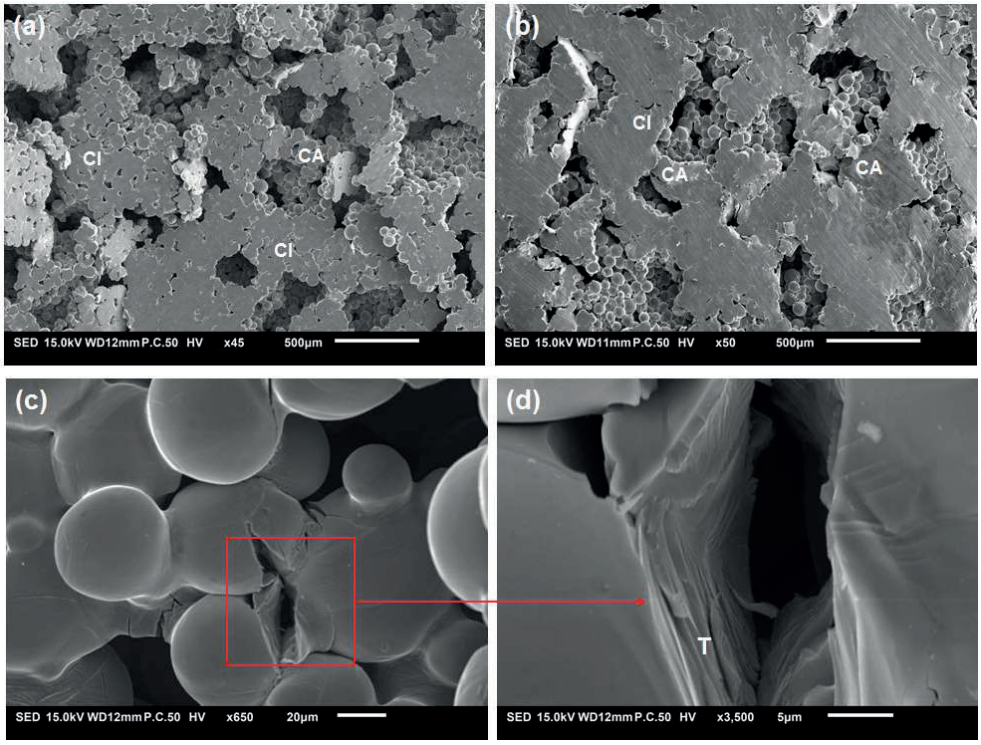

Fig. 6.14. Micrographs of the porous structures of the titanium scaffolds compressed to σ_c = 0.327 mm/mm, showing collision and slippage of fractured struts on the surface of the scaffold (a and b) and the fracture surface at the scaffold struts (c and d). (Reprinted with permission from Elsevier)

6.4. Discussion

6.4.1. Porous structures and open, interconnected pores in the titanium scaffolds

As shown in Fig. 6.3, the porosity of the titanium scaffolds could be controlled by adjusting the volume fraction of space-holding particles added to titanium during scaffold preparation. A linear relationship between the space holder volume fraction and the resulting porosity of the scaffolds, as seen in this figure, was confirmed by a model recently presented by Jian et al. [27].

The *Conn.D.* values obtained from the micro-CT analysis confirmed that pore interconnection inside the scaffold increased with rising porosity. Earlier studies reported an increasing number of interconnected pores with rising space holder volume fraction, as a result of an increasing number of interparticle contacts and the coalescence of space-holding particles during powder compaction [21, 26]. Correlations between *Th.Sp.* and porosity and between *Th.Ti*

and porosity also existed; *Th.Ti* decreased and *Th.Sp.* increased with rising porosity of the scaffold, or rising space holder volume fraction, as shown in Fig. 6.5. Considering a greater chance for space holder particles in a mixture with more space holder particle to coalesce, the determination of a mean pore size of the scaffold by using a *Th.Sp.* value tends to be less accurate in a scaffold with a higher porosity. To avoid this situation, the *Th.Sp.* value of the scaffold with p = 39.18% was used to determine a mean pore size of the titanium scaffold, i.e., d_p = 211 μm. This value appeared to be suitable for bone tissue engineering scaffolds, considering the fact that pore sizes between 200 – 500 μm have been widely accepted as suitable pore sizes for this application [28]. It has also been reported that the pore sizes of 75 - 100 μm were considered as the minimum required for the significant ingrowth of bone tissue in the scaffold [29].

The importance of *SSA* in determining cellular activities within the scaffold was studied by Murphy et al. [30] who considered this parameter to be critical for the initial attachment of cells to the interior of the scaffold. In their research, *SSA* reached a maximum value at p = 50 - 55%. A similar trend of the relationship between porosity and *SSA* was reported by Mitsak et al. [31] who obtained a larger surface area in a polycaprolactone scaffold with a porosity of 53.46% rather than in that with a 70% porosity.

It has been widely reported in the literature that open, interconnected pores within the scaffold can improve its biological and clinical performances by facilitating the transport of nutrients, oxygen and metabolic waste, needed during the regeneration process of bone tissue in the scaffold [25, 32, 33]. To ensure the presence of such open, interconnected pores, the measurement of the intrinsic permeability of the scaffold has been conducted as a supplement to the measurements of porosity and pore sizes [34, 4, 35, 36, 37, 33]. Onchoa et al. emphasized that the scaffolds with the same porosity might have different intrinsic permeability values, due to the differences in porous structure and morphology in the interior of the scaffolds [33]. Li et al. argued that permeability is more relevant than porosity and mean pore size to indicating the performances of the scaffold for tissue engineering [38]. The relationship between the permeability and biological performances of a scaffold has been indicated in several studies. Jones et al., for example, reported that a scaffold with a large number of isolated pores had a poor effective diffusivity and permeability, which in the end induced poor bone ingrowth after 9 weeks of implantation [39]. By using micro-CT, Mitsak et al. indicated better bone penetration in a highly permeable polycaprolactone scaffold [31].

As indicated in Fig. 6.7, the coefficient of permeability k increased from $2.04 \pm 0.22 \times 10^{-11}$ to $6.38 \pm 2.95 \times 10^{-11}$ m^2 with rising porosity from 31.18 – 61.03%. This correlation was in agreement with that reported in the open literature [17, 18, 33]. This finding was confirmed by increased *Conn.D.* value obtained from micro-CT with rising scaffold porosity (see Fig. 6.4). Despite being higher in the k and *Conn.D.* mean values than those of the scaffold with a lower porosity, the standard deviations of the k and *Conn.D.* values of the scaffold with porosity p = 61.03% were considerably larger, which might be related to a broader inter-sample variation of the porous structure of the scaffold interior. As noted earlier, it was harder to handle a scaffold green body with a larger space holder volume fraction, e.g., x = 80%, after the leaching process, due to its too low green strength that would lead to the disintegration of the titanium powder

compact and thus ruining of the porous structure of the scaffold. This limitation might still be encountered in the case of the scaffold green body prepared with $x = 70\%$.

Tortuosity reflects the actual path, through which fluid passes from one end to the other end of the scaffold, divided by the straight distance between these two parallel faces [25]. A higher T value would indicate a higher resistance that the fluid must overcome in order to penetrate into the core and reach the end face of a porous medium. In the current research, it was obvious that a decreased T value was obtained when the porosity of the scaffold was over 50%, which implied a greater number of pore interconnections in the scaffold with a higher porosity.

Based on all these findings, it can be concluded that the titanium scaffolds prepared in this research contained open, interconnected pores as a result of the interparticle contacts between space-holding particles in the green body of the scaffold. In a previous study, it was demonstrated that an effective diffusivity of dissolving space-holding particles inside the green body of the scaffold (D_e) increased due to more interconnections between space-holding particles in the scaffold green body with a higher space holder volume fraction [22]. The presence of the throats that linked the macro-pores in the interior of the scaffold was also clearly shown in the micrograph (Fig. 6.13a).

Since the intrinsic permeability value is independent of the working fluid or the thickness of the porous sample used in the characterization [34, 40], it was interesting to compare the k values of the scaffolds prepared in this study with those of other scaffolds that had been reported in the open literature. As shown in Fig. 6.8, the k values in the current study did not deviate greatly from the results obtained in other research [4, 35, 33, 36, 37, 8]. In the case of titanium scaffolds, the k values obtained in this study were similar to those obtained by Singh et al. [32] and Dabrowski et al. [4] over a porosity range of $p = 30 – 70\%$.

To predict the biological performances of the scaffolds prepared in the current study, it was of interest to compare the k values of the scaffolds with the k value of a graft that has been successfully used to heal bone defects. Hui et al. conducted an in vivo study to investigate the permeability of porcine cancellous bone and its effect on biological response, when the graft was implanted in a rabbit bone [41]. In this study, the k value of 3×10^{-11} m^2 was considered to be a threshold intrinsic permeability constant that could ensure vascularization and mineralization in the graft. Accordingly, titanium scaffolds with porosity $p > 50\%$ in this work were preferably to be used as bone tissue engineering scaffolds.

6.4.2. Diametral compression behavior of the titanium scaffolds

As mentioned earlier, in this research, DC tests were chosen to evaluate the mechanical properties of the titanium scaffolds with low H/D ratios, i.e., < 1. With the space holder method, the scaffold green body may be ruined during processing while space-holding particles are being removed [21, 42, 43, 44]. As a result, the porous structure inside the scaffold product may be deteriorated. This phenomenon is particularly encountered when a region with a lower green density and green strength relative to the rest of the scaffold preform is present, as a consequence of the friction between the compact and die wall during powder compression with a single-acting cold-die press, as that used in this study. The difference in green density between the densest

and the least dense parts in the scaffold preform can be reduced by lowering the H/D ratio of the powder compact [13]. Despite being largely used in the characterization of biomedical ceramic foams [17, 18], the DC tests have rarely been reported in the literature for use in determining the elastic modulus and compressive strength of porous metallic materials. Therefore, it was of critical importance to investigate the compression behavior and mechanisms involved in the deformation of porous metallic material during a DC test.

As shown in Fig. 6.10, the stress-strain diagrams obtained from the DC tests of the sintered titanium scaffolds appeared to be similar to those obtained from uniaxial compression (UC) tests in the work of Esen and Bor [5]. The first region of these diagrams was characterized by a linear part, which corresponded to the elastic behavior of the scaffold [5]. In the current study, this elastic region was confirmed by the measured deformation level (R_x, R_y and R_z), porosity p, and spacing between scaffold struts *Th.Sp.* as well as the micrograph showing interparticle necks in the scaffold. All these remained unchanged from their initial values after compression to ε_c = 0.02 mm/mm (point A). In this region, bending of scaffold struts was considered to be the dominant mechanism during the compression of the titanium scaffold [8, 45]. To ascertain that point A was indeed the elastic limit of the scaffold, the deformation level and porous structure of the titanium scaffold at the end of the non-linear part, i.e., region II of the stress-strain diagram in Fig. 6.10, needed to be examined. As clearly seen in Fig. 6.10a-b, the R_x, R_y, R_z and p values at point B, i.e., ε_c = 0.073 mm/mm, were all no longer equal to those at point A, although the changes in *Th.Ti* and *Th.Sp.* values were not really visible. The decreased R_y and p values without a decrease in *Th.Sp.* might indicate macroscopic deformation governed by the collapse of some of micro-pores, rather than the collapse of macro-pores in the scaffold. At this point, the elastic limit had already been surpassed and the titanium scaffold was deformed plastically. As expected, the R_x and R_z values increased at this point, demonstrating lateral expansion of the scaffold as compression proceeded in the y-direction. It is important to note that the fracture of necks formed during sintering between neighboring titanium matrix powder particles was observed in Fig. 6.13c, indicating that the failure of the scaffold had already started at point B in Fig. 6.10. This finding confirmed that the failure of the titanium scaffold under compressive loading was initiated by stress concentrations at pores and necks, which subsequently resulted in cracks and intergranular fracture of scaffold struts [8, 45, 46]. On the basis of this analysis, the non-linear part after the elastic region in the stress-strain diagram of the DC test could be established as a transition from the elastic behavior of the scaffold to the plastic behavior.

Apparently, point C in Fig. 6.10 corresponds to a transition from two linear parts with different slopes in the DC stress-strain diagram, i.e., regions III and IV. In a typical UC test, the region III and IV correspond to the plateau stage where scaffold struts collapse and solid densification occurs in the scaffold, respectively [5, 47]. At this point, R_y and *Th.Sp.* values became lower, while R_x and R_z values became higher, as compared with those at points A and B. As shown in Fig. 6.11d, the compression behavior of the titanium scaffold at point C, corresponding to ε_c = 0.163 mm/mm, was characterized by the initiation of the bending of the scaffold body along the x-axis. The micrographs in Figs. 6.13d - 6.13f clearly show the intergranular fracture with a terraced pattern (marked with T in Figs. 6.13e - 6.13f) and dimples

(marked with D in Fig. 6.13e) on the fracture surface of sintered titanium matrix particles. A similar observation was made during the UC test performed by Li et al. [8]. Thus, the fracture surface with a terraced pattern, together with dimples corresponding to a ductile fracture characteristic of necks, was a feature of the titanium scaffold prepared with the space holder method.

As noted earlier, the bending of the titanium scaffold body was observed at high compressive strains, starting from ε_c = 0.163 mm/mm (see Fig. 6.11d), which was caused by the differences in the deformability of titanium struts between the top side and bottom side of the scaffold. As shown in Fig. 6.11e, the deformability of titanium struts on the top side, i.e., the region inside the red circle mark, was higher than that on the bottom side of the scaffold, resulting in the bending of the scaffold along the x-axis. Intergranular fracture and subsidence of broken titanium struts on the top side of the scaffold after compression to ε_c = 0.327 mm/mm took place (Fig. 6.14a), confirming that this region was damaged by compression. On the other hand, it was observed that the bottom side of the scaffold suffered from tension, as indicated by the intergranular cracks and fractures without the evidence of strut subsidence after compression to ε_c = 0.327 mm/mm. Özkan and Briscoe [13] reported that the center of the top side was one of the regions with the lowest green density in a cylindrical powder compact. Since an increased green density could enhance the sintering rate of a metal powder as a result of an increased number of interparticle contacts [45], it was thought that the higher deformability of the top side than that of the bottom side of the scaffold was caused by the weaker bonding strength between sintered titanium particles (necks). In the top side region, crack could initiate from the edges of macro-pores or from micro-pores within scaffold struts, as also indicated by Li et al. [8].

On the basis of the above analysis, the deformation and failure mechanisms of a disc-shaped titanium scaffold during the DC test could be established.

1. Elastic deformation occurs at the beginning. It can be characterized from the linear part of the stress-strain diagram obtained from the DC test of a disc-shaped titanium scaffold.
2. The transition from elastic deformation to plastic deformation is indicated by the non-linear part of the stress-strain diagram and intergranular cracks at the necks of sintered titanium powder in the scaffold.
3. As the compression progresses, plastic deformation occurs, followed by the collapse of macro-pores and ductile fracture of titanium struts.
4. To higher compressive strains, i.e., ε_c = 0.163 - 0.327 mm/mm, densification takes place to a certain extent but macro-pores with distorted shapes are still present. The bending of the scaffold body along its horizontal axis occurs as a result of green density variation inside the scaffold preform and thus the inhomogeneity of the bonding strength between necks inside the scaffold.

Making use of the elastic region in the stress-strain diagrams obtained from the DC tests, one can establish a relationship between total porosity p and elastic modulus E. In this research, the relationship was established between porosity over a range of p = 31.18 to 61.03% and elastic modulus E over a range of 0.64 – 3.47 GPa, as shown in Fig. 12. With the 0.2% strain offset method, the yield strength σ_y values were determined, i.e., 28.67 to 80 MPa, over a porosity

range of p = 31.18 to 61.03%. In this research, the σ_y value was taken as a measure of the compressive strength of the titanium scaffold. As clearly indicated in Table 1, the E and σ_y values over a porosity range from 31.18 – 61.03% in this study, i.e., 0.64 – 3.47 GPa and 28.67 – 80 MPa, were comparable with those of the titanium scaffolds reported by Esen and Bor [5] and Dabrowski et al. [4].

To establish the relationships of porous structures between porosity p and E and between porosity p and σ_y, many researchers have tried to fit the data set obtained from compression tests into empirical models, e.g., Gibson model [47], as expressed in Eqs. 6.6 and 6.7:

$$E/E_s = C_1(1-p)^a \tag{6.6}$$

$$\sigma_y/\sigma_{y,s} = C_2(1-p)^b \tag{6.7}$$

where E_s and $\sigma_{y,s}$ are the elastic modulus and yield strength of solid grade 1 titanium, as used in this study, i.e., 100 GPa and 170 MPa, respectively [48]. C_1 and C_2 are the constants related to the cell geometry, while a and b equal to 2 and 1.5, respectively [47]. In this research, an attempt was made to fit the E and σ_y values obtained from the DC stress-strain diagrams into Eqs. 6.6 and 6.7. The C_1, C_2, a and b constants were then determined and presented in Table 6.2, together with those of the titanium scaffolds that have been found in the literature [5, 10, 49, 50].

Table 6.2. Constants derived from the Gibson model [47]

References	Relative density, 1 - ε	C_1	C_2	a	b
This study	0.38-0.65	0.220	1.54	3.56	2.38
Esen and Bor [5]	0.3-0.55	1.598	2.13	4.72	3.57
Niu et al. [49]	0.25-0.45	0.193	0.375	1.43	2.06
Mansourighasri et al. [10]	0.21-0.36	N/A	N/A	2.96	1.36
Lee et al. [50]	0.57-0.84	1.08	1.44	2.34	2.87

As shown in Table 6.2, the a and b constants were not equal to 2 and 1.5, respectively. Also, the C_1 and C_2 constants were not equal to 0.98 and 0.3, respectively, as suggested by Gibson [47]. This finding might reflect the differences in porous structure between the scaffold in the current study and that used by Gibson to derive his empirical model [5]. The Gibson model is applicable to the scaffolds with porosities higher than 70% (or relative density of <0.3) and tetrakaidodecahedral pores, instead of those with lower porosities, i.e., <65%, irregularly structured and shaped pores, as in this study. Wen et al. [11] also noticed the discrepancy in elastic modulus between the experimental and calculated values based on Eq. 6.5, in the case of titanium scaffolds with porosities lower than 80%.

A number of researchers have also reported the elastic modulus E and yield strength σ_y values of bone tissue. For instance, Yang et al. noted that the elastic moduli of cancellous and cortical bone tissue were 0.02 – 0.5 GPa and 3 – 30 GPa, respectively [51]. The yield strengths of cancellous and cortical bone tissue were 4 – 12 MPa and 130 – 180 MPa, respectively. The work of Bayraktar et al. revealed an elastic modulus of 18 and 19.9 GPa for trabecular and cortical bone tissue, respectively, and 135.3 MPa as the yield strength of the latter bone tissue [52]. Similarly, as noted by Karageorgiou and Kaplan [28], the elastic modulus and ultimate strength of cortical bone subjected to longitudinal compression were 17 GPa and 193 MPa, respectively. Recently, based on a review of Alvarez and Nakajima [53], the elastic modulus E of cortical bone tissue has been generalized over a range from 14.1 to 27.6 GPa. The compressive strengths have been determined to be 219 MPa and 153 MPa, measured in the longitudinal and transversal direction, respectively. The E and σ_y values of trabecular bone tissue have been generalized in the ranges from 0.1 - 0.4 GPa and 1.5 – 9.3 MPa, respectively.

As noted earlier, the intrinsic permeability constant k values of the titanium scaffolds with p > 50% were close to the threshold value for revascularization [41]. However, the interior of the titanium scaffold with $p \approx 65\%$ might have been ruined to some extent, as implied by the large standard deviations of the *SSA*, *Conn.D.*, k and T values. Accordingly, the titanium scaffolds with $p = 50 – 55\%$ would be the preferred ones as the products with an optimum design of the porous structure suitable for bone tissue engineering. Over a porosity range of 50 – 55%, the elastic modulus E and yield strength σ_y values of the titanium scaffolds were 1.53 – 1.98 GPa and 35.3 – 49.2 MPa, respectively. These E and σ_y values are quite close to the measured values of trabecular or cancellous bone tissue reported in the literature [51, 53]. Therefore, the titanium scaffolds with porosity of 50 – 55% prepared in this study might be applicable for cancellous bone tissue engineering.

6.5. Conclusions

In this research, open, interconnected pores and mechanical properties of biomedical titanium scaffolds prepared by using the space holder method were characterized. The results from micro-CT analysis and permeability tests confirmed the presence of open, interconnected pores in the titanium scaffolds with porosity over a range of 31 – 61%. A maximum specific surface area could be achieved in the scaffold with a total porosity of 50 - 55%. Such titanium scaffolds would have elastic moduli of 0.64 – 3.47 GPa and yield strengths of 28.67 – 80 MPa.

Deformation and failure occurring during the DC tests of the scaffolds were initiated by elastic deformation, which was characterized from the linear part of the stress-strain diagram obtained from the DC test. As compression proceeded further, plastic deformation took place, followed by the collapse of macro-pores and ductile fracture of titanium struts. At high compression strains, densification occurred, resulting in distortions of macro-pores.

In conclusion, on the basis of the measured specific surface area, permeability and mechanical properties, the titanium scaffolds with porosities of 50 - 55% appeared to be the most suitable ones to be used in cancellous bone tissue engineering.

References

[1] G. Ryan, A. Pandit and D. P. Apatsidis, "Fabrication methods of porous metals for use in orthopaedic applications," *Biomaterials,* vol. 27, pp. 2651-2670, 2006.

[2] R. Singh, P. D. Lee, R. J. Dashwood and T. C. Lindley, "Titanium foams for biomedical applications: A review," *Materials Technology,* vol. 25, pp. 127-136, 2010.

[3] T. Imwinkelried, "Mechanical properties of open-pore titanium foam," *Journal of Biomedical Materials Research A,* vol. 81, pp. 964-970, 2007.

[4] B. Dabrowski, W. Swieszkowski, D. Godlinski and K. J. Kurzydlowski, "Highly porous titanium scaffolds for orthopaedic applications," *Journal of Biomedical Materials Research B: Applied Biomaterials,* vol. 95, pp. 53-61, 2010.

[5] Z. Esen and S. Bor, "Processing of titanium foams using magnesium spacer particles," *Scripta Materialia,* vol. 56, pp. 341-344, 2007.

[6] I. Gligor, O. Soritau, M. Todea, C. Berce, A. Vulpoi, T. Marcu, V. Cernea, S. Simon and C. Popa, "Porous c.p. titanium using dextrin as space holder for endosseous implants," *Particulate Science and Technology,* vol. 31, pp. 357-365, 2013.

[7] S. W. Kim, H. D. Jung, M. H. Kang, H. E. Kim, Y. H. Koh and Y. Estrin, "Fabrication of porous titanium scaffold with controlled porous structure and net-shape using magnesium as spacer," *Materials Science and Engineering C,* vol. 33, pp. 2808-2815, 2013.

[8] B. Q. Li, C. Y. Wang and X. Lu, "Effect of pore structure on the compressive property of porous Ti produced by powder metallurgy technique," *Materials and Design,* vol. 50, pp. 613-619, 2013.

[9] D. Mondal, J. Datta Majumder, N. Jha, A. Badkul, S. Das, A. Patel and G. Gupta, "Titanium-cenosphere syntactic foam made through powder metallurgy route," *Materials and Design,* vol. 34, pp. 82-89, 2012.

[10] A. Mansourighasri, N. Muhamad and A. B. Sulong, "Processing titanium foams using tapioca starch as a space holder," *Journal of Materials Processing Technology,* vol. 212, pp. 83-89, 2012.

[11] C. E. Wen, Y. Yamada, K. Shimojima, Y. Chino, T. Asahina and M. Mabuchi, "Processing and mechanical properties of autogenous titanium implant materials," *Journal of Materials Science: Materials in Medicine,* vol. 13, pp. 397-401, 2002.

[12] R. Singh, P. Lee, T. Lindley, C. Kohlhauser, C. Hellmich, M. Bram, T. Imwinkelried and R. Dashwood, "Characterization of the deformation behavior of intermediate porosity

interconnected Ti foams using micro-computed tomography and direct finite element modeling," *Acta Biomaterialia,* vol. 6, pp. 2342-2351, 2010.

[13] N. Ozkan and B. Briscoe, "Characterization of die-pressed green compacts," *Journal of European Ceramics Society,* vol. 17, pp. 697-711, 1997.

[14] J. Fell and J. Newton, "Determination of tablet strength by the diametral-compression test," *Journal of Pharmaceutical Science,* vol. 59, pp. 688-691, 59.

[15] P. Jonsén, H. Häggblad and K. Sommer, "Tensile strength and fracture energy of pressed metal powder by diametral compression test," *Powder Technology,* vol. 176, pp. 148-155, 2007.

[16] G. Kamst, J. Vasseur, C. Bonazzi and J. Bimbenet, "A new method for the measurement of the tensile strength of rice grains by using the diametral compression test," *Journal of Food Engineering,* vol. 40, pp. 227-232, 1999.

[17] A. Almirall, G. Larrecq, J. Delgado, S. Martinez, J. Planell and M. Ginebra, "Fabrication of low temperature macroporous hydroxyapatite scaffolds by foaming and hydrolysis of an alpha-TCP paste," *Biomaterials,* vol. 25, pp. 3671-3680, 2004.

[18] R. Pilliar, M. Filiaggi, J. Wells, M. Grynpas and R. Kandel, "Porous calcium polyphosphate sca!olds for bone substitute applications - In vitro characterization," *Biomaterials,* vol. 22, pp. 963-972, 2001.

[19] M. Es-Saheb, A. Albedah and F. Benyahia, "Diametral compression test: Validation using finite element analysis," *International Journal of Advanced Manufacturing Technology,* vol. 57, pp. 501-509, 2011.

[20] A. Procopio, A. Zavaliangos and J. Cunningham, "Analysis of the diametral compression test and the applicability to plastically deforming materials," *Journal of Materials Science,* vol. 38, pp. 3629-3639, 2003.

[21] B. Arifvianto, M. Leeflang and J. Zhou, "The compression behaviors of titanium/carbamide powder mixtures in the preparation of biomedical titanium scaffolds with the space holder method," *Powder Technology,* vol. 284, pp. 112-121, 2015.

[22] B. Arifvianto, M. Leeflang, J. Duszczyk and J. Zhou, "Characterisation of space holder removal through water leaching for preparation of biomedical titanium scaffolds," *Powder Metallurgy,* vol. 57, pp. 9-12, 2014.

[23] T. Ferreira and W. Rasband, ImageJ User Guide, 2012.

[24] M. Doube, M. Klosowski, I. Arganda-Carreras, F. Cordelieres, R. Dougherty, J. Jackson, B. Schmid, J. Hutchinson and S. Shefelbine, "BoneJ: Free and extensible bone image analysis in ImageJ," *Bone,* vol. 47, pp. 1076-1079, 2010.

[25] T. S. Karande, J. L. Ong and C. M. Agrawal, "Diffusion in musculoskeletal tissue engineering scaffolds: Design issues related to porosity, permeability, architecture, and nutrient mixing," *Annals of Biomedical Engineering,* vol. 32, p. 1728–1743, 2004.

[26] Y. Torres, J. Rodríguez, S. Arias, M. Echeverry, S. Robledo, V. Amigo and J. Pavón, "Processing, characterization and biological testing of porous titanium obtained by space-holder technique," *Journal of Materials Science,* vol. 47, pp. 6565-6576, 2012.

[27] X. Jian, C. Hao, Q. Guibao, Y. Yang and L. Xuewei, "Investigation on relationship between porosity and spacer content of titanium foams," *Materials and Design,* vol. 88, pp. 132-137, 2015.

[28] V. Karageorgiou and D. Kaplan, "Porosity of 3D biomaterial scaffolds and osteogenesis," *Biomaterials,* vol. 26, pp. 5474-5491, 2005.

[29] S. F. Hulbert, F. A. Young, R. S. Mathews, J. J. Klawitter, C. D. Talbert and F. H. Stelling, "Potential of ceramic materials as permanently implantable skeletal prostheses," *Journal of Biomedical Materials Research,* vol. 4, pp. 433-456, 1970.

[30] C. M. Murphy, M. G. Haugh and F. J. O'Brien, "The effect of mean pore size on cell attachment, proliferation and migration in collagen-glycosaminoglycan scaffolds for bone tissue engineering," *Biomaterials,* vol. 31, pp. 461-466, 2010.

[31] A. Mitsak, J. Kemppainen, M. Harris and S. Hollister, "Effect of polycaprolactone scaffold permeability on bone regeneration in vivo," *Tissue Engineering A,* vol. 17, pp. 1831-1839, 2011.

[32] R. Singh, P. Lee, T. Lindley, R. Dashwood, E. Ferrie and T. Imwinkelried, "Characterization of the structure and permeability of titanium foams for spinal fusion devices," *Acta Biomaterialia,* vol. 5, pp. 477-487, 2009.

[33] I. Ochoa, J. Sanz-Herrera, J. Garcia-Aznar, M. Doblare, D. Yunos and A. Boccaccini, "Permeability evaluation of 45S5 Bioglass-based scaffolds for bone tissue engineering," *Journal of Biomechanics,* vol. 42, pp. 257-260, 2009.

[34] M. Chor and W. Li, "A permeability measurement system for tissue engineering scaffolds," *Measurement Science and Technology,* vol. 18, pp. 208-216, 2007.

[35] M. Innocentini, R. Faleiros, R. Pisani, I. Thijs, J. Luyten and S. Mullens, "Permeability of porous gelcast scaffolds for bone tissue engineering," *Journal of Porous Materials,* vol. 17, pp. 615-627, 2009.

[36] P. Sepulveda, F. Ortega, M. Innocentini and V. Pandolfelli, "Properties of highly porous hydroxyapatite obtained by the gelcasting of foams," *Journal of Americal Society of Ceramics,* vol. 83, p. 3021–3024, 2000.

[37] D. Shimko, V. Shimko, E. Sander, K. Dickson and E. Nauman, "Effect of porosity on the fluid flow characteristics and mechanical properties of tantalum scaffolds," *Journal of Biomedical Materials Research B: Applied Biomaterials,* vol. 73, pp. 315-324, 2005.

[38] S. Li, J. de Wijn, J. Li, P. Layrolle and K. De Groot, "Macroporous biphasic calcium phosphate scaffold with high permeability/porosity ratio," *Tissue Engineering,* vol. 9, pp. 535-548, 2003.

[39] A. Jones, C. Arns, D. Hutmacher, B. Milthorpe, A. Sheppard and M. Knackstedt, "The correlation of pore morphology, interconnectivity and physical properties of 3D ceramic scaffolds with bone ingrowth," *Biomaterials,* vol. 30, pp. 1440-1451, 2009.

[40] D. Shimko and E. Nauman, "Development and characterization of a porous poly(methyl methacrylate) scaffold with controllable modulus and permeability," *Journal of Biomedical Materials Research B: Applied Biomaterials,* vol. 80, pp. 360-369, 2007.

[41] P. Hui, P. Leung and A. Sher, "Fluid conductance of cancellous bone graft as a predictor of graft-host interface healing," *Journal of Biomechanics,* vol. 29, pp. 123-132, 1996.

[42] Y. Torres, J. J. Pavón and J. A. Rodríguez, "Processing and characterization of porous titanium for implants by using NaCl as space holder," *Journal of Materials Processing Technology,* vol. 212, pp. 1061-1069, 2012.

[43] A. Laptev, M. Bram, H. P. Buchkremer and D. Stöver, "Study of production route for titanium parts combining very high porosity and complex shape," *Powder Metallurgy,* vol. 47, pp. 85-92, 2004.

[44] A. Laptev, O. Vyal, M. Bram, H. Buchkremer and D. Stöver, "Green strength of powder compacts provided for production of highly porous titanium parts," *Powder Metallurgy,* vol. 48, pp. 358-364, 2005.

[45] Z. Esen and S. Bor, "Characterization of Ti–6Al–4V alloy foams synthesized by space holder technique," *Materials Science and Engineering A,* vol. 528, pp. 3200-3209, 2011.

[46] I. -H. Oh, N. Nomura, N. Masahashi and S. Hanada, "Microstructures and mechanical properties of porous titanium compacts prepared by powder sintering," *Materials Transactions,* vol. 43, pp. 443-446, 2002.

[47] L. Gibson, "Mechanical behavior of metallic foams," *Annual Review of Materials Science,* vol. 30, p. 191–227, 2000.

[48] M. Donachie Jr., Titanium: A technical guide, Ohio: ASM International, The Materials Information, 2000.

[49] W. Niu, C. Bai, G. Qiu and Q. Wang, "Processing and properties of porous titanium using space holder technique," *Materials Science and Engineering A,* vol. 506, pp. 148-151, 2009.

[50] B. Lee, T. Lee, Y. Lee, D. Lee, J. Jeong, J. Yuh, S. Oh, H. Kim and C. Lee, "Space-holder effect on designing pore structure and determining mechanical properties in porous titanium," *Materials and Design,* vol. 57, p. 712–718, 2014.

[51] S. Yang, K.-F. Leong, Z. Du and C.-K. Chua, "The design of scaffolds for use in tissue engineering. Part I. Traditional factors," *Tissue Enginnering,* vol. 7, pp. 679-689, 2001.

[52] H. Bayraktar, E. Morgan, G. Niebur, G. Morris, E. Wong and T. Keaveny, "Comparison of the elastic and yield properties of human femoral trabecular and cortical bone tissue," *Journal of Biomechanics,* vol. 37, pp. 27-35, 2004.

[53] K. Alvarez and H. Nakajima, "Metallic scaffolds for bone regeneration," *Materials,* vol. 2, pp. 790-832, 2009.

Chapter 7

Conclusions, general discussion and recommendations

7.1. Conclusions

The research presented in this thesis has delivered general conclusion as the following.

> **General conclusion:** By using the space holder method, titanium scaffolds with controllable porous structure and mechanical properties can be achieved through the adjustments of the volume fraction of space-holding particles and process parameters such as compacting pressure and duration for the removal of the space holder material.

The general conclusion above can be broken down into the more specific conclusions in Section 7.1.1 – 7.1.3, which are drawn based on the research in Chapters 3 – 6 of this thesis.

7.1.1. Characterization of the fabrication processes for titanium scaffolds with the space holder method

The results of the study on powder compaction in the preparation of titanium scaffold preforms in Chapter 3 led to Conclusion 1.

> **Conclusion 1:** The critical compacting pressure for the preparation of titanium scaffolds with carbamide space holder depends on the volume fraction of space-particles in the mixture (x).

Furthermore, the study on the water leaching process for removing the space holder material from the scaffold preform led to Conclusion 2, based on the work in Chapters 4 and 5.

> **Conclusion 2:** The green body of titanium scaffold containing a higher volume fraction of the space holder material required a shorter duration to completely remove carbamide space-holding particles.

7.1.2. Control of scaffold porous structure

The characterization of porous structure in titanium scaffolds prepared under the optimized conditions established in this study led to Conclusion 3, based on the work in Chapter 5.

> **Conclusion 3:** Porous structure of titanium scaffolds that were processed with sintering at 1200ºC for 3 h could be controlled by adjusting the volume fraction of space-holding particles in the scaffold green body.

7.1.3. Characterization of the physical and mechanical properties of scaffolds prepared with optimized fabrication process parameters

The evaluation of mechanical properties, permeability tests and micro-CT analysis in Chapter 6 led to Conclusion 4.

> **Conclusion 4:** The space holder method was an appropriate technique for the fabrication of titanium scaffolds with porosity of ~50% to replace defected cancellous bone tissue.

7.2. General discussion

In the last decade, bone tissue engineering as an alternative approach to the reconstruction of defects in bone tissue has received increasing attention in the biomedical research community. With this approach, large fracture in bone tissue can be repaired and remodelled with new bone cells in a medium implanted at the defect site [1]. In taking this approach, scaffold with an appropriate porous structure is required to facilitate cellular activities, such as the migration and proliferation of osteoblasts and mesenchymal cells, as well as the transport of nutrients and oxygen required for vascularization during bone tissue development [2, 3, 4]. Up till now, titanium and its alloys have been selected as preferred biomaterials for bone tissue engineering scaffolds, owing to their excellent mechanical properties and biocompatibility. Since titanium and its alloys are non-degradable materials, in order to minimizing stress shielding, the mechanical properties of these materials should be adjusted to be as close to the properties of bone tissue as possible, for instance by creating porous structure. Powder metallurgy has been recognized as an appropriate technique for the fabrication of scaffolds made of titanium or its alloys. In order to generate a highly porous structure with interconnected pores suitable for bone tissue engineering, a temporary space-holding powder as a pore former is needed [5, 6, 7].

7.2.1. Characterization of the fabrication process of titanium scaffolds with the space holder method

Despite a large number of studies on the fabrication of titanium scaffolds with the space holder method, the mechanisms involved in the scaffold fabrication with this method have not been fully understood. Instead of being optimized through a series of systematic studies and on the basis of the concepts of powder metallurgy, the fabrication process of titanium scaffolds

with the space holder method had been explored mostly by trial-and-error. These could lead to difficulties in ensuring the reproducibility of scaffold properties and, in the end, might result in the uncertainties of scaffold performance to heal the bone defect of the patient. Therefore, the objective of this thesis is to give an insight into the way to control and to optimize the porous structure of biomedical titanium scaffolds prepared with the space holder method in order to meet the requirements of scaffolds in physical and mechanical properties for bone tissue engineering. On the basis of the knowledge of the mechanisms involved in their fabrication processes with the space holder method, titanium scaffolds with porous structures that could meet the requirements for bone tissue engineering were proposed at the end of this thesis.

In this thesis, the attempt to control and optimize the porous structure of titanium scaffolds was first made by characterizing the powder compaction process of titanium matrix and carbamide space-holding particles, as presented in Chapter 3. In this case, a too high compacting pressure could lead to excessive deformation and even breakage of space-holding particles embedded in the titanium matrix powder, which might in the end lead to distortion of macro-pore geometry in scaffold products. On the other hand, a too low compacting pressure could result in scaffold green body with low green strengths, which might in the end cause ruining of the scaffold green body during or after the space holder removal process to generate macro-pores. Considering these two scenarios, an appropriate pressure should be applied in the compaction of titanium/carbamide powder mixtures. In this connection, a research question arose as to how appropriate pressures for compacting titanium/carbamide powder mixtures could be determined.

As presented in Chapter 3, appropriate compacting pressures for the preparation of titanium scaffolds with carbamide space-holding particles were determined, based on the compression behaviors of these two powders under uniaxial compressive stresses. The titanium matrix powder and carbamide space-holding particles exhibited dissimilar compression behaviors under the compressive stresses applied. To quantify these behaviors, the yield pressures of titanium powder, carbamide particles and their mixtures were determined with the aid of the Heckel model [8]. Since the yield pressure of titanium powder was higher than that of carbamide particles, the critical compacting pressure decreased with rising volume fraction of carbamide particles in the mixture. Thus, the measured yield pressure should be used as a critical pressure [8, 9, 10], with which a titanium/carbamide powder mixture could be compacted to generate the scaffold green body with a sufficient green strength but without causing excessive deformation and breakage of space-holding particles. As indicated in Chapter 3, the rule of mixtures could be applied with caution to predict the critical pressure for compacting a titanium/carbamide powder mixture with a predetermined space holder volume fraction. Nevertheless, by applying this approach for compacting titanium/carbamide powder mixtures, carbamide space-holding particles inside the scaffold green body remained intact, as demonstrated in an optical microscopic study. By means of micro-computed tomography (micro-CT), it was confirmed in Chapter 5 that the application of compressive stresses based on the rule of mixtures and yield pressures resulted in the sintered titanium scaffolds with acceptable pore sizes for bone tissue engineering, i.e., within the range of 200 – 500 μm [11, 12]. A similar approach to determine the

appropriate compacting pressure by using the rule of mixtures was adopted in the research of Mondal et al. [13] and Jha et al. [14]. In their research, instead of the yield pressures (P_y), the strengths ($\bar{\sigma}$) of elemental powder particles were applied in the rule of mixtures (Eq. 2.3). However, the application of P_y was considered more relevant and appropriate because this parameter was derived on the basis of the powder behaviour during uniaxial cold compaction used in this research [8].

To generate macro-pores in the scaffold, space-holding particles inside the titanium/carbamide powder compact should be removed. It is important to note that inappropriate removal of space-holding particles might result in ruined scaffold green body or contamination due to the presence of residues inside the scaffold preform. At this processing step, two fundamental questions remained unanswered as to how to characterize and then to optimize the space holder removal process during scaffold preparation with the space holder method.

In Chapter 4, a novel and precise weight measurement technique for the characterization of the removal process of carbamide space-holding particles by the water leaching method is presented based on the ASTM B963-08 standard. With this technique, the mechanisms operating during space holder removal by using water leaching could be determined with the aid of the existing solvent debinding models for powder injection moulded parts [15, 16]. Three primary regimes representing the leaching behavior of carbamide particles in the scaffold preform were recognized, namely (i) rapid dissolution, (ii) dissolution and diffusion and (iii) saturation. Based on these mechanisms, the influence of space holder volume fraction on the duration and efficiency of the leaching process to remove carbamide space-holding particles was investigated and the appropriate durations required for the leaching process to remove carbamide particles were determined (Chapters 5). It was concluded that the green body of titanium scaffold containing a higher volume fraction of the space holder material required a shorter duration to completely remove carbamide space-holding particles. The x = 70% was the highest space holder volume fraction that could be used for processing scaffolds with this method, beyond which disintegration of titanium powder from the scaffold green body took place. Disintegration of titanium powder occurred during the leaching process, mainly at the circumference of the bottom part of the scaffold green body. As noted in Chapter 4, the new method proposed in this research was precise and able to minimize the chance of the ruining of the scaffold green body due to multiple-step handling for weighing and determining weight loss [17, 18]. Based on the work reported in Chapter 5, the accuracy of this technique remained a challenge, owing to the disintegration of titanium particles in the region of the scaffold green body with a low green strength. The powder compaction technique that could ensure a homogeneous green density and minimize the presence of regions with a low green strength over the scaffold green body was therefore suggested.

7.2.2. Control of the scaffold porous structure

With the powder compaction and space holder removal processes optimized, the fabrication of titanium scaffolds with a controllable porous structure and structural integrity and without

contamination could be executed. However, another fundamental question as to whether the final porous structure of the sintered titanium scaffold could reflect powder particle arrangements inside the scaffold green body remained unanswered. As discussed in Chapter 2, the shrinkage of the porous green body of titanium scaffold inevitably occurred due to sintering. Excessive shrinkage might lead to the deviations of the final porosity and macro-pore geometry of the sintered scaffold from the volume fraction and geometry of space-holding particles in the green body of the scaffold. Therefore, the information on the changes of 3-dimensional (3D) porous structure from the green body to sintered titanium scaffolds should be obtained.

In Chapter 5, the 3D porous structures of the green body and sintered titanium scaffolds prepared under the optimized conditions reported in Chapters 3 and 4 were characterized by means of micro-CT. This study concluded that the porous structures of the titanium scaffolds processed through water leaching and sintering at 1200 ºC for 3 h did not deviate significantly from their green structures. Thus, the control of the final porous structure of titanium scaffold from its green body would be feasible by applying these sintering parameters. As a consequence, the desired porous structure of a titanium scaffold could be realized conveniently and efficiently by selecting the right space holder volume fraction, thereby avoiding multiple attempts based on trial and error to realize such a desired porous structure. The results of the work reported in Chapter 5 also revealed the important parameters that could be optimized by adjusting the volume fraction of space-holding particles in the scaffold. For instance, maximum specific surface area values of the green body and sintered scaffold could be obtained by adding 60 – 65 vol.% carbamide space-holding particles, which corresponded to a total porosity of 50 – 55% in the sintered scaffold. In addition, the connectivity density measured by means of micro-CT increased with rising space holder volume fraction in the scaffold green body.

7.2.3. Characterization of physical and mechanical properties of the scaffolds prepared with optimized fabrication process parameters

To evaluate the performance of titanium scaffold products prepared after a series of experimental studies presented in Chapters 3 – 5, the presence of open, interconnected pores in the scaffold interior was confirmed and the elastic modulus and the yield strength of the scaffold were determined. As shown in Chapter 6, micro-CT and permeability analyses were carried out to quantify the porous structures and to ascertain the presence of open, interconnected pores in the scaffolds with porosity in a range of 31 – 61%. The elastic moduli and yield strengths of the scaffolds were also determined with the aid of the stress-strain diagrams obtained from diametral compression (DC) tests.

The results of the micro-CT and permeability analyses confirmed the presence of open, interconnected pores in the titanium scaffolds with total porosity in a range of 31 – 61%. Interestingly, the intrinsic permeability constant k value of the scaffold with total porosity of ~50% was close to that of the threshold value for revascularization, i.e., 3×10^{-11} m^2 inside the bone graft [19]. Elastic moduli and yield strengths of titanium scaffolds having this level of porosity could be achieved in the ranges of 0.64 – 3.47 GPa and 28.67 – 80 MPa, respectively. The elastic moduli of the titanium scaffolds with porosity in a range of 50 – 55%, i.e., 1.53 –

1.98 GPa, were comparable to the elastic modulus of cancellous bone tissue reported in the literature, i.e., 0.02 – 0.5 GPa [20]. The yield strengths of the scaffolds at this level of porosity, i.e., 35.3 – 49.2 MPa, were higher than the yield strength of cancellous bone, i.e., 4 – 12 MPa [20], which demonstrated that the strengths of the titanium scaffolds prepared with the method in this research were sufficient to meet the criterion for scaffolds to replace defected cancellous bone tissue. In conclusion, based on a series of experimental studies performed in this research, the space holder method was confirmed to be an appropriate technique for the fabrication of titanium scaffolds with porosity of ~50% for replacement of defected cancellous bone tissue.

To summarize the discussion, the research presented in this thesis is schematically illustrated in Fig. 7.1, which is developed on the basis of Fig. 1.1.

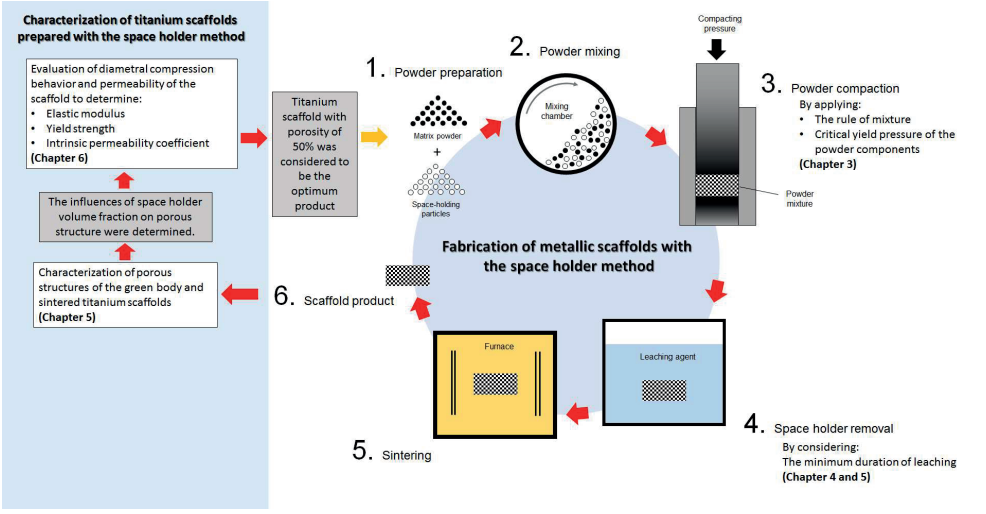

Fig. 7.1. Schematic illustration of the research presented in this thesis. A series of systematic studies have been conducted to determine the mechanisms involved and to optimize the powder compaction (Step 3) and space holder removal process (Step 4) in the fabrication of titanium scaffold with the space holder method. The scaffold products fabricated under the optimized powder compaction and space holder removal process were then characterized, to determine their porous structure and mechanical properties. Based on this research, the space holder method is appropriate for the fabrication of titanium scaffolds with 50% porosity for replacement of defected cancellous bone tissue.

7.3. Recommendations

Although the research presented in this thesis has led to the successful development of the specific methods for the characterization and optimization of process parameters in the fabrication of titanium scaffolds with the space holder method, a number of limitations of this research have been recognized. As noted in Chapter 5, the deviations of the space holder volume fractions of the scaffold green body from the nominal volume fractions of the space holder prior to mixing are too large to be ignored. This may be related to the efficiency of powder mixing,

which is in turn related to the parameters employed during the mixing of the titanium powder and carbamide particles. The control of the mixing process is an important issue that is not studied in this thesis. Therefore, a systematic study to characterize and optimize the parameters involved in the mixing process of the matrix powder and space-holding particles in the preparation of titanium scaffolds is suggested as a supplement to the research presented in this thesis.

Furthermore, it will be highly interesting to extend this work by conducting numerical analysis, making use of the scaffold properties that have been experimentally determined in this research. With this approach, a consecutive model will be established, in the first instance, to predict the scaffold performances based on the geometrical characteristics and physical and mechanical properties of scaffolds fabricated under optimized conditions. It is cautioned that despite being able to reveal mechanical properties similar to the standardized uniaxial compression tests, the DC tests reported in Chapter 6 will not indicate the load and stress distributions all over the body of the titanium scaffold. By means of micro-CT analysis, the changes in the pore morphology of diametrically-compressed titanium scaffolds can be observed and quantified, which may in turn indirectly indicate the stress distributions all over the body of the scaffold. However, the results of such a micro-CT study will not indicate the stress distribution at the cell walls of the scaffold, which is of critical importance for the identification of local failure that leads to the final damage of the whole scaffold under the compressive loads. Therefore, it is highly challenging to develop a validatable model that takes into account the changing geometrical characteristics along the scaffold fabrication route and is able to predict the mechanical behaviour of the scaffolds as influenced by the starting powdered material characteristics and scaffold fabrication process parameters.

References

[1] A. Vats, N. S. Tolley, J. M. Polak and J. E. Gough, "Scaffolds and biomaterials for tissue engineering: A review of clinical applications," *Clinical Otolaryngology,* vol. 28, pp. 165-172, 2003.

[2] S. Bose, M. Roy and A. Bandyopadhyay, "Recent advances in bone tissue engineering scaffolds," *Trends in Biotechnology,* vol. 30, pp. 546-554, 2012.

[3] V. Karageorgiou and D. Kaplan, "Porosity of 3D biomaterial scaffolds and osteogenesis," *Biomaterials,* vol. 26, pp. 5474-5491, 2005.

[4] C. M. Murphy, M. G. Haugh and F. J. O'Brien, "The effect of mean pore size on cell attachment, proliferation and migration in collagen-glycosaminoglycan scaffolds for bone tissue engineering," *Biomaterials,* vol. 31, pp. 461-466, 2010.

[5] B. Arifvianto and J. Zhou, "Fabrication of metallic biomedical scaffolds with the space holder method: A review," *Materials,* vol. 7, pp. 3588-3622, 2014.

[6] R. Singh, P. D. Lee, R. J. Dashwood and T. C. Lindley, "Titanium foams for biomedical applications: A review," *Materials Technology,* vol. 25, pp. 127-136, 2010.

[7] G. Ryan, A. Pandit and D. P. Apatsidis, "Fabrication methods of porous metals for use in orthopaedic applications," *Biomaterials,* vol. 27, pp. 2651-2670, 2006.

[8] R. Heckel, "Density-pressure relationships in powder compaction," *Transactions of the Metallurgical Society of AIME,* vol. 221, pp. 671-675, 1961.

[9] P. Denny, "Compaction equations: A comparison of the Heckel and Kawakita equations," *Powder Technology,* vol. 127, pp. 162-172, 2002.

[10] J. Sonnergaard, "A critical evaluation of the Heckel equation," *International Journal of Pharmaceutics,* vol. 193, pp. 63-71, 1999.

[11] C. E. Wen, M. Mabuchi, Y. Yamada, K. Shimojima, Y. Chino and T. Asahina, "Processing of biocompatible porous Ti and Mg," *Scripta Materialia,* vol. 45, pp. 1147-1153, 2001.

[12] S. F. Hulbert, F. A. Young, R. S. Mathews, J. J. Klawitter, C. D. Talbert and F. H. Stelling, "Potential of ceramic materials as permanently implantable skeletal prostheses," *Journal of Biomedical Materials Research,* vol. 4, pp. 433-456, 1970.

[13] D. Mondal, J. Datta Majumder, N. Jha, A. Badkul, S. Das, A. Patel and G. Gupta, "Titanium-cenosphere syntactic foam made through powder metallurgy route," *Materials and Design,* vol. 34, pp. 82-89, 2012.

[14] N. Jha, D. Mondal, J. Dutta Majumdar, A. Badkul, A. Jha and A. Khare, "Highly porous open cell Ti-foam using NaCl as temporary space holder through powder metallurgy route," *Materials and Design,* vol. 47, pp. 810-819, 2013.

[15] T. Shivashankar and R. German, "Effective length scale for predicting solvent-debinding times of components produced by powder injection molding," *Journal of the American Ceramics Society,* vol. 82, pp. 1146-1152, 1999.

[16] S. Kim, H. Lee, H. Song and B. Kim, "Pore structure evolution during solvent extraction and wicking," *Ceramics International,* vol. 22, pp. 7-14, 1996.

[17] Y. Torres, J. J. Pavón and J. A. Rodríguez, "Processing and characterization of porous titanium for implants by using NaCl as space holder," *Journal of Materials Processing Technology,* vol. 212, pp. 1061-1069, 2012.

[18] H. Bafti and A. Habibolahzadeh, "Production of aluminum foam by spherical carbamide space holder technique," *Materials and Design,* vol. 31, pp. 4122-4129, 2010.

[19] P. Hui, P. Leung and A. Sher, "Fluid conductance of cancellous bone graft as a predictor of graft-host interface healing," *Journal of Biomechanics,* vol. 29, pp. 123-132, 1996.

[20] S. Yang, K.-F. Leong, Z. Du and C.-K. Chua, "The design of scaffolds for use in tissue engineering. Part I. Traditional factors," *Tissue Enginnering,* vol. 7, pp. 679-689, 2001.

Summary

Loss of function and impaired life quality as a result of large bone defects remain a serious problem in the society. Basically, the bone tissue has the capability of healing by itself when fractured. However, impaired healing may occur, leading to delayed union or even non-union when a bone segment is excised above a critical size. In recent years, bone tissue engineering has received increasing attention in the biomedical research community as an alternative approach to bone defect reconstruction. With this approach, damaged bone tissue can be repaired and remodelled with new bone cells at the defect site. For this purpose, a synthetic porous material, namely scaffold, is needed to act as a template to facilitate cellular activities, such as the migration and proliferation of osteoblasts and mesenchymal cells, as well as the transport of nutrients and oxygen required for vascularization during bone tissue development at the defect site. Currently, titanium is considered to be a preferred biomaterial for bone tissue engineering scaffolds owing to its excellent biocompatibility and mechanical properties. So far, the space holder method has been preferably used for the fabrication of titanium scaffolds with high porosity and open, interconnected pores for bone tissue engineering. Despite a large number of studies on the scaffold fabrication with this method, the mechanisms involved and the way to control the porous structure of scaffolds during fabrication have not yet been fully understood.

The work reported in this thesis is aimed to give an insight into the way to control the porous structure of biomedical titanium scaffolds prepared with the space holder method in order to meet the requirements of scaffolds in physical and mechanical properties for bone tissue engineering. Although the general principle of scaffold fabrication with this method has been described in the literature, detailed protocols for the fabrication and characterization of scaffolds are not available in the open literature and complex relationships of fabrication process parameters with the geometrical characteristics and physical and mechanical properties of scaffolds are largely unknown. Obviously, these issues must be addressed before scaffolds with controllable and consistent porous structures and performances can enter the phase of tissue engineering product development for clinical applications. In this thesis work, the characterization and optimization of the fabrication processes for titanium scaffolds prepared with the space holder method were carried out. Then, the physical and mechanical properties of the scaffolds prepared under the optimized process conditions were evaluated against the requirements of scaffolds for bone tissue engineering.

On the basis of an extensive literature study (Chapter 2), key challenges in the fabrication processes for titanium scaffolds with the space holder method were identified. The control of space holder geometry during powder compaction and the retention of structure integrity and also complete removal of space holder to generate macro-pores in the scaffold were recognized as the primary challenges. Despite being critically important in determining the porous structure of the scaffold, both the powder compaction process and the space holder removal process were rarely studied. The characterization of these two processing steps was considered to be the basis for the optimization of the whole scaffold fabrication process with the space holder method.

In the powder compaction process, an appropriate compressive stress must be applied to prevent either the scaffold green body from being ruined due to a too low compacting pressure or the macro-pore geometry from distortion as a result of heavy deformation and even breakage of space-holding particles due to a too high compacting pressure. In this thesis work (Chapter 3), the appropriate compacting pressures for the preparation of titanium scaffolds with carbamide space-holding particles were determined, based on the dissimilar compression behaviors of these two powders under uniaxial compressive stresses. The yield pressures of the titanium powder, carbamide particles and their mixtures were determined with the aid of the Heckel model. The measured yield pressure of a titanium/carbamide powder mixture was used as a critical pressure, with which the mixture could be compacted to generate the scaffold green body with a sufficient green strength but without causing excessive deformation and breakage of space-holding particles. The rule of mixtures was found to be applicable with caution to predict the critical pressure for compacting a titanium/carbamide powder mixture with a predetermined space holder volume fraction. In conclusion, by applying this approach to compacting titanium/carbamide powder mixtures, carbamide space-holding particles inside the scaffold green body remained intact, as demonstrated in an optical microscopic study. Micro-computed tomography (micro-CT) confirmed that the application of compressive stresses based on the rule of mixtures and yield pressures resulted in the sintered titanium scaffolds with acceptable pore sizes for bone tissue engineering.

In the space holder removal process, in order to prevent the scaffold green body from being ruined or the contamination by the residues inside the scaffold preform it was of critical importance to develop a reliable method to monitor the progress of this process. A novel precise weight measurement technique for the characterization of the removal process of carbamide space-holding particles by the water leaching method was developed (in Chapter 4). With this technique, the mechanisms operating during space holder removal by using water leaching were determined with the aid of the existing solvent debinding models for powder injection moulded parts. Three primary regimes representing the leaching behavior of carbamide particles in the scaffold preforms were recognized, namely (i) rapid dissolution, (ii) dissolution and diffusion and (iii) saturation. Based on these mechanisms, the influence of the space holder volume fraction on the duration and efficiency of the leaching process to remove carbamide space-holding particles was investigated and the appropriate durations required for the leaching process to remove carbamide particles were determined. It was concluded that the green body of titanium scaffold containing a higher volume fraction of the space holder material required a shorter duration to completely remove carbamide space-holding particles. Disintegration of titanium powder still occurred during the leaching process, mainly at the circumference of the bottom part of the scaffold green body and in the scaffold preforms with high carbamide volume fractions, i.e., $x > 70\%$.

The next challenge was to answer the fundamental question as to whether the final porous structure of the sintered titanium scaffold could reflect powder particle arrangements inside the scaffold green body, as shrinkage of the porous green body of titanium scaffold would inevitably take place during sintering. Excessive shrinkage might lead to the deviations of the final porosity

and macro-pore geometry of the sintered scaffold from the volume fraction and geometry of space-holding particles in the green body of the scaffold. Therefore, the information on the changes of 3-dimensional (3D) porous structure from the green body to sintered titanium scaffolds should be obtained. In this thesis work (Chapter 5), the 3D porous structures of the green body and sintered titanium scaffolds prepared under the optimized conditions were characterized by means of micro-CT. It was found that the porous structures of the titanium scaffolds processed through water leaching and sintering at 1200 ºC for 3 h did not deviate significantly from their green structures. Thus, the control of the final porous structure of the titanium scaffold from its green body would be feasible by applying these sintering parameters. It was also found that maximum specific surface area values of the green body and sintered scaffold could be obtained by adding 60 – 65 vol.% carbamide space-holding particles, which corresponded to a total porosity of 50 – 55% in the sintered scaffold. In addition, the connectivity density measured by means of micro-CT increased with rising space holder volume fraction in the scaffold green body.

To meet the criteria of scaffolds for bone tissue engineering, scaffolds with open, interconnected pores and appropriate mechanical properties are required to support and to guide the formation and development of new tissue. In principle, open, interconnected pores could be produced by increasing the porosity of the scaffold. However, as the porosity increased the mechanical properties of the scaffold decreased. Therefore, an attempt was made to balance these two conflicting property requirements. In this thesis work (Chapter 6), open, interconnected pores and mechanical properties of titanium scaffolds with porosity in a range of 31 – 61% were characterized. Micro-CT and permeability analyses were carried out to quantify the porous structures and to ascertain the presence of open, interconnected pores in the scaffolds. The elastic moduli and yield strengths of the scaffolds were determined with the aid of the stress-strain diagrams obtained from diametral compression (DC) tests. The results of the micro-CT and permeability analyses confirmed the presence of open, interconnected pores in the titanium scaffolds with total porosities in a range of 31 – 61%. Interestingly, the intrinsic permeability constant k value of the scaffold with a total porosity of ~50% was close to that of the threshold value for revascularization, i.e., 3×10^{-11} m^2 inside the bone graft. Elastic moduli and yield strengths of titanium scaffolds in the ranges of 0.64 – 3.47 GPa and 28.67 – 80 MPa, respectively, could be achieved. The elastic moduli of the titanium scaffolds with porosities in a range of 50 – 55%, i.e., 1.53 – 1.98 GPa, were comparable to the elastic modulus of the cancellous bone tissue reported in the literature, i.e., 0.02 – 0.5 GPa. The yield strengths of the scaffolds at this level of porosity, i.e., 35.3 – 49.2 MPa, were higher than the yield strength of the cancellous bone, i.e., 1.5 – 30 MPa, which demonstrated that the strengths of these titanium scaffolds were sufficient to meet the criterion for the scaffolds to replace the defective cancellous bone tissue.

In conclusion, the space holder method was confirmed to be an appropriate technique for the fabrication of titanium scaffolds with porosity of ~50%.

Samenvatting

De gevolgen van grote bot defecten zoals functieverlies en een afname in kwaliteit van leven blijven een ernstig probleem voor de samenleving. In principe heeft botweefsel het vermogen zichzelf te helen wanneer het gebroken is. Echter, wanneer een botsegment boven een kritische grootte is verwijderd, kan dit leiden tot vertraagde botheling of zelfs pseudartrose. De belangstelling in botweefsel engineering als een alternatieve aanpak voor de reconstructie van botdefecten is bij de biomedische onderzoeksgemeenschap in de afgelopen jaren toegenomen. Door middel van deze aanpak kunnen nieuwe botcellen op de defecte locatie remodelleren en het beschadigde botweefsel herstellen. Hiervoor is een synthetisch, poreus materiaal nodig, een scaffold genoemd, die als patroon kan dienen voor zowel cellulaire activiteiten, zoals de migratie en proliferatie van osteoblasten en mesenchymale cellen, als de transport van nutriënten en zuurstof die nodig is voor vascularisatie tijdens de ontwikkeling van botweefsel op de defecte locatie. Op basis van zijn uitmuntende biocompatibiliteit en mechanische eigenschappen geniet titanium momenteel de voorkeur als biomateriaal. Voor de vervaardiging van titanium scaffolds met hoge porositeit en open, onderling verbonden poriën wordt, tot nu toe, voornamelijk de space-holder methode gebruikt. Ondanks de grote hoeveelheid aan studies op het gebied van scaffoldvervaardiging met deze methode, zijn de betrokken mechanismen en de wijze waarop de poreuze structuur beheerst kan worden tijdens vervaardiging nog niet volledig doorgrond.

Het doel van het werk beschreven in dit proefschrift is het geven van inzicht in de wijze waarop er met de space-holder methode een poreuze structuur voor een biomedische titanium scaffold geprepareerd kan worden die vervolgens voldoet aan de fysische en mechanische eisen voor botweefsel engineering. Hoewel het algemene principe van deze methode is beschreven in de literatuur, zijn er geen gedetailleerde procedures beschikbaar in de open literatuur voor de vervaardiging en karakterisering van scaffolds en blijven complexe relaties, tussen fabricageprocesparameters en geometrische, fysische en mechanische eigenschappen, grotendeels onbekend. Het is evident dat deze punten behandeld moeten worden voordat scaffolds met beheersbare en consistente poreuze structuren en prestaties de productontwikkelingsfase van tissue engineering voor klinische toepassingen kunnen binnentreden. De karakterisering en optimalisatie van het vervaardigingsproces voor titanium scaffolds met de space-holder methode zijn binnen dit proefschrift uitgevoerd. Opvolgend zijn de fysische en mechanische eigenschappen van de scaffolds, vervaardigd met geoptimaliseerde procescondities, geëvalueerd tegen de eisen voor scaffolds voor botweefsel engineering.

Op basis van een uitgebreide literatuurstudie (Chapter 2), werden de belangrijkste uitdagingen in het vervaardigingsproces voor titanium scaffolds met de space-holder methode geïdentificeerd. Het beheersen van de space-holder geometrie tijdens poedercompactie en de retentie van de integriteit van de structuur maar ook de complete verwijdering van de space-holder om de macro-poriën te genereren werden gezien als primaire uitdagingen. Ondanks het cruciale belang van de poedercompactie en de space-holder verwijdering voor het verkrijgen van de poreuze structuur werden deze processen nauwelijks bestudeerd. De karakterisering van deze

processen werden beschouwd als de basis voor de optimalisatie van het complete scaffold vervaardigingsproces met de space-holder methode.

Tijdens poedercompactie moet een geschikte druk worden toegepast om te voorkomen dat aan de ene kant het ongesinterde werkstuk verbrokkeld door een te lage druk en aan de andere kant de macro-poriën vervormen als gevolge van grove deformatie of zelfs breuk van de space-holder deeltjes door een te hoge druk. In dit proefschrift (Chapter 3), werd de juiste druk voor het vervaardigen van titanium scaffolds met carbamide als space-holder deeltjes bepaald op basis van het ongelijke compressiegedrag van deze twee poeders onder uni-axiale drukspanningen. De vloeidruk van het titanium poeder, carbamide deeltjes en hun mengsels werden bepaald aan de hand van het Heckel model. De gemeten vloeidruk van een titanium/carbamide mengsel werd gebruikt als een kritische druk waarmee het mengsel kon worden samengedrukt tot een scaffold met genoeg stekte in ongesinterde staat maar zonder bovenmatige deformatie of breuk van space-holder deeltjes. De mengregels bleken toepasbaar, met enige voorzichtigheid, om de kritische druk te voorspellen waarmee een titanium/carbamide poedermengsel, met een vooraf bepaalde space-holder volumefractie, samengedrukt kon worden. Aan de hand van optische microscopie kon worden aangetoond dat door deze aanpak toe te passen voor het compacteren van titanium/carbamide poedermengsels, space-holder deeltjes binnen in de scaffold intact bleven. Door middel van micro computergestuurde tomografie (micro-CT) werd bevestigd dat het toepassen van drukspanningen op mengregels en vloeidrukken resulteerde in gesinterde titanium scaffolds met toereikende poriegroottes voor botweefsel engineering.

Om te voorkomen dat, tijdens het verwijderen van de space-holder, de scaffold in ongesinterde staat verbrokkeld of residuen de scaffold vervuilen moest een betrouwbare methode ontwikkeld worden om de voortgang van dit proces te monitoren. Een unieke precisie gewichtmeting werd ontwikkeld voor de karakterisering van het verwijderen van carbamide deeltjes door middel van water-uitloging (Chapter 4). Met deze techniek werden de mechanismen, die tijdens space-holder uitloging optreden, bepaald met hulp van bestaande modellen voor het ontbinden van spuitgietproducten. Drie primaire regimes die het uitlogingsgedrag van carbamide deeltjes in scaffold voorvormen weergeven werden bepaald, namelijk (i) snelle oplossing, (ii) oplossing en diffusie en (iii) saturatie. Op basis van deze mechanismen werd de invloed van de space-holder volumefractie op de duur en efficiëntie van het uitlogingsproces voor de verwijdering van carbamide deeltjes onderzocht en de juiste tijden die nodig waren voor het uitlogen van carbamide deeltjes bepaald. Er werd geconcludeerd dat titanium scaffolds met een hogere volumefractie aan space-holder, in ongesinterde staat, minder tijd nodig hadden voor het volledig verwijderen van de carbamide space-holder deeltjes. Tijdens het uitlogingsproces trad er disintegratie van titanium deeltjes op, voornamelijk aan de omtrek van de onderkant van de ongesinterde scaffold en in de scaffolds met hoge carbamide volumefracties, namelijk $x > 70\%$.

De volgende uitdaging was het beantwoorden van de fundamentele vraag of de poederdeeltjes van het gesinterde eindproduct dezelfde architectuur hadden als de deeltjes van de scaffolds in de ongesinterde staat, omdat krimp tijdens sinteren een onvermijdelijk verschijnsel is. Derhalve moest informatie over de veranderingen van de drie dimensionale (3D)

poreuze structuur van de titanium scaffolds tijdens sinteren verkregen worden. In dit proefschrift (Chapter 5) zijn de 3D poreuze structuren van zowel de ongesinterde als gesinterde scaffolds, vervaardigd onder optimale condities, gekarakteriseerd door middel van micro-CT. Er werd vastgesteld dat de poreuze structuren van de titanium scaffolds, vervaardigd via water-uitloging en sintering op 1200 °C voor 3 uur niet significant afweken van hun ongesinterde structuur. Het was daarom haalbaar om de uiteindelijke poreuze structuur van de titanium scaffolds te beheersen wanneer deze sinterparameters werden toegepast. Bovendien werd er vastgesteld dat het maximale specifieke oppervlak van de ongesinterde en gesinterde scaffolds behaald konden worden door toevoeging van 60 – 65 vol.% carbamide deeltjes, wat overeenkwam met een totale porositeit van 50 -55 % in de gesinterde scaffold. Verder steeg de connectiviteitsdichtheid, gemeten met micro-CT, met toenemende volumefractie van space-holder in de ongesinterde scaffold.

Om aan de criteria te voldoen van scaffolds voor botweefsel engineering moeten scaffolds met open, onderling verbonden poriën en geschikte mechanische eigenschappen de formatie en ontwikkeling van nieuw weefsel ondersteunen en leiden. In principe zouden open, onderling verbonden poriën geproduceerd kunnen worden door de porositeit van de scaffold te vergroten. Echter, wanneer de porositeit toeneemt, nemen de mechanische eigenschappen van de scaffold af. Er is derhalve getracht een balans te vinden tussen deze twee conflicteerde eigenschappen. In dit proefschrift (Chapter 6) werden open, onderling verbonden poriën en mechanische eigenschappen van titanium scaffolds met een porositeit van 31 – 61% gekarakteriseerd. Micro-CT en permeabiliteitanalyses werden uitgevoerd om de poreuze structuren te kwantificeren en de aanwezigheid van open, onderling verbonden poriën in de scaffold vast te stellen. De elasticiteitsmoduli en vloeigrenzen van de scaffolds werden bepaald aan de hand van spanning-rek diagrammen verkregen met diametrale compressietesten (DC). De resultaten van de micro-CT en permeabiliteit analyses bevestigde de aanwezigheid van open, onderling verbonden poriën in de titanium scaffolds met een totale porositeit van 31 – 61%. Interessant was dat de intrinsieke permeabiliteit van de scaffolds met een totale porositeit van ~ 50% dicht bij dat van de drempelwaarde voor revascularisatie lag, namelijk 3×10^{-11} m², binnen in het bottransplantaat. Met de titanium scaffolds konden elasticiteitsmoduli en vloeigrenzen in de reikwijdte van, respectievelijk, 0.64 – 3.47 GPa en 28.67 – 80 MPa worden bereikt. De elasticiteitsmoduli van de titanium scaffolds met een porositeit in het bereik van 50 – 55%, namelijk 1.53 – 1.98 GPa, waren vergelijkbaar met die van spongieus botweefsel, gerapporteerd in de literatuur, namelijk 0.02 - 0.5 GPa. In dit gebied van porositeit besloeg de vloeigrens van de scaffolds 35.5 – 49.2 MPa en was hoger dan dat van spongeus bot, namelijk 1.5 – 30 MPa, wat demonstreerde dat de stekte van deze titanium scaffolds voldoende was om aan de criteria te voldoen voor vervanging van defect spongieuze botweefsel.

Tot besluit kon worden vastgesteld dat de space-holder methode een geschikte techniek is voor de fabricage van titanium scaffolds met een porositeit van ~50%.

Acknowledgments

To me, this thesis is one of important chapters in a story book about my academic carrier. Also, it is like a mirror, to which I looked back at all memories from every single moment that happened during the period of 2012 – 2016, when I was studying and enjoying the life in the Netherlands. At that time, I learned many things, not only about research but also about the life from many great and inspiring people who always stayed around and gave their supports to me. I dedicate these three pages for them, to express my gratitude to all these special people.

Prof. Frans van der Helm. I am so lucky to have a chance to be one of his Ph.D. students in TU Delft. From him, I learned that we should first be skeptical to the data we acquired from an experimental or research work, though they looked good and so convincing. Frans, thank you for all your helps and time for me.

Dr. Jie Zhou. Jie is the very first person who opened the way for me to TU Delft and then gave a warm welcome when I entered this university. I will never forget the moment when he made his first call to me from Delft for a short interview. Also, the time when he picked me up in Schiphol Airport upon my first arrival in Delft was so difficult to forget. He supervised, assisted, trained and sometimes challenged me to become a good and reputable research her in my field. He trusted my ideas and always kept his door open for all my questions, complains and problems. It happened many times; I came to him, bringing a big box of problems from my work in the lab, but he never refused to give his help. His attention to my personal life and my family has made me having a feeling that Delft is my second home in this world. Jie, thank you for everything.

Ing. Sander Leeflang. It must be very hard to run all my experiments without the helps from Sander. I spent most of my time working together with him. It happened many times, that a scientific discussion with him turned into an informal but very interesting discussion, about the life, culture, history, family and his cats! I will always remember his favorite quote: Be optimistic! Sander, thank you so much for all your helps, assistance and cooperation.

Dr. Iulian Apachitei and Dr. Lidy Fratila-Apachitei. I would like to thank to Iulian and Lidy, for their warm welcome in TU Delft. They are among the people in this university who always trusted me and my expertise. I felt of being trusted and honored when they appointed me several times to supervise M.Sc. students in their mini-research projects.

Dr. Amir A. Zadpoor. Amir is truly an inspiring young researcher and leader of the Section of Biomaterials and Tissue Biomechanics. I was impressed to his dedication to the group and the way he managed his own big research projects. I would like to express my gratitude to him for some discussions and informal talks during the group meeting and coffee time.

Prof. Jenny Dankelman. Professor Dankelman was the chairwoman of the Department of Biomechanical Engineering when I joined TU Delft in 2012. I am grateful for her permission to become the member of big family of this multidiscipline department.

Prof. Bart Verkerke. In the mid of 2006, I met Professor Bart Verkerke in University of Groningen. Bart introduced me to the world of biomedical engineering. Also, he also introduced me to the Netherlands and the Dutch academic culture. Therefore, I felt his contribution in every step of my life in the Netherlands. Bart, thank you so much.

Dineke Heersma and Mirjam Bierhuizen. Without numerous helps from Dineke and Mirjam, I must be trapped in many difficult situations when dealing with all administrative works during my study in TU Delft. I am grateful to both of them. Also, I would like to thank to **Mascha Toppenberg** for her patience in assisting me to proceed all administrations of the graduate school of 3mE faculty and TU Delft. And, to all the secretaries in this department: **Anouk, Nancy, Diones, Hanneke, Sabrina,** and **Karin,** thank you for all your helps.

To my roommates and lab-mates: **Vahid, Shahram, Sina, Gerwin, Nazli, Mohammed, Reza, Franscois, Yageng, Saber, Steven, Helene, Arjo, Gianni, Bram, Chunman, Anand, William, Alexandra,** and **Linda**. I was so lucky to see and interact with all of you guys! Thanks a lot, and all the best to you.

To all my colleagues in several labs and departments around TU Delft: **Wim, Arjan, Sander van Asperen, Maiko, Ger, Hans, Ton, Kees** and **Karel**. I might not be able to finish this thesis without your assistance and cooperation. Thank you so much!

To all my Indonesian colleagues: **Dieky, Ficky, Yudha, Anggrit, Ardhi, Dwi, Giga, Muhammad, Agung Purniawan, Andri, Pandu, Junaedy, Agung Wahyudi, Inung, Mutia, Ajenk, Arif, Hermin, Jejey, Tri Budi** and **others** in *Perhimpunan Pelajar Indonesia di Delft* (PPI Delft; Indonesian Students Association in Delft) and *Keluarga Muslim Delft* (KMD). Thanks for the friendship, jokes, foods, and other things which could not be mentioned here.

To **Yazdi** and **Ely, Adhi** and **Erma, Senot** and **Pungky, Tofan** and **Ainil, Hedi** and **Putri**, **Jumari** and **Etty, Marwan** and **Ririn, Dhata** and **Maya,** Pak **Satria** and Teh **Irma**, Pak **Gerri** and Mbak **Lina**; thank you for being a warm place for me and my family in the Netherlands. A special thank goes to **Yazdi**, for many discussions about dreams, research, aircraft, organization, family and life. Also, for his contribution in designing the cover page of this thesis book and his assistance during the preparation of my Ph.D. defense.

Dr. Suyitno, **Dr. Muslim Mahardika**, **Dr. Punto Dewo** and **Dr. Titis Wijayanto** in Gadjah Mada University, Indonesia. They are all among the great people, who had become my mentor

and good friends before I moved to Delft in 2012. Thank you so much for the lessons, discussion and cooperation.

I would like to thank to Pak **Archi Sanwikrama**, Pak **Adhi Wibawa** and their families, Pak **Hendi**, Bli **Kadek Yota** and mbak **Shanti** who had become my big family when I and my wife lived in Groningen, before we moved to Delft. There were many hard moments there, but fortunately we had their kindness and endless supports.

I am grateful to the **Ministry of Education and Culture (**later, **Ministry of Research and Technology and Higher Education Affair), Republic of Indonesia** for the financial support through DIKTI-NESO scholarship scheme, especially during my first three years in TU Delft. Also, thank you for some of the DIKTI-NESO scholarship holder in 2012: **Ajeng, Alfi, Richo, Galuh** and **Rosa**.

To **my parents** and **parents-in-law**; their constant prayers had become a booster of my energy and motivation of my life in the Netherlands, though we were separated about 11,340 kilometers. Bapak, Ibu, *matur nuwun*. To **my brothers** and **sisters**: **Hanif, Arina, Fiki** and **Barra**, thanks for all your supports.

I would also like to thank to my uncle, **Listyo Sumitro**, and his family for their support to me when I had to stay in Jakarta several times to prepare and submit all the documents required for applying the DIKTI scholarship and the visa to enter the Netherlands.

Finally, all my achievements since the period before I moved and lived in Delft (and then Schiedam) would never be real without the endless supports and prayers from my wife, **Nida**, and my daughter, **Azkia**. Their presence to accompany me in the Netherlands was indeed a very special gift from Him. Thank you so much my dear. It was a very touching moment when I could bring you both back to the Netherlands in 2014. Then, we lived, grew and learned together in Delft and Schiedam. And now, we realize that it is too hard to forget all the memories about our life in the Netherlands.

Delft, October 25th, 2017

Budi Arifvianto

About the author

Budi Arifvianto was born in Yogyakarta, Indonesia. He started his academic career in 2005 when he was appointed as technical assistant in the laboratory of aerodynamics, Department of Mechanical and Industrial Engineering, Universitas Gadjah Mada (UGM), Indonesia. At the same year, he obtained his bachelor degree in mechanical engineering from the same university. In 2008, he obtained his M.Biotech. after completing a two-year master program in biomedical engineering, also in UGM. Soon after, he was involved in some research projects in the field of biomaterials processing technology, with financial supports mainly from UGM and Ministry of Education and Culture, Republic of Indonesia. His research concerned the investigation of mechanical surface treatments and their influences on mechanical and surface properties of metallic biomaterials, such as stainless steel, titanium and magnesium alloy. In September 2012, he moved to Delft to start his Ph.D. in Department of Biomechanical Engineering, TU Delft, under the supervision of Dr. Jie Zhou and Prof. Frans van der Helm. He worked on a project to develop titanium scaffolds for bone tissue engineering by using powder metallurgy approach and space holder method. This thesis was adapted from his work in this project. After completing his Ph.D., he will return to UGM and work as a researcher and lecturer in the Department of Mechanical and Industrial Engineering of this university.

List of publications

A. Journal publications

1. Diametral compression behavior of biomedical titanium scaffolds with open, interconnected pores prepared with the space holder method
   B. Arifvianto, M.A. Leeflang, J. Zhou, **Journal of the Mechanical Behavior of Biomedical Materials**, 68 (2017) pp. 144-154.

2. Characterization of the porous structures of the green body and sintered biomedical titanium scaffolds with micro-computed tomography
   B. Arifvianto, M.A. Leeflang, J. Zhou, **Materials Characterization**, 121 (2016) pp. 48-60.

3. The compression behaviors of titanium/carbamide powder mixtures in the preparation of biomedical titanium scaffolds with the space holder method
   B. Arifvianto, M.A. Leeflang, J. Zhou, **Powder Technology**, 284 (2015) pp. 112-121.

4. Fabrication of metallic biomedical scaffolds with space holder method: A review
   B. Arifvianto, J. Zhou, **Materials**, 7 (2014) pp. 3588-3622.

5. Characterization of space holder removal through water leaching for preparation of biomedical titanium scaffolds
   B. Arifvianto, M.A. Leeflang, J. Duszczyk, J. Zhou, **Powder Metallurgy**, 57 (2014) pp. 9-12.

6. A new technique for the characterization of the water leaching behavior of space holding particles in the preparation of biomedical titanium scaffolds
   B. Arifvianto, M.A. Leeflang, J. Zhou, **Materials Letters**, 120 (2014) pp. 204-207.

7. Surface modification of titanium using steel slag ball and shot blasting treatment for biomedical implant applications
   B. Arifvianto, Suyitno, M. Mahardika, **International Journal of Minerals, Metallurgy and Materials**, 20 (2013) pp. 788-795.

8. Effect of cold working and sandblasting on microhardness, tensile strength and corrosion resistance of AISI 316L stainless steel
   Suyitno, B. Arifvianto, T.D. Widodo, M. Mahardika, P. Dewo, U.A. Salim, **International Journal of Minerals, Metallurgy and Materials**, 19 (2012) pp. 1093-1099.

9. Influence of grit blasting treatment using steel slag balls on subsurface microhardness, surface characteristics and chemical composition of medical grade 316L stainless steel
B. Arifvianto, Suyitno, K.A. Wibisono, M. Mahardika, **Surface and Coatings Technology**, 210 (2012) pp. 176-182.

10. Effect of slag ball blasting treatment on surface structure, roughness and wettability of 316LVM stainless steel
B. Arifvianto, G.A. Pohan, Suyitno, M. Mahardika, **Procedia Engineering**, 50 (2012) pp. 142-151.

11. Effects of surface mechanical attrition treatment (SMAT) on a rough surface of AISI 316L stainless steel
B. Arifvianto, Suyitno, M. Mahardika, **Applied Surface Science**, 258 (2012) pp. 4538-4543.

12. Effect of surface mechanical attrition treatment (SMAT) on microhardness, surface roughness and wettability of AISI 316L
B. Arifvianto, Suyitno, M. Mahardika, P. Dewo, P.T. Iswanto, U.A. Salim, **Materials Chemistry and Physics**, 125 (2011) pp. 418-426.

13. Effect of sandblasting and surface mechanical attrition treatment on surface roughness, wettability, and microhardness distribution of AISI 316L
B. Arifvianto, Suyitno, M. Mahardika, **Key Engineering Materials**, 462-463 (2011) pp. 738-743.

Note: Articles no. 1 – 6 were published based on the research presented in this thesis.

B. Published works in conference proceedings and book of abstracts

1. B. Arifvianto, M.A. Leeflang, J. Zhou, Influences of macro-pores and compacting pressure on the geometry of micro-pores and mechanical properties of biomedical titanium scaffolds prepared with the space holder method, **Book of Abstract: Advanced Materials Processing and Technologies Conference** (2015), Madrid, Spain.

2. B. Arifvianto, M.A. Leeflang, J. Zhou, Appropriate compacting pressures for the preparation of biomedical titanium scaffolds with the space holder method, **Ph.D. Day 3mE TU Delft** (2015) Delft, The Netherlands (with poster presentation).

3. B. Arifvianto, M.A. Leeflang, J. Zhou, Analysis of densification behaviour of titanium/carbamide powder mixtures in the preparation of biomedical titanium scaffolds with the space holder method, **Book of Abstract: The 5th Dutch BioMedical**

Engineering Conference (2015), Egmond aan Zee, The Netherlands (with poster presentation).

4. B. Arifvianto, M.A. Leeflang, J. Duszczyk, J. Zhou, Characterization of space holder removal through water leaching for the preparation of biomedical titanium scaffolds, **Proceeding of Euro Powder Metallurgy 2013 Congress and Exhibition, Vol. 3: Powder Metallurgy for Biomaterials** (2013), Gothenburg, Sweden.

5. B. Arifvianto, Suyitno, M. Mahardika, Hybrid surface treatment for improving mechanical and surface properties of AISI 316L stainless steel, **Proceeding of the 2nd International Conference on Instrumentation, Communications, Information Technology and Biomedical Engineering (ICICI-BME)/Biomedical Engineering Days 2011** (2011), Bandung, Indonesia`

6. B. Arifvianto, Suyitno, M. Mahardika, Roughness reduction in AISI 316L stainless steel after surface mechanical attrition treatment (SMAT), **The 4th Nanoscience and Nanotechnology Symposium (NNS2011): An International Symposium. AIP Conference Proceedings**, Vol. 1415, (2011) Bali, Indonesia.

7. B. Arifvianto, M. Mahardika, Suyitno, Surface structure of AISI 316L after sandblasting and surface mechanical attrition treatment, **Proceeding of the 1st International Conference on Materials Engineering (ICME) and 3rd AUN/SEED-Net Regional Conference on Materials (RCM)** (2011) Yogyakarta, Indonesia.

8. B. Arifvianto, Suyitno, M. Mahardika, Surface mechanical attrition treatment on AISI 316L with different milling ball parameters, **Proceeding of 2nd AUN/Seed-Net Regional Conference on Manufacturing Engineering** (2009) Bandung, Indonesia.

9. B. Arifvianto, Suyitno, A. Widyaparaga, Effect of surface mechanical attrition treatment on roughness and wettability of AISI 316L, **Proceeding of International Conference on Materials and Metallurgical Technology (ICOMMET)**, (2009) Surabaya, Indonesia.

Note: Articles no. 1 – 4 were published based on the research presented in this thesis.